

**Systemic Delivery of Phosphorylated Nucleoside Analogues and siRNA via LCP  
Nanoparticles for Cancer Therapy**

Yuan Zhang

A dissertation submitted to the faculty of the University of North Carolina at Chapel Hill in  
partial fulfillment of the requirements for the degree of Doctor of Philosophy in the  
Eshelman School of Pharmacy.

Chapel Hill  
2013

Approved by,

Leaf Huang, Ph.D.

William Y Kim, MD.

Sam Lai, Ph.D.

Philip C. Smith, Ph.D.

Xiao Xiao, Ph.D.

© 2013  
Yuan Zhang  
ALL RIGHTS RESERVED

## ABSTRACT

YUAN ZHANG: Systemic Delivery of Phosphorylated Nucleoside Analogues and siRNA via LCP Nanoparticles for Cancer Therapy  
(Under the direction of Leaf Huang, Ph.D.)

Nucleoside analogues are a significant class of anticancer agents. As prodrugs, they terminate the DNA synthesis upon transforming to their active triphosphate metabolites. However, several *in vivo* delivery hurdles compromise their application in clinical settings. To address these delivery problems, we encapsulated the phosphorylated nucleoside analogues (i.e. gemcitabine triphosphate (GTP), or gemcitabine monophosphate (GMP)) into a novel Lipid/Calcium/Phosphate nanoparticle (LCP) platform. The therapeutic efficacy of drug loaded LCPs was evaluated in a panel of human non-small-cell lung cancer (NSCLC) or human pancreatic cancer xenograft models. Drug-loaded LCPs induced cell death and arrested the cell cycle in the S phase. *In vivo* efficacy studies in mice showed that intravenously injected drug-loaded LCPs triggered effective apoptosis of tumor cells, significant reduction of tumor cell proliferation and cell cycle progression, leading to dramatic inhibition of tumor growth, with little *in vivo* toxicity. Additionally, LCPs significantly prolonged the blood circulation of the entrapped GTP as compared to the free drug. The current study offers preclinical proof-of-principle that many active nucleotide or phosphorylated nucleoside analogues could be encapsulated in the LCP nanoplatform for systemic delivery.

In order to suppress the tumor progression more effectively, gene therapy by RNAi was combined with gemcitabine chemotherapy, by formulating multiple therapeutic agents into one single nanoparticle. LCP encapsulating both VEGF siRNA and GMP, or LCP encapsulating both c-Myc siRNA and GMP were constructed. *In vivo* responses of combined

therapies were compared with individual monotherapies in NSCLC xenograft model or NSCLC orthotopic model. *In vivo* efficacies of LCP formulations were evaluated by caspase activation, apoptosis induction and proliferation reduction, as well as tumor growth inhibition. Anti-angiogenic effects and *in vivo* toxicities were also evaluated. The current studies demonstrated the plausibility of incorporating multiple nucleic acid molecules and phosphorylated small molecule drugs, targeting to different pathways, into a single nanoparticle formulation for profound therapeutic effect.

## **ACKNOWLEDGEMENTS**

I would like thank my academic advisor, Dr. Leaf Huang, for his guidance and support of my research. I also thank my committee members, Drs. Kim, Lai, Smith and Xiao for their suggestions on my dissertation project. The kind assistance from the Huang lab during my graduate research and study is acknowledged. I also appreciate the supports from my friends and family, especially my mother Weijun Zheng.

Drs. Srinivas Ramishett, Nicole Schwerbrock, Yang Yang, Jinfeng Du, Hong Yuan and Arlin Rogers are acknowledged for their help on this project.

## LIST OF ABBREVIATIONS

NSCLC	Non-Small-Cell-Lung Cancer
GTP	Gemcitabine Triphosphate
GMP	Gemcitabine Monophosphate
LCP	Lipid Calcium Phosphate nanoparticle
VEGF	Vascular Endothelial Growth Factor
VEGFR	Vascular Endothelial Growth Factor Receptor
Gem	Gemcitabine
dCK	deoxycytidine kinase
AA	anisamide
CMP	Cytidine Monophosphate
Con	Control siRNA
PEG	Polyethylene glycol
TEM	Transmission Electron Microscope
EE%	Encapsulation Efficiency
TUNEL	TdT-mediated dUTP Nick-End Labeling
BUN	Blood Urine Nitrogen
AST	Aspartate aminotransferase
ALT	Alanine aminotransferase
CaP	Calcium Phosphate

## TABLE OF CONTENTS

LIST OF FIGURES .....	<b>XV</b>
LIST OF TABLES.....	<b>XVIII</b>
1.0 RNA DRUG DELIVERY APPROACHES .....	<b>1</b>
1.1 INTRODUCTION .....	1
1.2 RNA MOLECULES WITH POTENTIAL FOR CANCER TREATMENT ...	1
1.3 CHEMICAL MODIFICATION STRATEGIES .....	2
1.3.1 Sugar modification.....	3
1.3.2 Nucleobase modification .....	4
1.3.3 Terminal modification .....	4
1.4 CHALLENGE IN RNA DELIVERY .....	5
1.4.1 Chemical stability and structure modification .....	5
1.4.2 Extracellular delivery stage.....	7
1.4.3 Target-cell specificity and uptake via targeting ligands .....	8
1.4.4 Endosomal release .....	8
1.5 POTENTIAL ADVERSE EFFECTS OF RNA THERAPY .....	10
1.5.1 Induction of immune responses .....	10
1.5.2 Off-target effect .....	11
1.5.3 Saturation of endogenous silencing pathway.....	11
1.6 RNA DELIVERY .....	12
1.6.1 Physical method.....	12
1.6.1.1 Hydrodynamic injection .....	12
1.6.1.2 Electroporation .....	14

1.6.1.3	Particle bombardment .....	15
1.6.2	Chemical vectors for RNA delivery .....	15
1.6.2.1	Cationic lipids/liposomes and cationic lipid nanoparticles (lipoplex).....	15
1.6.2.2	Ionizable lipids.....	17
1.6.2.3	Lipid-like delivery molecules (lipidoids) .....	18
1.6.2.4	Cationic polymers (polyplexes).....	19
1.6.2.5	Core/membrane lipid-based nanoparticles (lipopolyplex).....	24
1.6.2.6	Aptamer-siRNA chimeras .....	29
1.7	TARGETING LIGANDS .....	30
1.7.1	Aptamers .....	30
1.7.2	Cell penetrating peptides.....	31
1.7.3	Antibodies .....	31
1.7.4	Peptides and Proteins .....	32
1.7.5	Small molecular weight ligands.....	33
1.8	THERAPEUTIC APPLICATION FOR TREATMENT OF CANCER .....	34
1.8.1	siRNA therapeutic mechanisms.....	34
1.8.2	Examples in cancer treatment by RNA delivery technology.....	34
1.9	CONCLUSION.....	37
2.0	<i>IN VIVO</i> GENE DELIVERY BY NON-VIRAL VECTORS: OVERCOMING HURDLES? .....	38
2.1	INTRODUCTION .....	38
2.2	CHALLENGES OF GENE DELIVERY .....	40



2.2.1	Off-target effect .....	40
2.2.2	Immune stimulation .....	40
2.2.3	Delivery.....	41
2.2.4	Serum inactivation and enzyme degradation .....	41
2.2.5	RES recognition .....	42
2.2.6	The EPR effect.....	43
2.2.7	Entrance into cells: The PEG dilemma .....	44
2.2.8	Endosome escape .....	45
2.2.9	Nuclear entry.....	47
2.3	NON-VIRAL VECTOR DESIGN FOR <i>IN VIVO</i> GENE DELIVERY .....	49
2.3.1	Lipoplex/Polyplex.....	49
2.3.2	Lipopolyplex .....	51
2.3.3	Aptamer-siRNA chimeras.....	54
2.4	LOCAL GENE DELIVERY .....	56
2.4.1	Bubble liposomes by ultrasound exposure .....	56
2.4.2	Heat and irradiation.....	56
2.4.3	Magnetofection .....	57
2.5	CONCLUSION AND PERSPECTIVE.....	57
3.0	SYSTEMIC DELIVERY OF GEMCITABINE TRIPHOSPHATE VIA LCP NANOPARTICLES FOR NSCLC AND PANCREATIC CANCER .....	59
3.1	INTRODUCTION .....	60
3.2	MATERIALS AND METHODS .....	63

3.2.1	Materials .....	63
3.2.2	Cell culture.....	63
3.2.3	Experimental animals.....	64
3.2.4	Preparation of GTP-loaded LCPs .....	64
3.2.5	Characterization of GTP-loaded LCPs .....	65
3.2.6	<i>In vitro</i> cellular uptake .....	65
3.2.7	<i>In vitro</i> cytotoxicity assay .....	66
3.2.8	Cell cycle analysis.....	67
3.2.9	Caspase activation.....	67
3.2.10	Western blot analysis .....	68
3.2.11	Immunostaining .....	69
3.2.12	Pharmacokinetic profile of GTP-loaded LCPs .....	70
3.2.13	Tumor growth inhibition and toxicity study .....	71
3.2.14	Statistical analysis.....	72
3.3	RESULTS .....	72
3.3.1	Characterization of GTP-loaded LCPs .....	72
3.3.2	<i>In vitro</i> specific tumor cell targeting.....	74
3.3.3	GTP-loaded LCPs reduced the cell viability .....	76
3.3.4	GTP-loaded LCPs arrested the cell cycle in the S phase .....	78
3.3.5	GTP-loaded LCPs induced caspase activation <i>in vitro</i> and <i>in vivo</i> .....	78
3.3.6	GTP-loaded LCPs triggered PARP cleavage and inhibited cell cycle progression <i>in vivo</i> .....	81
3.3.7	GTP-loaded LCPs triggered tumor cell apoptosis and	

	inhibited tumor cell proliferation <i>in vivo</i> .....	82
3.3.8	GTP-loaded LCPs prolonged blood circulation time <i>in vivo</i> .....	86
3.3.9	Tumor growth inhibition study .....	87
3.4	DISCUSSION .....	90
3.5	CONCLUSION .....	93
4.0	CO-DELIVERY OF VEGF SIRNA AND GEMCITABINE MONOPHOSPHATE IN A SINGLE NANOPARTICLE FORMULATION FOR EFFECTIVE TREATMENT OF NSCLC .....	94
4.1	INTRODUCTION .....	95
4.2	MATERIALS AND METHODS .....	97
4.2.1	Materials .....	97
4.2.2	Cell culture .....	98
4.2.3	Experimental animals .....	98
4.2.4	Preparation of VEGF-LCP-AA, GMP-LCP-AA and (GMP+VEGF)-LCP-AA .....	98
4.2.5	Characterization of VEGF-LCP-AA, GMP-LCP-AA and (GMP+VEGF)-LCP-AA .....	100
4.2.6	Western blot analysis .....	100
4.2.7	Caspase activation .....	101
4.2.8	TUNEL assay .....	101
4.2.9	Immunohistochemistry .....	102
4.2.10	Tumor growth inhibition .....	102
4.2.11	<i>In vivo</i> toxicity .....	103

4.2.12	Statistical analysis.....	103
4.3	RESULTS .....	104
4.3.1	Characterization of drug-loaded LCPs.....	104
4.3.2	Drug-loaded LCPs induced VEGF down-regulation and apoptosis <i>in vivo</i> .....	105
4.3.3	Drug-loaded LCPs triggered caspase activation and tumor cell apoptosis <i>in vivo</i> .....	108
4.3.4	Drug-loaded LCPs inhibited the formation of tumor vasculature .....	110
4.3.5	Drug-loaded LCPs triggered tumor cell apoptosis and inhibited tumor cell proliferation <i>in vivo</i> .....	113
4.3.6	Drug-loaded LCPs inhibited mitotic figures in tumors.....	114
4.3.7	Tumor growth inhibition.....	118
4.3.8	(GMP+VEGF)-LCP-AA reduced the <i>in vivo</i> toxicity .....	120
4.4	DISCUSSION.....	122
5.0	CO-DELIVERY OF C-MYC SIRNA AND GEMCITABINE MONOPHOSPHATE VIA LCP NANOPARTICLES TO NSCLC SUBCUTANEOUS AND ORTHOTOPIC MOUSE MODELS. ....	126
5.1	INTRODUCTION .....	127
5.2	MATERIALS AND METHODS .....	128
5.2.1	Materials .....	128
5.2.2	Cell culture.....	129
5.2.3	Experimental animals.....	129
5.2.4	Preparation of cMyc-LCP-AA, GMP-LCP-AA and	

	(GMP+cMyc)-LCP-AA .....	130
5.2.5	Characterization of cMyc-LCP-AA, GMP-LCP-AA and (GMP+cMyc)-LCP-AA .....	132
5.2.6	Western blot analysis .....	132
5.2.7	Caspase activation.....	133
5.2.8	TUNEL assay.....	133
5.2.9	Immunohistochemistry .....	134
5.2.10	Tumor growth inhibition.....	134
5.2.11	<i>In vivo</i> toxicity .....	135
5.2.12	Statistical analysis.....	135
5.3	RESULTS .....	135
5.3.1	Characterization of drug-loaded LCPs.....	135
5.3.2	Drug-loaded LCPs induced VEGF down-regulation and apoptosis <i>in vivo</i> . .....	136
5.3.3	Drug-loaded LCPs triggered caspase activation and tumor cell apoptosis <i>in vivo</i> .. .....	137
5.3.4	Drug-loaded LCPs inhibited tumor cell proliferation <i>in vivo</i> .....	140
5.3.5	Tumor growth inhibition.....	142
5.3.6	<i>In vivo</i> toxicity .....	144
5.4	DISCUSSION.....	144
6.0	SUMMARY .....	149
6.1	SUMMARY OF RESEARCH RESULTS .....	149
6.2	FUTURE DIRECTIONS.....	152

<b>APPENDIX.....</b>	<b>153</b>
<b>BIBLIOGRAPHY.....</b>	<b>155</b>

## LIST OF FIGURES

Figure 1.1 The mechanism of RNAi .....	2
Figure 1.2 Challenges of <i>in vivo</i> siRNA delivery .....	10
Figure 1.3 Schematic formation of lipoplex .....	16
Figure 1.4 Schematic formation of polyplexes .....	20
Figure 1.5 Schematic structure of polyconjugates.....	24
Figure 1.6 Structure and preparation scheme of LPD nanoparticles. ....	25
Figure 1.7 The schematic structure of MEND nanoparticle. ....	26
Figure 1.8 A schematic diagram illustrating the strategy of releasing gene cargo in MEND nanoparticles by PPD modification. ....	27
Figure 1.9 A diagram illustrating the limited release of siRNA from LPD condensed core.....	28
Figure 1.10 The formation process and entrapped siRNA release mechanism of LCP nanoparticles .....	29
Figure 1.11 Schematic structure of aptamer-siRNA chimeras .....	30
Figure 2.1 Representative scheme of <i>in vivo</i> gene delivery barriers. . ....	49
Figure 2.2 The structure and preparation scheme of LPD (LPD-II)/LPH nanoparticles.....	52
Figure 3.1 <i>In vivo</i> delivery hurdles of Gemcitabine. ....	61
Figure 3.2 Physiochemical characterization of GTP-loaded LCPs... ..	73
Figure 3.3 The cellular uptake of GTP-LCP-PEG and GTP-LCP-PEG-AA at 37°C for 1 h on H460 cells. ... ..	75
Figure 3.4 <i>In vitro</i> cell viability and cell cycle arrest of GTP-loaded LCPs. ....	77
Figure 3.5 Caspase activation and western blot analysis after different treatments.. ..	80

Figure 3.6 GTP-loaded LCPs triggered tumor cell apoptosis and inhibited tumor cell proliferation effectively <i>in vivo</i> in H460 and BxPC-3 xenografts.....	84
Figure 3.7 AA-targeted and GTP-loaded LCPs triggered tumor cell apoptosis and inhibited tumor cell proliferation effectively <i>in vivo</i> in NSCLC A549 tumor and a panel of pancreatic tumor xenografts.....	85
Figure 3.8 Percentage of the GTP injected dose (%ID) in blood after intravenous bolus administration of GTP-loaded LCPs and free GTP in H460 tumor-bearing mice .....	87
Figure 3.9 GTP-loaded LCPs inhibited the tumor growth on H460 (A) and BxPC-3 (B) xenografts. The relative body weight changes of H460 (C) and BxPC-3 (D) xenografts were calculated.....	89
Figure 4.1 Schematic illustration of the <i>in vivo</i> co-delivery mechanism.....	97
Figure 4.2 Schematic illustration of the preparation procedure of GMP- and/or VEGF siRNA- loaded LCP formulations. ....	104
Figure 4.3 TEM pictures of drug-loaded LCPs. . ....	105
Figure 4.4 Western blot analysis and VEGF mRNA level after systemic treatments.. ....	107
Figure 4.5 The caspase activation and induction of apoptosis after the systemic administration of different LCPs in H460 exnografts.....	110
Figure 4.6 CD31 immunohistochemistry staining of H460 xenograft tumors after (A) short term treatment and (B) long term treatment of different LCP formulations...112	
Figure 4.7 Immunostaining and mitotic figures after long term treatments.. ....	118
Figure 4.8 Tumor growth inhibition of different LCPs after systemic treatments. ....	120
Figure 4.9 Histopathology of different organs evaluated by H&E stain. ....	122



Figure 5.1 Graphical illustration of the establishment of NSCLC (A549)	
orthotopic model. ....	130
Figure 5.2 TEM pictures of (GMP+cMyc)-LCPs. ....	136
Figure 5.3 Western blot analysis for VEGF and cleaved PARP expressions	
<i>in vivo</i> after systemic treatment of different LCP formulations	
on H460 subcutaneous xenograft model. ....	137
Figure 5.4 The caspase activation and induction of apoptosis	
after the systemic administration of different LCPs in A549	
lung orthotopic xenografts . ....	139
Figure 5.5 Tumor cell proliferation after the systemic administration of	
different LCPs in A549 lung orthotopic xenografts.. ....	141
Figure 5.6 Tumor growth inhibition after systemic treatment of different LCPs.....	143

## LIST OF TABLES

Table 1.1 Some structures of siRNA modifications .....	6
Table 1.2 RNA interference (RNAi) drugs in clinical trials .....	36
Table 3.1 Particle size and zeta potential of LCPs.....	72
Table 3.2 IC <sub>50</sub> values in each treatment group in MTT assay on H460 and BxPC-3 cells. ....	78
Table 3.3 The key pharmacokinetic parameters of GTP-loaded LCPs and free GTP in H460 xenograft model.....	87
Table 3.4 Serum levels of BUN, creatinine, AST, ALT after 3 daily IV injections .....	90
Table 4.1 Serum levels of BUN, creatinine, AST, ALT after 3 daily IV injections in H460 xenograft model.. .....	121
Table 5.1 Serum levels of BUN, creatinine, AST, ALT after long term treatment. ....	144

## **1.0 RNA DRUG DELIVERY APPROACHES**

### **1.1 INTRODUCTION**

siRNA has a high potential in therapeutic applications. siRNAs are noncoding for proteins and they induce a sequence specific mRNA degradation. Since they do not interact with DNA transcription, there is a reduced concern about possible adverse gene alteration<sup>1</sup>. siRNA can be utilized as a therapeutic drug for gene silencing for a wide range of target proteins to potentially treat various diseases<sup>2</sup>. The drug siRNA molecule can target any mRNA of interest, regardless of their cellular location of the translated proteins. Furthermore, siRNA is very potent, as only a few siRNA molecules per cell are enough to produce effective gene silencing<sup>3,4</sup>.

### **1.2 RNA MOLECULES WITH POTENTIAL FOR CANCER TREATMENT**

RNA interference (RNAi) is a process that a specific messenger RNA (mRNA) is targeted for degradation to inhibit the synthesis of the encoded protein. Two types of small RNA molecules – microRNA (miRNA) and small interfering RNA (siRNA) – are central to the RNAi function. It is known that both miRNA and siRNA participate in carcinogenesis, either inhibiting suppressor genes, or stimulating oncogenes.

The initiation step of RNAi pathway is that the double strand (ds) RNAs are processed into 21-23 nucleotide small interfering RNAs (siRNA) by an RNase III-like enzyme called Dicer. Then, the siRNA assemble into endoribonuclease-containing complexes known as RNA-induced silencing complexes (RISCs). RISC uses the siRNA

as a template for recognizing complementary mRNA. The proteins in RISC unwind siRNA, keep the antisense strand and degrade the sense strand. The antisense strand in the RISC recruits the corresponding mRNA in a sequence-specific manner, at which time a protein component of RISC called Slicer cuts the mRNA in the middle of the binding region. The cut mRNA is recognized by the cell as being abnormal and is subsequently destroyed, resulting in gene silencing (**Fig. 1.1**). As RNAi relies on the sequence-specific interaction between siRNA and mRNA, siRNA can be tailored to silence almost any gene. Besides naturally generated siRNA from a long dsRNA, siRNAs that have been chemically synthesized or created by in vitro transcription systems can also induce gene silencing. Moreover, the multiple administration of synthetic siRNAs achieved long-term silencing effect of the target gene without disrupting the endogenous miRNA pathways<sup>5</sup>.

In the case of miRNA, a miRNA-induced silencing complex (miRISC) associates with the mature miRNA, and the complex binds to the 3' untranslated region of mRNA and blocks translation. Many miRNAs form imperfectly complementary stem-loop structures on the target sense strand of mRNA, as opposed to siRNA, which require near-perfect match.

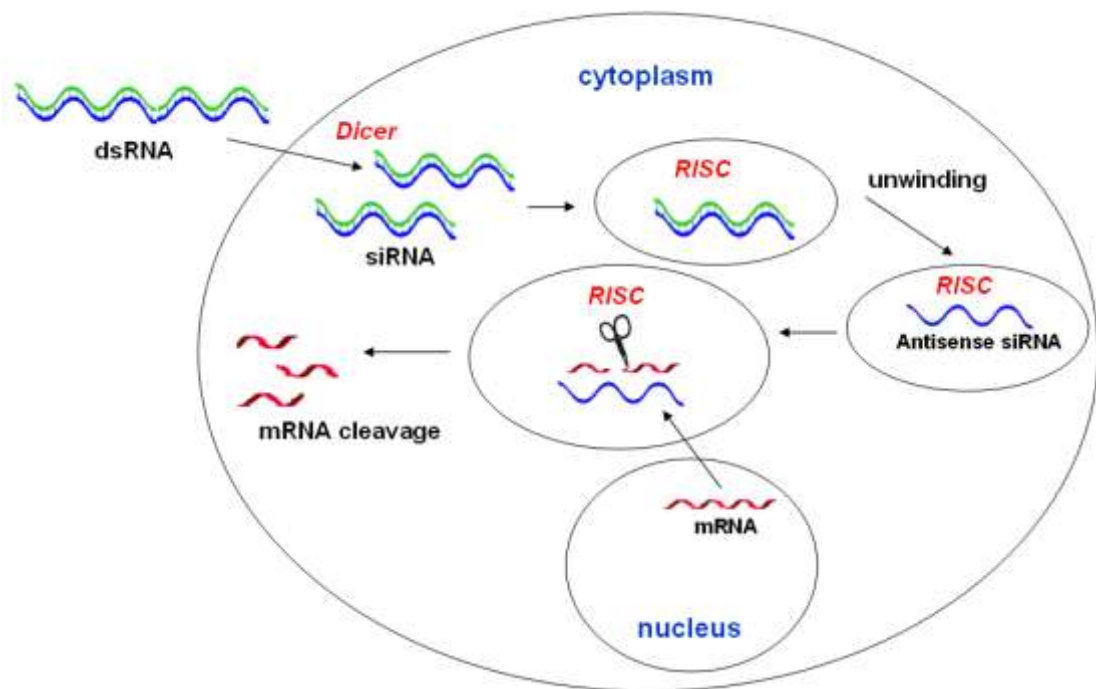


**Figure 1.1 The mechanism of RNAi** (Adapted from Hannon GJ, Nature 418, 244-251, 2002)

### 1.3 CHEMICAL MODIFICATION STRATEGIES

Although a double-stranded RNA is more stable than a single stranded RNA, unprotected siRNA can be quickly degraded in and outside the cells. In order to improve the stability of siRNA for prolonged circulation, chemical modification of siRNA has been attempted without compromising its potency. Various positions within the siRNA duplex have been chemically modified in a wide variety of ways to confer nuclease resistance.

As increasing requirements for effective RNAi, chemical modifications can also be used to optimize potency as well, via features such as target-binding affinity by modulating hybridization on-rate and off-rate, conformational preorganization (A-form helical structure) and duplex flexibility. Part of the increase in potency may be due to the increased nuclease stability of the chemically modified siRNA.

Chemical modifications can also be used to reduce the immunostimulatory properties of siRNAs<sup>6</sup>, which is considered a potentially dangerous off-target effect.

### **1.3.1 Sugar modification**

The most widely used siRNA modifications are on the sugar moiety. Early studies showed that A-form duplex structure is important, the 2'-OH is not required for active siRNA<sup>7</sup>. So the 2' position has been extensively modified. For example, 2'-O-methylation of RNA increases binding affinity and nuclease stability. Bulky 2'-substituents are not well-tolerated in the siRNA duplex. The 2'-OH groups of siRNA in both strands can be converted at random into 2,4-dinitrophenyl ethers (2'-O-DNP), which shows improved binding affinity, nuclease resistance and potency. Fluorine substituent at the 2'-position can be functional and active throughout the sense and antisense strands. The 2'-F-RNA-modified siRNA duplex can increase serum stability and the duplex binding affinity. Capodici et al<sup>8</sup> incorporated fluorinated CTP and UTP modifications into siRNA, and these fluorine-derivatized siRNAs yielded equivalent activity to unmodified siRNA. The modification could protect the siRNA from RNase A and could be delivered without the transfection reagent in the presence of serum. A fully modified siRNA composed of 2'-O-Me and 2'-F-RNA modified nucleotides showed 500 times more potency than the unmodified RNA<sup>9</sup>, and significantly reduced immunostimulatory activity<sup>10</sup>.

Locked Nucleic Acid (LNA) is an RNA mimic in which the ribose sugar moiety is locked by an oxymethylene bridge connecting 2'-C and 4'-C. LNA modification possesses high binding affinity and excellent specificity toward complementary DNA or RNA oligonucleotides. In addition, LNA modified oligonucleotides improve the resistance to

enzymatic degradation and show high stability in biological system<sup>11, 12</sup>. Introduction of LNA nucleotides in siRNA, namely, LNA-modified siRNA or siLNA, could substantially increase the thermal stability of the modified RNA duplex without compromising the efficacy of RNAi<sup>13</sup>, and reduce the off-target gene regulation comparing to the corresponding unmodified siRNA<sup>14</sup>.

### **1.3.2 Nucleobase modification**

Some modified bases can be used to stabilize A-U base pairs, although the activity of the modified RNA may be somewhat reduced. Examples are 5-Br-Ura and 5-I-Ura instead of uracil, diaminopurine instead of adenine. 2-thiouracil, 4-thiouracil, dihydrouracil and some uracil analogs are also used, which could increase binding affinity, potency and specificity if placed appropriately within the duplex. For example, 2-thiouracil base at the 3'-end of the antisense strand and a dihydrouracil base at the 3'-end of the sense strand make the modified siRNA duplex more active<sup>15</sup>.

### **1.3.3 Terminal modification**

The terminal end of each strand can be modified by 5'-end chemical phosphorylation. Antisense strand phosphorylation helps to ensure high potency, especially when the strand is modified. Furthermore, various groups can be conjugated to the ends of a siRNA duplex, especially the terminal end of the sense strand. Fluorescent dyes or biotin are conjugated to the RNA terminal ends to allow biochemical studies. Cell penetrating peptides (CPPs) are short peptides that facilitate cellular uptake of various cargos. Conjugation of cell penetrating peptides (CPPs) via disulfide bond and lipophilic groups such as steroids and lipids may help with siRNA delivery through improving its stability, facilitating penetration and cellular uptake. Abes et al<sup>16</sup> and Moulton et al<sup>17</sup> conjugated

arginine-rich CPPs and penetratin to oligonucleotides for efficient delivery of nucleic acid cargos. Generally, the 5'-end of the antisense strand is most sensitive to modifications<sup>18</sup>. Attaching a group to an antisense 5'-phosphate does not necessarily eliminate RNAi activity<sup>19</sup>.

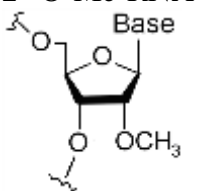
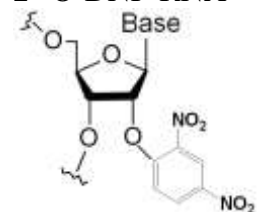
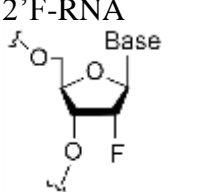
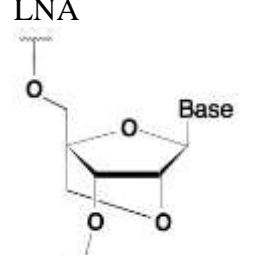
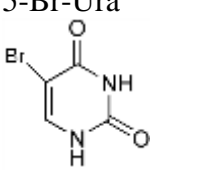
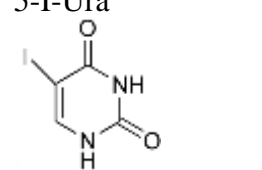
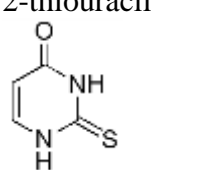
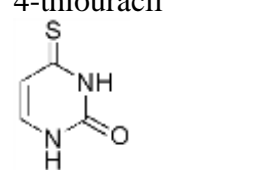
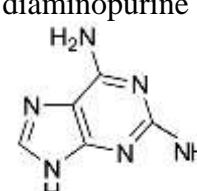
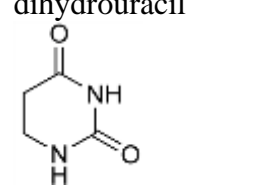
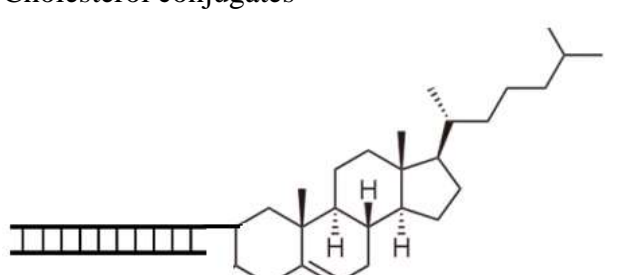

## **1.4 CHALLENGE IN RNA DELIVERY**

### **1.4.1 Chemical stability and structure modification**

Naked siRNAs are highly susceptible to nuclease degradation especially *in vivo*. In order to allow siRNA to survive long enough to maintain an acceptable level in tissues, its degradation must be minimized or at least significantly delayed. Chemical modifications of siRNA have been extensively used to achieve enhanced resistance to nuclease-induced degradation<sup>20</sup>. Chemical modifications can be induced to the 5'- or 3'- terminus, backbone, sugar and nucleobase of siRNA, which could increase the stability of siRNA duplex and retain or enhance their gene-silencing activity, and in some cases, significantly reduce the immunogenicity as well. Effective design and modification of siRNA can also allow minimization of the potential sequence-dependent off-target effects. For example, 2'-O-methyl ribosyl group substitution at position 2 in the sense strand could reduce silencing of most off-target transcripts<sup>21</sup>.



**Table 1.1 Some structures of siRNA modifications**

Sugar modification	2'-O-Me-RNA 	2'-O-DNP-RNA 
	2'-F-RNA 	LNA 
	5-Br-Ura 	5-I-Ura 
	2-thiouracil 	4-thiouracil 
Nucleobase modification	diaminopurine 	dihydrouracil 
	Cholesterol conjugates 	
	CPP conjugates 	

### 1.4.2 Extracellular delivery stage

The most important challenge in siRNA therapy is the issue of delivery. siRNA is negatively charged hydrophilic molecules so that it has difficulty in passing through negatively charged hydrophobic cellular membranes by passive diffusion. *In vivo* delivery of naked siRNA to appropriate disease sites remains a considerable obstacle because of rapid enzymatic digestion in the plasma and renal elimination. Limited penetration across the tumor capillary endothelium and inefficient cellular uptake by cancer cells further limit the use naked siRNA as a drug formulation<sup>3</sup>. Thus, developing effective *in vivo* delivery systems is critical to overcome these difficulties. The delivery vectors should be biocompatible, biodegradable, nonimmunogenic, and can provide target tissue-specific distribution after systematic administration, avoiding rapid hepatic or renal clearance. Generally, nanoparticles with a mean size around 100-200 nm are ideal for tumor targeting, because they can accumulate in the tumor leaky vasculature via the enhanced permeability and retention (EPR) effect after i.v. administration. However, the circulating nanoparticles are prone to the capture by the reticuloendothelial system (RES), such as the liver Kupffer cells and the splenic macrophages, causing a major loss of the injected dose (>50%) within a few hours after i.v. injection. So the nanoparticles need to have a prolonged circulation half-life and the ability to escape the surveillance of RES, in order to encounter the leaky tumor vasculature before they are cleared from the *in vivo* circulation<sup>22</sup>. For the sake of improve the pharmacokinetic properties of delivery vectors after intravenous administration mentioned above, poly(ethylene glycol) (PEG) was introduced to modify the surface of nanoparticles. This hydrophilic polymer imparts a steric barrier on the surface of nanoparticles and minimizes the opsonization effect.

PEGylation on the surface of the nanoparticles exhibit stealth properties, shielding the nanoparticles and help them escape the surveillance of RES.

#### **1.4.3 Target-cell specificity and uptake via targeting ligands**

The delivery vectors need to interact with cell membrane, internalize and localize in the intracellular compartment before releasing the nucleic acid cargo. Though PEGylation mentioned above can largely facilitate the accumulation of nanoparticles in the tumor leaky vasculature and confer stability in the systemic circulation, it hinders the uptake of the nanoparticles by the tumor cells once they extravasate<sup>22</sup> because of its steric configuration coating on the outer surface of the nanoparticles. In order to solve the PEG dilemma, promote the interaction with target cells and prevent side effects by avoiding non-specific binding to non-diseased cells, many cell specific targeting ligands (e.g. small molecules, antibodies, aptamers, peptides) that can recognize unique biomarkers (e.g. antigens, receptors) on the diseased cell surface, are modified on the surface of the vectors to construct functional nanoparticles.

#### **1.4.4 Endosomal release**

In intracellular condition, inefficient release of the nucleic acid cargo complexes from endocytic vesicles into the cytoplasm is one of the primary causes of poor gene delivery. After delivery into target cells via endocytosis, the delivery systems should promote the endosomal release of siRNA from nanoparticles into the cytoplasm, followed by the interaction of siRNA with endogenous RISC in order to be bioactive. In detail, once the delivery vectors have been internalized into cells and arrive in an endosomal compartment, two essential processes have to occur in order to achieve higher gene transfection: one is dissociation of the nucleic acid from the delivery vector; the other is

the destabilization of the endosomal membrane to allow the release of the nucleic acid into the cytosol where is the site of action for siRNAs, and the release process is also critical to make the other nucleic acid cargo (e.g. plasmid DNA) accessible for transport to the nucleus for transcription.

To overcome this obstacle, exogenous agents such as chloroquine<sup>23</sup> or activated adenovirus<sup>24</sup> were added to affect escape from the endosome and lysosomes, but they have cellular toxicity, immunogenicity and other side effects which make them impractical for in vivo gene therapy.

Thus, a variety of stimulus responsive nanoparticle formulations for enhancing drug endosomal release and subsequently therapeutic effect, have been designed. Generally, several models have been proposed to interpret the possible mechanism of lipid/polymer based nanoparticles disrupting the endosome membrane and fleeing from the endosome/lysosome. These accepted models include the ion-pairing model ( $H_{II}$  phase formation), the proton sponge model and the charge-charge destabilization model<sup>22</sup>, which will be explained in the following paragraphs in detail.

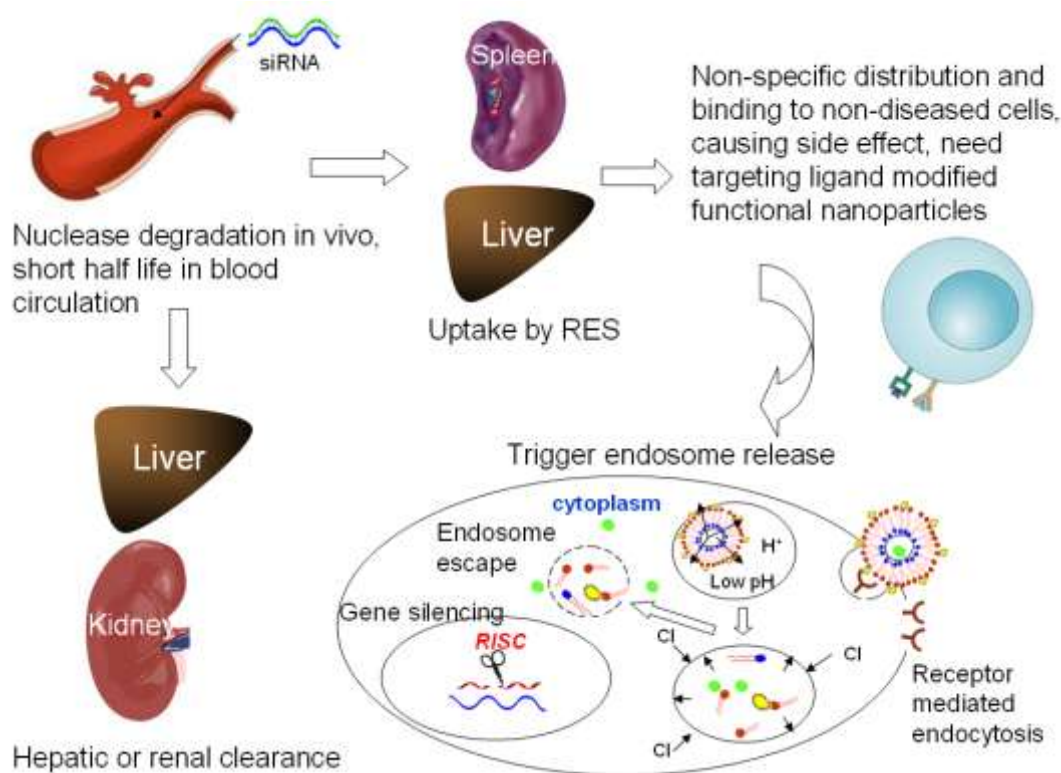


**Figure 1.2 Challenges of *in vivo* siRNA delivery**

## **1.5 POTENTIAL ADVERSE EFFECTS OF RNA THERAPY**

### **1.5.1 Induction of immune responses**

siRNA therapy could induce 'immune stimulation'; this is the recognition of a RNA duplex by the innate immune system. GU-rich regions in a particular sequence motif can lead to secretion of inflammatory cytokines in a cell-type and sequence-specific manner<sup>25</sup>. siRNA-mediated immune induction seems to rely on the TLR receptors located in the endosome<sup>26</sup>, such that the mode of delivery and hence compartmentalization of the siRNA greatly influences the cellular response. Not all siRNAs could induce immune stimulation. The stimulation of innate immune responses by siRNA may be related to a specific nucleotide sequence, or motif. The TLR7-mediated interferon-alpha induction by siRNA was shown to be sequence specific<sup>27, 28</sup>.

### **1.5.2 Off-target effect**

The ‘off-target’ effect is the inhibition of a gene not intended for silencing. It may occur because the gene shares a partial homology with the siRNA. For example, one class of siRNA off-target effects involves partial hybridization with the wrong mRNA, or the sense strand can cause off-target effects if it hybridizes to an irrelevant mRNA<sup>29</sup>. Silencing of an off-target is clearly unwanted as the cellular consequence of altered gene activity is unknown and unpredictable<sup>25</sup>. So one of the solutions is to increase the selective uptake of the antisense strand and decrease incorporation of the sense strand via appropriate siRNA duplex modifications. The undesired silencing of nontarget genes may lead to data misinterpretation and toxicity. Thus, the design and selection of a specific siRNA may involve consideration of internal repeated sequence, GC content, appropriate siRNA length, specific base preference in the sense strand, secondary structure. Some studies suggest that some of the off-target gene changes may be due to the delivery system itself, e.g. cationic lipids<sup>30, 31</sup>. Above all, off targeting remains a critical issue for therapeutic applications of RNAi and tolerable levels of off targeting effect are required for siRNA gene therapy.

### **1.5.3 Saturation of endogenous silencing pathway**

siRNA relies on the endogenous miRNA machinery in order to achieve potent target silencing. The risk of saturating such pathways and hence perturb the natural system has been reported<sup>25</sup>. siRNA resembles miRNA precursors before and after Dicer processing, so all component of the miRNA pathway might be blocked by high doses of the ectopic RNA.

## **1.6 RNA DELIVERY**

Getting siRNA into cells is one of the biggest challenges of any application of RNAi. Naked siRNAs appear to be poorly transported into cells, and even there is a little free siRNAs that can eventually enter the cells, most of them would remain sequestered within endosomal/lysosomal vesicles where it may likely undergo degradation by nucleases. Therefore, in order to achieve siRNA-mediated gene silencing in cells, a feasible delivery system is required to improve cellular uptake and intracellular trafficking of the encapsulated siRNAs, facilitating their binding with the complementary mRNA in RISC in cytosolic compartment before gene silencing.

### **1.6.1 Physical method**

Multiple physical and mechanical approaches have been used for *in vivo* gene delivery, which are considered the simplest way to deliver gene *in vivo* for transfection, such as hydrodynamic i.v. injection, intraportal injection, electroporation, mechanical liver massage, particle bombardment etc.

#### **1.6.1.1 Hydrodynamic injection**

An efficient gene transfer and expression can be achieved by a rapid injection of a large volume of naked DNA solution into animals via the tail vein. This hydrodynamic based gene delivery is a simple and highly efficient procedure in gene expression to deliver and express exogenous genes to almost all major organs, especially the liver in small animals, such as mice and rat. There are two basic requirements for the hydrodynamic injection in order to achieve an appropriate hydrodynamic pressure in targeted tissues: one is to inject rapidly in 5-7 seconds; the other is to inject a huge volume at one time. This hydrodynamic pressure can facilitate DNA solution to transiently permeabilize the

endothelium and plasma membrane of parenchyma cells and allow efficient intracellular gene transfer. For example, naked DNA in 2 ml volume of saline solution could be injected into mice weighing 20 g in just 5-7 seconds. Liu et al<sup>32</sup> used this hydrodynamic procedure to transfect up to 40% of liver cells after a single injection of naked plasmid DNA, showing that the level of gene expression in different organs increased with the increasing volume of the injected DNA solution, and the optimal transgene expression requires an injection volume of approximately 8-12% of the body weight.

Manual control of the injection speed and strength is hard to standardize, which makes the results insufficiently reliable when the experiment is operated by different individual. In order to minimize the problem, Suda<sup>33</sup> developed a computer-controlled injection device that uses real-time intravascular pressure as a regulator for the injection and can program the computer according to the need. This device can self-adjust the volume needed to develop the sufficiently elevated pressure that can thereby help to achieve a successful gene transfer. The self-adjustment of the device is base on the size and anatomical structure of the selected organ of interest. This device enabled safe and effective gene delivery to mouse liver, and kidney and muscle cells in rats with plasmids or adenoviral vectors as gene carriers. Gene transfer to the liver of pigs was also successful. The study also showed that larger animals tend to require higher pressure for successful gene transfer to a given organ, and the liver shows the highest gene delivery efficiency probably due to the high elasticity of the liver vasculature and parenchyma cells.

Though the tissue damage caused by the hydrodynamic pressure after injection can recover in rodents, rapid injection of large volume of plasmid DNA is invasive and can



not be applied to humans. High level of gene expression achieved by this simple method may be useful to analyze the function and molecular mechanism of different genes involved in many genetic and acquired diseases within the whole animal.

#### **1.6.1.2 Electroporation**

Electroporation is a simple and convenient way to deliver nucleic acids (e.g. DNA) into cells. Cells act as an electrical capacitor which is generally unable to pass current. Subjecting the cells to an electric field creates transient permeable structures or micropores on the cell membrane, which last long enough after electroporation to allow penetration of pharmaceuticals or nucleic acids into the cell. Over time, the micropores on the cell membrane close and cell becomes impermeable again. It can be applied, in principle, to any types of cells and tissues so long as the target is accessible. The advantages of electroporation include controllable tissue or cell damage, flexibility in the structure of DNA to be transfected, and the possibility of transfecting cells deep inside a specific tissue. The transfection efficiency by electroporation is many times greater than that of naked DNA and with reduced inter-individual variability<sup>34, 35</sup>.

Various devices have been designed for effective electroporation, including electro square-wave porator, caliper electrodes, syringe electrode, flow-through electroporation. The caliper electrodes consist of a caliper and a pair of adjustable end plates. The electrodes sandwich the target area and deliver electric pulses following the injection of the molecule of interest. Liu & Huang<sup>36</sup> invented a syringe electrode device for both DNA injection and electroporation. It applies a voltage to the syringe needle, and this allows the needle to be used not only for injection but also as an electrode. This is particularly advantageous as the electric field is applied to the same area as the injected

fluid. And the injected DNA can be confined to the high intensity region of the field, thus the required electric field strength can be reduced without compromising the transfection efficiency. Tissue damage could be minimized due to the low electric power used. Geng<sup>37</sup> introduced a novel flow-through electroporation method for gene delivery into cells at high flow rate based on disposable microfluidic chips and a direct current power supply that provide a constant voltage. With the optimal parameter design, approximately 75% of CHO cells were transfected by this method without apparent toxicity.

### **1.6.1.3 Particle bombardment**

Particle bombardment is a commonly used method for genetic transformation to a broad range of cell and tissue types. Colloid gold particles coated with DNA (microprojectiles) are shot directly into the target cells or tissues by a burst of helium gas using a biolistic device or gene gun. The particles or macromolecules can be delivered through membranes and extracellular matrices. They can penetrate 100  $\mu\text{m}$  into the skin by this method, and transfect some skin Langerhan cells for antigen presentation. Particle bombardment is the only reproducible means for delivering DNA to mitochondria<sup>38</sup>. Therefore, the method could have a significant impact on the gene expression within the cytoplasmic organelles<sup>39</sup>.

## **1.6.2 Chemical vectors for RNA delivery**

### **1.6.2.1 Cationic lipids/liposomes and cationic lipid nanoparticles (lipoplex)**

Various cationic lipids can form complex with negatively charged DNA or siRNA. The complex, called lipoplex, at suitable N/P ratios interact with cells in culture by non-specific charge interaction, followed by endocytosis. Lipofectamine is a commonly used cationic liposome reagent for nucleic acid transfection that provides high transfection

efficiency and high levels of transgene expression in a range of mammalian cell types *in vitro*. It can transfect siRNA or plasmid DNA into cells in culture by altering the cell plasma membrane and allowing nucleic acids to get access into the cytoplasm.

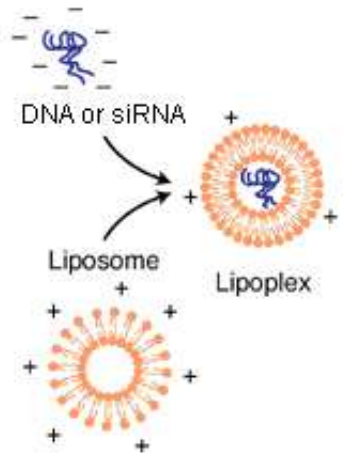


**Figure 1.3 Schematic formation of lipoplex** (adapted from [www.google.com/images](http://www.google.com/images))

Liposomes prepared from cationic amphiphiles interact with polyanionic DNA or RNA, spontaneously forming lipoplexes driven by electrostatic interaction forces. Lipoplexes are efficient nonviral vectors to introduce nucleic acids into the desired target cells. Cationic lipids mediated gene transfer has the advantages over viral gene transfer because it is less immunogenic, easier to produce and not oncogenic. Most studies have been performed on the synthesis and investigation of new cationic lipid for DNA or RNA complexing, used either alone or combined with particular helper lipid, such as cholesterol and dioleoylphosphatidyl-ethanolamine (DOPE) which are neutral lipids and can participate in bilayer formation when combined with a cationic lipid<sup>40</sup>. The presence of helper lipid affects the association of nucleic acids with lipoplexes<sup>41</sup> and can help to facilitate the release of the cargo from endosome and achieve higher transfection

efficiency by promoting the inverted hexagonal H<sub>II</sub> phase transition. The inverted hexagonal phase has a negative spontaneous curvature and the tendency of membranes to form inverted micellar structure, which allows to de-stabilize the endosomal membrane and de-assemble the lipoplex<sup>42</sup>, resulting in concomitant release of the nucleic acid cargo from endosome. For example, cationic lipid DOTAP prefer a bilayer organization, however, mixing with helper lipid like DOPE will affect the packing parameter and mediate fusion between the liposomes and the endosomal membrane after endocytosis, reverting to a H<sub>II</sub> phase, which results in the destabilization of the endosomal membrane and release of the nucleic acid cargo to the cytosol<sup>43-45</sup>. The nonbilayer H<sub>II</sub> phase structure is also formed due to the formation of ion pairs between cationic lipids and the anionic phospholipids in the endosome membrane<sup>46</sup>. Several studies have investigated the correlation between the structural properties of lipoplexes and their transfection efficiency, and revealed that lipoplexes that adopt the H<sub>II</sub> phase strongly facilitate intracellular release of nucleic acid cargo from the endosomal compartment<sup>42</sup> and display the highest transfection efficiency<sup>47</sup>. Cationic lipids with multiple cis double bond, small or less hydrophilic head group and unsaturated bulky acyl or alkyl chains favor H<sub>II</sub> phase formation and resulted in higher transfection efficiency<sup>40, 42</sup>. To avoid non-specific binding *in vivo* of the positively charged lipoplex, PEG derivatized lipids are often included to decrease the net positive charge<sup>48</sup>, providing stealth properties that stabilize the lipoplexes.

#### **1.6.2.2 Ionizable lipids**

Recently, Alnylam Pharmaceuticals designed some ionizable cationic lipids to formulate lipid nanoparticles (LNPs) to deliver siRNA *in vivo*, such as 1,2-dilinoleyloxy-3-

dimethylaminopropane (DLinDMA) and other DLinDMA-based lipids. The ionizable cationic lipids contain weak basic lipid headgroups, which affect the surface charge of the particles in a pH-dependent manner, rendering them positively charged at acidic pH but close to neutral charge at physiologic pH<sup>49</sup>. LNPs comprised of different lipid compositions and ratios as well as different sizes and structures using different methods, which are characterized by very high siRNA encapsulation efficiency, small uniformly sized particles as well as superior delivery capacity and therapeutic gene silencing effect. One of the newly invented ionizable LNPs termed stable nucleic acid lipid particles (SNALP) substantially improved in vivo endogenous gene silencing activity with siRNA doses as low as 0.01 mg/kg in rodents and 0.1 mg/kg in nonhuman primates<sup>50</sup>. The rational lipid design for SNALP-mediated delivery lies in the pKa of the ionizable cationic lipid and the abilities of these lipids to induce the nonbilayer hexagonal H<sub>II</sub> phase structure with anionic phospholipids of endosomal membrane when protonated in acidic pH environment in the endosome<sup>50</sup>. The efficient delivery mechanism of these ionizable LNPs (iLNPs) involves endogenous apolipoprotein E (apoE) by targeting to the low-density lipoprotein receptor (LDLR) in the hepatocytes<sup>49</sup>. Briefly, iLNPs behave as neutral liposomes in circulation to absorb apoE as an endogenous targeting ligand and deliver siRNA to hepatocytes in an endogenous targeting manner. The exogenous targeting approach via asialoglycoprotein receptor (ASGPR) expressed on hepatocytes is also highly effective<sup>49</sup>.

#### **1.6.2.3 Lipid-like delivery molecules (lipidoids)**

Akinc *et al*<sup>51</sup> developed chemical synthesis methods based on the conjugate addition of alkyl-acrylates or alkyl-acrylamides to primary or secondary amines, to rapidly generate

substantial and diverse collection of lipid-like molecules, termed lipidoids. They are structurally distinct from other classes of lipid delivery vectors since they contained multiple protonable amine groups connected to relatively short alkyl chains. Materials with good *in vitro* and *in vivo* efficacy could be identified within the large library, including a lead material 98N<sub>12</sub>-5 that was shown to be efficacious in primates. In addition, the *in vivo* delivery efficacy of the novel lipid-like material can be affected by many parameters, such as the formulation composition, nature of PEGylation on the particle, degree of drug loading, particle size, changes in PEG lipids anchor chain length and so on<sup>52</sup>, resulting in distinct gene silencing effects. The side chains of the molecule can be further altered to obtain different capacities for hydrogen bonding, hydrophobic interactions, and protonated states, enabling the exploration of functionalized lipidoids for efficient siRNA delivery<sup>53</sup>.

#### **1.6.2.4 Cationic polymers (polyplexes)**

Cationic polymers include natural DNA-binding proteins, such as histones, synthetic polypeptides, poly(ethylenimine) (PEI), cationic dendrimers, carbohydrate-based polymers such as chitosan<sup>40</sup>. The self assembly of cationic polymers with nucleic acids in solution forms a particulate complex and leads to a strong condensation and large size reduction of nucleic acid drug, which is favorable to improve *in vivo* transfection efficiency<sup>54</sup>.

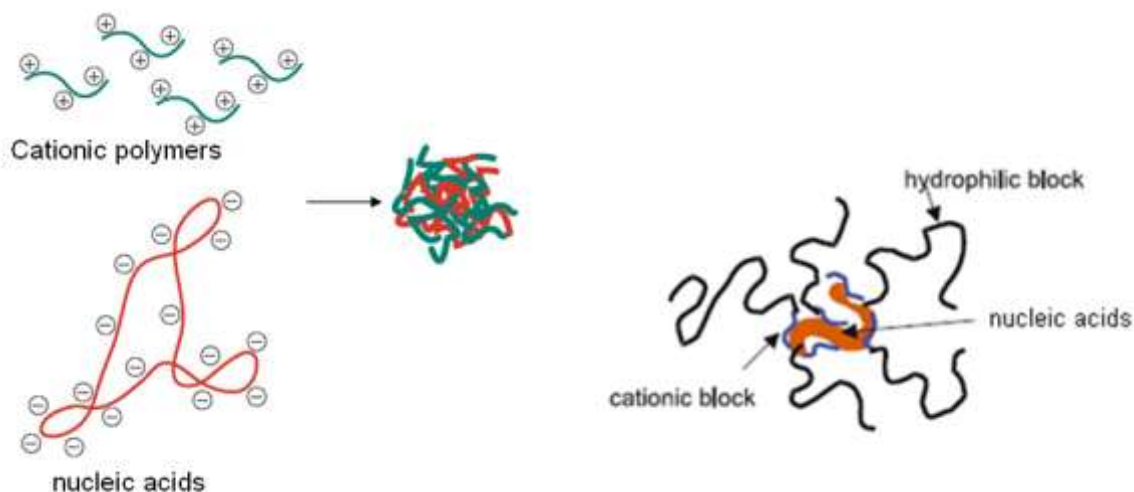


**Figure 1.4 Schematic formation of polyplexes** (Adapted from Nature Reviews Drug Discovery 4, 581-593, 2005; Adv Polym Sci 192, 1-8, 2006)

Polyethylenimine (PEI) has been widely used for non-viral transfection *in vitro* and *in vivo*. PEI exists as a branched polymer and in linear form as well. It is available in a broad range of molecular weights, from less than 1000 Da to 1600 kDa, and the PEIs with molecular weight between 5 and 25 kDa are most suitable for gene transfer<sup>55</sup>. Higher molecular weights lead to increased cytotoxicity, probably due to aggregation of huge clusters of the cationic polymer on the outer cell membrane, which may induce necrosis<sup>56</sup>.

Chitosan is a linear carbohydrate-based polymer comprising  $\beta(1,4)$ -linked D-glucosamine and N-acetyl-D-glucosamine. It is widely used in the field of non-viral gene delivery due to its good biocompatibility and high positive charge density<sup>57</sup>. The chitosan molecular weight, salt form, and the degree of deacetylation affect its gene delivery efficiency. The application of chitosan is also limited by its low water solubility, inefficient gene unpacking and relatively low gene transfection efficiency. Thus, various chitosan derivatives have been synthesized and the structures were further modified to alter its

hydrophilicity. Incorporation of negatively charged agents such as hyaluronic acid (HA) with chitosan has shown to increase the transfection efficiency significantly due to the low density of the HA chain which could improve the DNA release from the condensing compact nanoparticles<sup>58</sup>. Jiang<sup>59</sup> described the chitosan-polyethylenimine (PEI) hybrid systems, including chitosan/PEI blend and chitosan-graft-PEI, to enhance the transfection efficiency of the cells owing to a proton sponge effect (see below).

Dendrimers are three-dimensional polymers that can interact with various forms of nucleic acids, such as plasmid DNA, antisense oligonucleotides, and RNA, to form complexes that protect the nucleic acid from degradation. The cationic dendrimer condenses the anionic nucleic acids through electrostatic interaction. The positively charged dendrimer/nucleic acid complex can transfect cells by interact with the negatively charged cell membranes, though highly cationic systems are also cytotoxic. The properties of the dendrimer/nucleic acid complex depend on various factors, such as stoichiometry, concentration of dendrimer amines and nucleic acid phosphates, as well as solvent properties like pH, salt concentration, buffer strength, and dynamics of mixing. Dendrimer based transfection reagents could be used as routine tools for *in vitro* transfection, but *in vivo* delivery of therapeutic nucleic acids still remains a challenge.

Bartlett et al<sup>60</sup> have developed a synthetic delivery system based on a cyclodextrin-containing polycation (CDP) which can deliver various nucleic acid payloads including pDNA, siRNA and ribozyme. The nucleic acid and CDP complexes formed by adamantine (AD)-containing molecules and the  $\beta$ -cyclodextrin molecules could be attached to the poly (ethylene glycol) (AD-PEG) conjugates for steric stabilization and the targeting ligands (AD-PEG-transferrin) for cell-specific targeting. This CDP delivery



vehicle can encapsulate large amounts of payload molecules and shows superior physicochemical and biological characterizations.

Generally, the longer the polymer chain or the higher branched polymer leads to better condensation of nucleic acids. For example, low branched PEIs with low condensation capacity require higher N/P ratios to completely condense nucleic acid payloads compared to the highly branched counterparts<sup>56</sup>, most likely because of the lower content of primary amines in the low branched polymers. Highly branched PEIs form smaller polyplexes and usually achieve higher transfection efficiencies, but also show greater toxicity<sup>40</sup>. The complex condensation can confer protection against degradation in the extracellular environment and improve cell uptake by electrostatic interactions of the polycation with the negatively charged cell surface.

Unlike cationic lipids, cationic polymers are devoid of hydrophobic domain and hard to destabilize the endosome by direct interaction with the endosomal membrane. Instead, the cationic polymers, such as PEI, can mediate endosome disruption by the “proton sponge” effect to enhance the nucleic acid cargo release<sup>40</sup>. The proton sponge effect arises from a large number of weak conjugated bases as proton-buffering groups (e.g. amine groups in PEI) with high buffering capabilities at pH 5-6 in acidic organelles, leading to proton absorption (sponge) and simultaneously chloride ion accumulation in the endosome, which arouses the osmotic pressure buildup in the endosome. This osmotic pressure causes swelling and/or rupture of the endosomes and a release of the entrapped drug materials into the cytoplasm<sup>61</sup>.

In order to achieve higher transfection efficiency, rational design of the polymer structure and the systematic structure modification has been developed. The design of the proper polymers becomes a sophisticated task in terms of the different applications of polymers as gene carrier systems. The molecular weight, the degree of branching, surface charge and the composition of the complexes (e.g. the ratio of polymer to nucleic acid payload) have to be optimized in order to form stable complexes, and conduct desired *in vivo* release properties as well. Higher charge density and higher molecular weight of polymers are usually required to reach high condensation capability. For example, polyamidoamine dendrimers have a branched spherical shape and a high surface charge density. Their transfection ability depends on the size, shape and the number of primary amine groups on the polymer surface<sup>62, 63</sup>.

Rozema *et al*<sup>64</sup> invented a siRNA Dynamic PolyConjugate vehicle for the delivery of siRNA to hepatocytes both *in vitro* and *in vivo*. They use amphipathic poly(vinyl ether) termed PBAVE as a latent endosomolytic agent, whose amine groups are modified with a maleic anhydride to create acid-labile maleamate bonds. These bonds reversibly mask the activity of this polymer until it reaches the acidic environment of endosomes. These bonds can be cleaved in the endosome, exposing the agent's amines and activating its endosome release capacity. The siRNA cargo is attached to PBAVE through a disulfide linkage, and the shielding agent PEG and hepatocyte targeting ligand *N*-acetylgalactosamine (NAG) are attached to PBAVE by a bifunctional maleamate linkage to afford specific targeting to hepatocytes *in vivo* by i.v. injection. By this delivery technology, two endogenous genes apolipoprotein B (*apoB*) and peroxisome proliferator-

activated receptor alpha (*ppara*) in mouse liver were knocked down, consistent with the phenotypic changes of the gene functions.

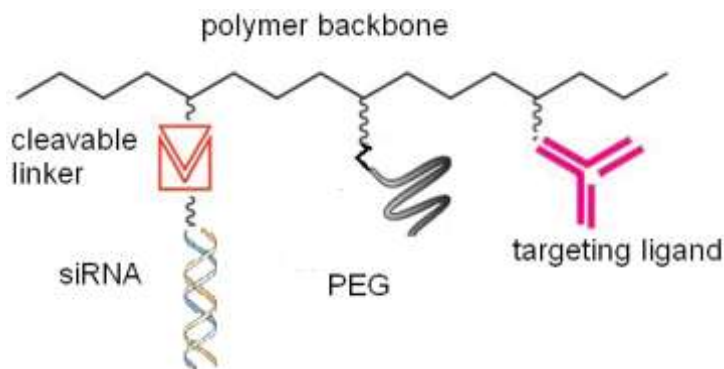


**Figure 1.5 Schematic structure of polyconjugates**

#### **1.6.2.5 Core/membrane lipid-based nanoparticles (lipopolyplex)**

The core/membrane nanoparticle Liposome-Polycation-DNA (LPD) was a DNA-protamine complex subsequently wrapped by cationic liposomes. It is further modified by post-insertion of PEG to impart a steric barrier for prolonged circulation time *in vivo*. Li et al.<sup>65</sup> developed the “LPDI” (Liposome-Polycation-DNA) formulation composed of protamine sulfate, DNA, and 1,2-dioleoyl-3-trimethylammonium-propane (DOTAP)/cholesterol liposome. The weakly immunogenic protamine sulfate condenses DNA or siRNA to form a relatively small and negatively charged complex core about 50 nm in diameter. The complex core structure has a high efficiency of encapsulation, control of particle size, controlled release of nucleic acid in cells<sup>66</sup>, and it can protect the nucleic acid cargo from enzymatic degradation by nucleases and other environmental assaults as well. The cationic liposome containing DOTAP wraps around the negatively charged complex core, and the resulting LPD nanoparticles are slightly less than 100 nm in diameter<sup>67</sup>. Lee & Huang<sup>68</sup> developed a similar LPD gene transfer vector (LPD-II),

where DNA was first complexed to polylysine to form a positively charged core. The major difference from LPDI is that LPD-II uses pH-sensitive anionic liposomes composed of dioleoyl phosphatidylethanolamine (DOPE)/cholesteryl hemisuccinate (CHEMS) instead of cationic liposomes. Above all, the liposomes added to the LPD complexes are either made of cationic (LPD-I) or anionic (LPD-II) lipids to form lipopolyplexes. In order to increase the circulation half-life, PEG was coated outside the LPD, and targeting ligands (e.g. anisamide, folate) were also tethered to the distal end of the PEG polymer chain to achieve specific internalization, enhanced cellular uptake and improved transfection efficiency<sup>69, 70</sup>.

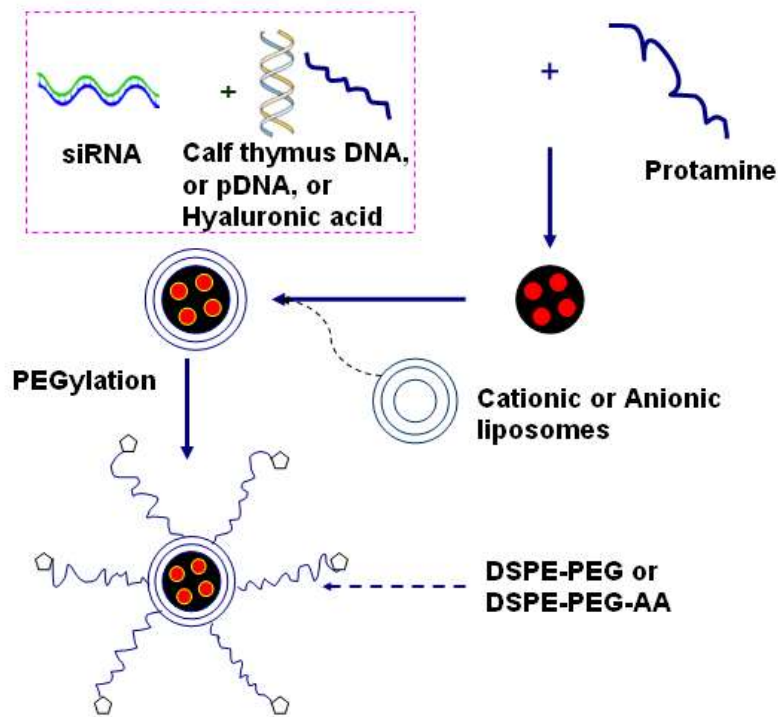


**Figure 1.6 Structure and preparation scheme of LPD nanoparticles.**

Nakamura et al<sup>66</sup> developed a multifunctional envelope-type nano device (MEND) as non-viral gene delivery for plasmid DNA (pDNA) and oligodeoxynucleotides (ODN),

similar to LPD-II<sup>68</sup>. MEND consists of a DNA core condensed by polycation and covered with lipid membranes, and the surface of the lipid envelope can be modified with various functional devices, such as PEG for prolonged circulation, specific ligand for targeting, or fusogenic peptide for endosomal escape<sup>71</sup>. The lipid membrane of MEND was composed of 1,2-dioleoyl-sn-glycero-3-phosphoethanolamine (DOPE) and cholesteryl hemisuccinate (CHEMS) without cationic lipids. Since PEG modification on the surface of nanoparticle is undesirable for the cellular uptake by interfering the interaction with the cell membrane<sup>22</sup>, Hatakeyama<sup>72</sup> used a biological responsive PEG-peptide-lipid ternary conjugate (PEG-peptide-DOPE conjugate (PPD)) to modify the MEND gene carrier. The PEG can be removed from the carriers via cleavage by a matrix metalloproteinase (MMP) which is specially expressed in tumor tissues. The results show MEND modified with PPD is stable in the systemic circulation and can facilitate tumor accumulation and transfection.

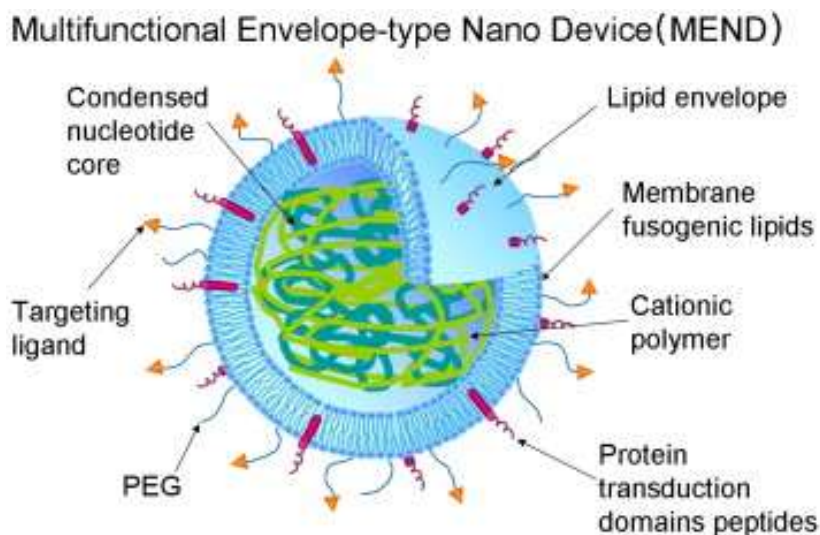


**Figure 1.7 The schematic structure of MEND nanoparticle.** (Ref: Advanced Drug Delivery Reviews, 2008, 60, 559-571)

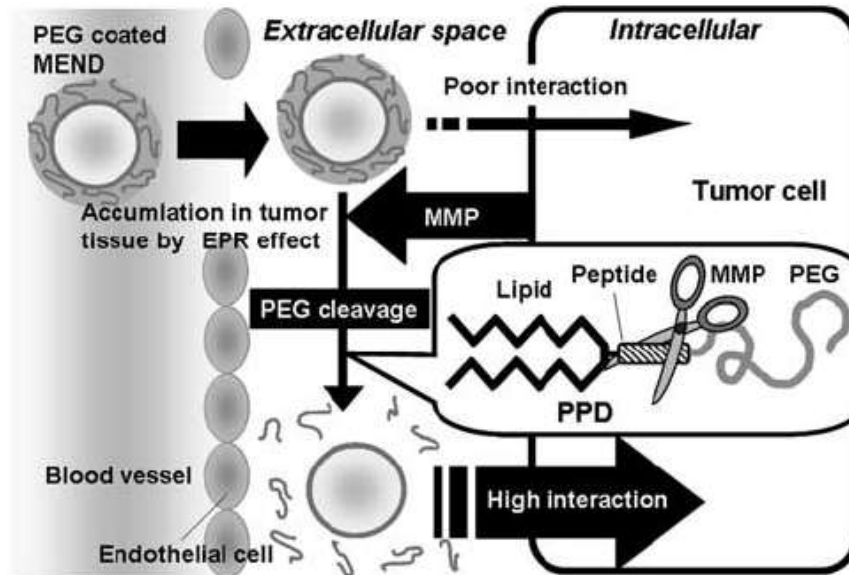


**Figure 1.8 A schematic diagram illustrating the strategy of releasing gene cargo in MEND nanoparticles by PPD modification.** (Ref: Gene Therapy, 2007, 14, 68-77)

From the xzy confocal microscopy images by Li et al, most of the siRNAs was delivered intracellularly in vivo when formulated in anisamide (AA) targeted LPD nanoparticles (**Fig 1.9c**), while siRNAs only remained in extracellular space when they are formulated in non-targeted nanoparticles (**Fig 1.9b**). Free siRNA and non-targeted nanoparticles showed little cellular uptake (**Fig 1.9a, 1.9b**). However, in **Fig 1.9c**, the siRNA fluorescence was not distributed homogeneously, instead, there were many granular dots dispersed in the cytoplasm. The data strongly indicate that the delivered siRNA was not completely dissociated from the nanoparticles. Although LPD nanoparticles were strikingly successful in delivering siRNA via intravenous administration, most of siRNA loaded into the vector is still associated with the cores in the cytoplasm such that most of the encapsulated siRNA is not bioavailable.

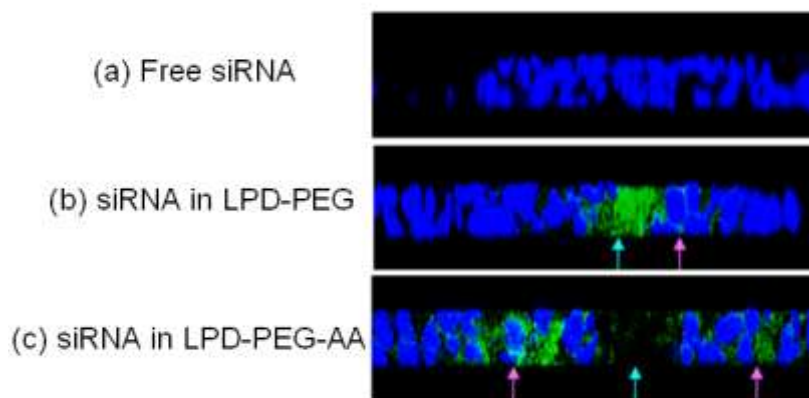


**Figure 1.9** A diagram illustrating the limited release of siRNA from LPD condensed core. Green fluorescence is FAM-siRNA. Blue arrows indicate the extracellular space and pink arrows indicate the intracellular uptake of siRNA. (Ref: Molecular Therapy, vol. 16, no. 1, 163-169, 2008)

In order to solve the problem regarding to the inefficient release of siRNA from LPD nanoparticles, Li et al<sup>70</sup> developed a lipid coated calcium phosphate (LCP) nanoparticle formulation for efficient delivery of siRNA to a xenograft tumor model by intravenous administration. Comparing to the LPD nanoparticle, the previous DNA-protamine complex core was replaced by a biodegradable nano-sized calcium phosphate precipitate prepared by using water-in-oil microemulsions, and siRNA was entrapped in the calcium phosphate precipitate in the microemulsion. The rationale for the LCP design is that the calcium phosphate precipitate in the core of LCP nanoparticles would dissolve and de-assemble at low pH in the endosome, increase the osmotic pressure, and cause endosome swelling and bursting to release the entrapped siRNA. This new formulation improved the *in vitro* silencing effect 3-4 folds comparing to the previous LPD formulation, and had decreased immunotoxicity to allow a potential application for clinical trial. The LCP nanoparticles can be further optimized by changing the precipitate core and the coating

lipids. **Fig 1.10** shows the formation process and the entrapped siRNA release mechanism of LCP-II nanoparticles.

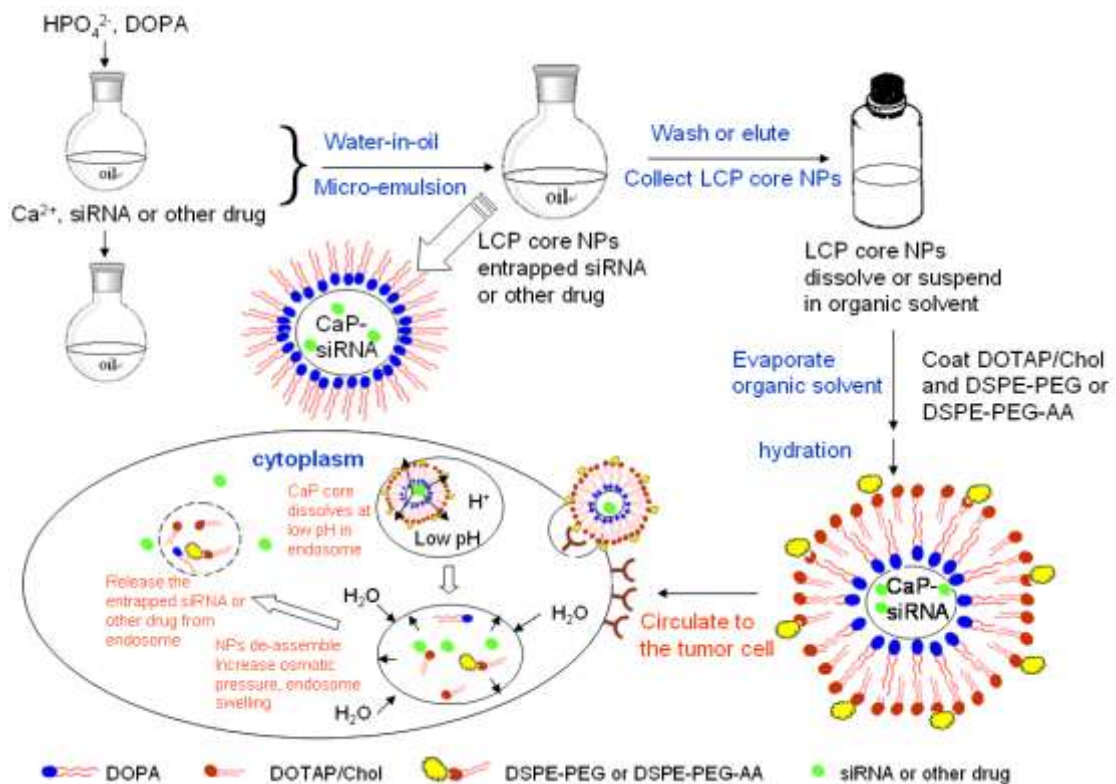


**Figure 1.10** The formation process and entrapped siRNA release mechanism of LCP nanoparticles

#### 1.6.2.6 Aptamer-siRNA chimeras

Cancer cells usually over-express certain surface markers<sup>73</sup> which can be exploited for targeted delivery of siRNA. Aptamers are ssDNA, RNA, or modified nucleic acids with high binding affinity specific to their targets which range from small molecules to proteins<sup>74</sup>. They have been isolated and identified for the recognition of molecular targets expressed on the surface membranes of specific cancer cells. Dassie et al<sup>75</sup> and McNamara et al<sup>76</sup> use aptamer-siRNA chimeras to target prostate-specific membrane



antigen (PSMA) expressed on prostate cancer cells, triggering cell type-specific gene silencing by chimeric RNAs via the RNAi pathway. The aptamer-siRNA chimeras show specific tumor inhibition and mediate tumor regression in a xenograft model of prostate cancer, which could prove to be useful therapeutics for targeting human prostate cancer in the future. The drawback of the vector is the lack of any endosome escape mechanism in the chimera.

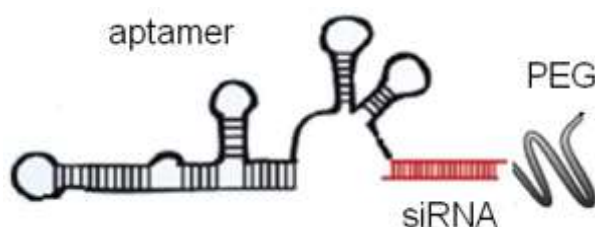


**Figure 1.11 Schematic structure of aptamer-siRNA chimeras** (Adapted from RNAi and small interfering RNAs in human disease therapeutic applications. Trends Biotechnol. 28 (11): 570-579, 2010)

## 1.7 TARGETING LIGANDS

### 1.7.1 Aptamers

Aptamers are short single-stranded DNA or RNA oligonucleotides ranging in size from 20 to 80 bases (~6 to 26 kDa) which are able to recognize and bind to their target molecules, such as proteins, phospholipids, sugars, nucleic acids, cell surface receptor, with high affinity and specificity<sup>11, 77</sup>. Aptamers are derived from a large random sequence pool through repeated rounds of in vivo selection for targets on the surface of tumor cells and in vitro selection using purified protein target. They can also be obtained via a process referred to as SELEX (systemic evolution of ligands by exponential enrichment)<sup>78</sup> to bind to various molecular targets, and even cells, tissues and organisms.

Receptor-binding RNA aptamers may help cell receptors to internalize cargos after the ligands interact with the receptors. Aptamers are also amenable to a wide variety of chemical modifications, such as radioactive or fluorescent reporters, affinity tags for molecular recognition, ribose ring modification, which makes aptamers resistant to nuclease. Aptamers can also be covalently conjugated to nanomaterials after appropriate chemical modification. Another attractive feature of aptamers in biological systems is their low toxicity, low immunogenicity<sup>79</sup> and long circulation half life.

### **1.7.2 Cell penetrating peptides**

Cell penetrating peptides (CPPs), also known as protein transduction domain (PTDs), are a class of short peptide sequences that can enter cells efficiently, either alone or linked to bulky cargos such as peptides, proteins, oligonucleotides, pDNA, or liposomes<sup>80, 81</sup>. Linking the cargo macromolecule to CPP can help to overcome the cell membrane barrier.

### **1.7.3 Antibodies**

Antibodies and antibody fragments have been fused to various drug delivery systems as a targeting agent, so that they can selectively deliver their payload to tumor cells. Xu et al<sup>82</sup> conjugated a single-chain monoclonal antibody fragment (scFv) that targeted to the transferrin receptor to cationic liposomes, and then mixed with plasmid DNA to produce scFv-Lip-DNA complex, which enhances the transfection efficiencies both in vitro and in vivo in a variety of human tumor models. Chen et al has also conjugated scFv to liposome-polycation-hyaluronic acid (LPH) nanoparticles to deliver both siRNA and miRNA for therapy in a murine B16F10 melanoma model<sup>83</sup>. The siRNA delivered by the

scFv targeted nanoparticles efficiently down-regulated the target genes in the lung metastasis and reduced the tumor load in the lung.

#### **1.7.4 Peptides and Proteins**

Some cancer cells up-regulate certain cell surface receptors that correspond to larger protein ligand, such as transferrin which is an iron-transporting serum glycoprotein. The transferrin modified drug delivery vectors can be efficiently taken up into cells by receptor-mediated endocytosis. Also, small immobilized peptides can be tethered on polymers as cell recognition motif which can resist enzymatic degradation and therefore exhibit excellent long term stability. In addition, unlike extracellular matrix (ECM) proteins that normally contain many different cell recognition motives, the small peptides represent only one single motif, so they can selectively address one particular type of cell receptors and trigger cell adhesion efficiently. Both linear peptides and cyclic peptides can be employed<sup>84</sup>. The Arg-Gly-Asp (RGD) sequence is one of the most effective and most often employed peptide sequences for stimulated cell adhesion, targeting to integrin family receptors on tumor vasculature, such as  $\alpha_v\beta_3$  which plays a significant role in tumor angiogenesis. Peptides containing RGD and RGD-mimetics have been coupled to liposomes, polymers, other peptides, small molecule drugs and radiotracers for therapeutic, diagnostic imaging of tumor angiogenesis<sup>85</sup>. Many multivalent RGD-constructs and multimeric cyclic RGD peptides have been used to increase the binding affinity and targeting capability to integrin  $\alpha_v\beta_3$ <sup>86, 87</sup>. Multivalency not only greatly improves affinity but also facilitate internalization via receptor-mediated endocytosis<sup>88</sup>. Besides RGD-mediated delivery of small molecule drugs, imaging agents, peptides and proteins, RGD-modification of non-viral and viral gene carriers have been successfully

exploited as well<sup>89</sup>. Similar to RGD, Asn-Gly-Arg (NGR) is another small peptide applied to target to aminopeptidase N (CD13) molecule which is over-expressed on certain tumor cells and most tumor endothelial cells<sup>90</sup>. Chen et al<sup>91</sup> conjugated NGR peptide to PEGylated LPD nanoparticles for efficient delivery of siRNA and doxorubicin into solid tumors. NGR-hTNF which consists of human tumor necrosis factor (hTNF) fused with NGR peptide showed efficient antitumour activity at low doses due to selective binding to CD13 over-expressed on tumor blood vessels, and the activity and safety of NGR-hTNF was further evaluated in clinical study on colorectal cancer (CRC) patients failing standard therapies<sup>92</sup>. The results showed NGR-hTNF was well tolerated on CRC patients, and deserves further evaluation in combination with standard chemotherapy. Thus, both RGD and NGR have been widely used in many drug delivery systems for active tumor targeting and enhanced antitumor therapeutic effect.

### **1.7.5 Small molecular weight ligands**

Folate receptors are over-expressed on several types of cancers and diseased cells but are expressed in minimal quantity in normal cells except the kidneys<sup>93</sup>. So folate conjugation presents an effective method of targeting drug/gene carriers to cancer cells. It has been successfully applied for the receptor-specific delivery of chemotherapy agents, liposomal drug carriers and gene transfer vectors<sup>90</sup>. Anisamide is a high affinity small molecular weight ligand for sigma receptors that are highly expressed on many epithelial cancer cells. It can be conjugated to lipid nanocarriers to deliver doxorubicin<sup>94</sup> and siRNA<sup>95, 96</sup> to tumors in animals. Other small molecules such as haloperidol, SA4503, and opipramol have also been reported as sigma receptor ligands<sup>97</sup>. Mukherjee et al<sup>98</sup> reported that haloperidol conjugated lipoplexes showed 10-fold greater delivery of DNA to breast

carcinoma cells than the control lipoplexes. The advantages of small molecular weight ligands are their small size, convenient availability, relatively simple conjugation chemistry, and reduced immunogenicity.

## **1.8 THERAPEUTIC APPLICATION FOR TREATMENT OF CANCER**

### **1.8.1 siRNA therapeutic mechanisms**

Many human diseases are often caused by inappropriate endogenous or exogenous gene expression that leads to angiogenic dysfunction. The role of angiogenesis in tumor growth is mediated by a balance of activators and inhibitors. siRNA can create new inhibitors that down-regulate angiogenesis through post-transcriptional gene silencing, such as regulation of VEGF receptor expression<sup>99</sup>. siRNA have already shown therapeutic effects from a number of animal disease models, demonstrating that anti-angiogenesis siRNA may play an important role in the treatment of human diseases in the near future<sup>100</sup>. Furthermore, siRNA targeting key elements of proliferation signal transduction pathways can prevent the development of specific human cancers. And siRNAs specifically down-regulating the expression of the target genes can induce the induction of cell cycle arrest, apoptosis and reduced cell proliferation *in vitro* or tumor growth *in vivo*. In addition, drug resistance in cancer cells can also be overcome by delivering c-myc siRNA<sup>101</sup>.

### **1.8.2 Examples in cancer treatment by RNA delivery technology**

Clinical trials using RNAi technology to treat human diseases were first launched in 2004<sup>102</sup>. siRNA is now being evaluated for almost all types of disease and more than 13 products have entered into clinical trials. Although it is a very promising class of drug, the Food and Drug Administration (FDA) has not approved any human gene therapy

product to date. Davis *et al*<sup>103</sup> has finished the first siRNA clinical trial using targeted nanoparticle delivery system invented by Calando Pharmaceuticals. This technology applied cyclodextrin polymer carriers to deliver the siRNA<sup>81</sup>. The synthetic delivery system tested in clinical trial contained a linear cyclodextrin-based polymer (CDP), a human transferrin protein (TF) as the targeting ligand, hydrophilic PEG polymers to improve nanoparticle stability in the circulation and siRNA designed to reduce the expression of RRM2<sup>103</sup>. This targeted nanoparticles were designed to circulate and then to accumulate and permeate in solid tumors after intravenously administration. The reduction of the RRM2 mRNA and protein by the RRM2-specific siRNA was observed in the tumor biopsies of melanoma patients. The experimental data demonstrated that siRNA administered systemically to human can produce a specific gene inhibition by an RNAi mechanism of action.

From this successful example of RNAi clinical trial, it is predictable that cancer treatment with siRNAs will be widely applicable in the near future once the challenges of targeting, potency, duration of effect, specificity and safety issues are overcome for the effective systemic delivery. **Table 1.2** summarized some ongoing clinical trials for RNAi based therapy to cancers and other wide range of diseases<sup>104-106</sup>.

**Table 1.2 RNA interference (RNAi) drugs in clinical trials**

Company	RNAi agent name	Disease	Target	RNA delivery method	Route of admin. and target tissue	Trial phase
Calando	CALAA-01 <sup>103</sup>	Solid tumors	RRM2	Targeted nanoparticle delivery system	Intravenous injection (systemic)	Phase I
Alnylam	ALN-VSP	Liver cancers and solid tumors	KSP, VEGF	Liposomal conjugation	Intravenous infusion (systemic)	Phase I
Silence Therapeutics	Atu027/Atu093 <sup>107</sup>	Lung cancers	PKN3	siRNA-lipoplex	Intravenous injections or infusions (systemic)	Phase I
Quark/Pfizer	PF-4523655/RTP-801i-14	AMD, diabetic macular degeneration	RTP801	Synthetic chemically modified siRNA molecule	Intravitreal injection (eye)	Phase II
Alnylam	ALN-RSV01 <sup>108</sup>	RSV infection	Nucleocapsid (N) gene of RSV genome	Minimally modified, unencapsulated siRNAs	Intranasal (respiratory tract)	Expanded Phase II
Quark	AKIi-5	ARF, AKI	TP53	Chemically modified siRNA formulation	Intravenous injection (systemic)	Phase II
Allergan	AGN-211745 (Sirna-027) <sup>109</sup>	AMD and CNV infection	VEGFA, VEGFR1	Sterile siRNA buffer or nuclease-free PBS	Intravitreal injection (eye)	Phase II
TransDerm	TD101 <sup>110</sup>	Pachyonychia congenita	Keratin 6a N171K	Unmodified TD101 siRNA	Intradermal injection (skin)	Phase I
University of Duisburg-Essen	BCR-ABL siRNA <sup>111</sup>	CML	bcr-abl	DLS lipid solution with anionic lipoplexes	Intravenous injection (systemic)	Single patient
Duke University Hospital	siRNA immunotherapy	Metastatic melanoma	Proteasome	Dendritic cell-based vaccine	intradermal injection (skin)	Phase I
Opko Health	bevasiranib	Wet AMD	VEGF	Direct inject siRNA to the eye	Intravitreal injection (eye)	Expanded Phase III

*Abbreviations:* AKI: Acute kidney injury; AMD: age-related macular degeneration; ARF: acute renal failure; CML: Chronic myeloid leukaemia; CNV: choroidal neovascularization; KSP: Kinesin spindle protein; PKN3: protein kinase N3; RRM2: M2 subunit of ribonucleotide reductase; RSV: respiratory syncytial virus; RTP801: hypoxia-inducible factor 1-responsive gene; TP53: tumor protein p53; VEGF: vascular endothelial growth factor; VEGFR-1: vascular endothelial growth factor receptor-1.

## **1.9 CONCLUSION**

Optimal siRNA delivery vectors discussed above are widely applied to improve the therapeutic nucleic acid based transfection efficiency with limited toxic side effects. In sum, RNAi has rapidly been recognized as an experimental tool and is expected to be used as a therapeutic treatment for various diseases.

This literature review leads to the project designs described in Chapter 4 and Chapter 5 of this thesis.



## **2.0    *IN VIVO* GENE DELIVERY BY NON-VIRAL VECTORS: OVERCOMING HURDLES?**

The promise of cancer gene therapeutics is hampered by difficulties in the *in vivo* delivery to the targeted tumor cells, and systemic delivery remains to be the biggest challenge to be overcome. Here, we concentrate on systemic *in vivo* gene delivery for cancer therapy using nonviral vectors. In this review, we summarize the existing delivery barriers together with the requirements and strategies to overcome these problems. We will also introduce the current progress in the design of nonviral vectors, and briefly discuss their safety issues.

### **2.1    INTRODUCTION**

Gene therapy holds the significance of correcting genetic defects, and there are many nucleic acid-based therapeutic strategies that can be used for gene therapy against cancer, including antisense and RNA interference (RNAi) mechanisms. Antisense oligonucleotides are typically 15-30 nucleotides long and block production of the disease-causing protein after complementarily hybridizing to their target mRNA and degrading

---

Reference: Yuan Zhang, Andrew Satterlee, Leaf Huang. *In vivo* gene delivery by non-viral vectors: overcoming hurdles? *Molecular Therapy* (2012); 20 (7), 1298-1304.

the mRNA by activating RNaseH. RNAi is a separate process in which a specific mRNA is targeted for degradation in order to inhibit the synthesis of its encoded protein. Two types of small RNA molecules – microRNA (miRNA) and small interfering RNA (siRNA) – are central to the RNAi function. After delivery into the cytoplasm, the antisense strand of RNAi molecules recruits the corresponding mRNA in a sequence-specific manner to the RNA-induced silencing complex (RISC), which is followed by cleavage of the target mRNA, resulting in gene silencing. Both antisense oligonucleotides and RNAi-based therapy target mRNA to inhibit transcription of an overexpressing endogenous gene or a cancer causing oncogene<sup>112</sup>, resulting in selectively inhibiting the expression of an unwanted protein (downregulation or loss of function). Plasmid DNA (pDNA) is also widely used to introduce a normal wild-type transgene into specific cells of the host where the endogenous gene is underexpressing<sup>112</sup>, resulting in expression of a deficient protein (upregulation or gain of function).

Currently, three different kinds of gene delivery systems have been explored: modified naked siRNA, viral vectors, and non-viral vectors. Modified naked siRNAs have increased nuclease stability and gene silencing efficiency, as well as reduced immune responses and off-target effects, when compared to unmodified RNAs.<sup>113</sup> Viral vectors have high gene transfection efficiency, but their residual viral elements can cause insertional mutagenesis and immunological problems. Non-viral vectors are constructed with biocompatible materials using innovative fabrication approaches, so that they can safely transport gene cargo *in vivo*, but their transfection efficiencies are not as high as viral vectors.

Therapeutic nucleic acids are potent in correcting genetic defects in cell and molecular levels, but in a real biological environment, their lack of serum stability and rapid clearance greatly compromise their *in vivo* delivery, which retards gene therapy application in clinical setting. In this review, we will summarize the existing delivery barriers, highlight the strategies to overcome these hurdles, and introduce the current progress of non-viral vectors constructed for cancer gene therapy.

## **2.2 CHALLENGES OF GENE DELIVERY**

### **2.2.1 Off-target effect**

siRNAs are capable of reducing expression of non-target genes due to interaction of the siRNA guide strand with a partially complementary site on an ‘off-target’ mRNA<sup>114</sup>. Careful selection of siRNA sequences to avoid off-target effects is an important issue, and can be minimized by avoiding certain sequence motifs. The design and selection of a specific siRNA may involve the consideration of internal repeated sequence, GC content, siRNA length, specific base preference, secondary structure, etc.<sup>115,116</sup>

### **2.2.2 Immune stimulation**

Innate immune activation via RNA represents a significant undesirable side effect due to the toxicities associated with excessive cytokine release<sup>117</sup> and inflammatory syndromes after systemic administration. The inflammatory response is mediated by Toll-like receptors (TLRs) TLR3, TLR7, TLR8 and TLR9, which are located in endosome compartments, and recognize unmethylated CpG DNA as well as various moieties in double-stranded RNA or their degraded products<sup>118</sup>. A number of parameters affect how delivery vehicles potentiate immune stimulation. These include the chemical composition of the delivery vehicles, physical properties such as the size and charge of formulated

materials, pharmacokinetics and biodistribution of formulated nucleic acids, and routes of administration.<sup>117</sup> TLR-mediated recognition and concomitant immune stimulation can be inhibited by chemical modifications, such as introduction of 2'-O-methyl (2'OMe)-modified nucleotides.<sup>119</sup>

### **2.2.3 Delivery**

The most important—and most difficult—challenge in gene therapy is the issue of delivery. Not only must the therapy evade the reticuloendothelial system as it circulates after systemic administration, but it must also cross several barriers before it arrives in the cytoplasm or nucleus of its target cells.

### **2.2.4 Serum inactivation and enzyme degradation**

Stabilization of RNA is regarded as a prerequisite for *in vivo* therapeutic applications, however, naked RNAs are rapidly degraded by nuclease in serum. Nuclease resistance can be enhanced by chemical modification of RNAs. Because the 2'-hydroxyl group of the ribose ring is not necessary for potent gene silencing by siRNAs, the most widely used RNA modifications are on sugar moieties. Common modifications are 2'-fluoro, 2'-O-methyl, and 2'-amine conjugations<sup>112</sup>. The locked nucleic acid (LNA) conformation has a 2'-O, 4'-C methylene bridge in the sugar ring. Such LNA molecules have the desirable features of increased nuclease stability and silencing potency, as well as reduced off-target effects and immune responses. Backbone modification by changing the internucleotide phosphate linkage, such as phosphorothioate (P = S) and boranophosphonate (P = B) modifications, can be placed in the RNA duplex at any desired position to enhance nuclease stability<sup>112</sup>.

Though modified RNAs are favorable for *in vivo* delivery when compared to naked RNAs, they lack specific tumor targeting and would be quickly excreted by the kidney upon systemic administration, so a large amount of modified RNAs are needed to attain desired therapeutic effects<sup>113</sup>. Generally, modified RNAs are delivered by local injection, but the local route is only accessible for certain cancers, such as skin cancer or head and neck cancer. Thus, most efforts have been concentrated on developing safe and effective nanoparticles for systemic gene delivery.

### **2.2.5 RES recognition**

In order to condense negatively charged nucleic acids into delivery vehicles, most nanoparticles contain polycations such as cationic polymers or lipids. The positive charge aids cellular uptake but also promotes non-specific interactions with non-target cells and extracellular components such as serum proteins and extracellular matrix<sup>122</sup>. Binding of plasma proteins is the primary mechanism for the reticuloendothelial system (RES) to recognize circulating nanoparticles<sup>123</sup>, causing the major injected dose (ID) to go to RES organs, such as the liver, spleen, and bone marrow, immediately after i.v. injection, with little accumulation in tumors.

The most common way to decrease non-specific interactions is to shield the nanoparticle surface with hydrophilic, uncharged polymers such as polyethylene glycol (PEG). Surface PEG coating sterically hinders the interaction and binding of blood components with the nanoparticle surface and prevents opsonization and recognition by phagocytes of the RES<sup>124</sup>, resulting in prolonged nanoparticle circulation in the blood. The nanoparticle circulation half-life may vary by changes in PEG chain length, PEG density, surface coating, particle size and surface charge of the underlying nanostructure.<sup>125</sup> PEGylated

(aka stealth) nanoparticles with a reduced RES uptake and a prolonged circulation half-life are a prerequisite for enhanced tumor targeting<sup>123</sup>.

### **2.2.6 The EPR effect**

Transport of macromolecules across the tumor endothelium is more efficient than that of normal endothelium because of its leaky and discontinuous vascular structures (permeation) with poor lymphatic drainage (retention), which is referred to the ‘enhanced permeability and retention (EPR) effect’.<sup>126</sup> In other words, tumor endothelium allows the penetration of macromolecules and most nanoparticles. The EPR effect can be enhanced by PEGylation because the amount of blood that circulates through the tumor is usually far less than that of the RES organs, and only those nanoparticles that are not rapidly cleared from the circulation will have a chance to encounter the leaky tumor vasculature<sup>123</sup>.

Not all human tumors are equally leaky; for tumors with less leaky vasculatures, nanoparticles with small size (less than 30 nm) are desirable<sup>124</sup>, but for most tumors, nanoparticles with a mean size around 100 nm are attractive for tumor targeting. Particles that are 100 nm in size also allow easier surface modification with PEG arranged in a brush mode, a conformation that efficiently prevents serum opsonization. Particles larger than 400 nm can not easily enter the capillary gaps in the tumor vasculature, while particles smaller than 70 nm are able to access the parenchymal cells in the liver (i.e., hepatocytes) after crossing the liver blood vessels (known as the sinusoidal space), since the sinusoidal vessels contain fenestrae that have an average diameter of 100 nm<sup>122</sup>. Small particles are also prone to renal excretion through the glomeruli in the kidney, and their large surface curvature presents difficulties for PEG shielding.

### 2.2.7 Entrance into cells: The PEG dilemma

PEGylation may protect nanoparticles from protein agglomeration and macrophage capture, controlling their biodistribution and tumor accumulation, but the PEG coating prevents the formation of essential non-bilayer intermediates<sup>127</sup> and inhibits fusion with the cell and/or the endosomal membrane, thus reducing the potential of nanoparticle cellular uptake and cargo release from endosomes, decreasing silencing or transfection efficiency.

To solve this PEG dilemma, labile bonds can be introduced in the PEG chain, so that nanoparticles become unPEGylated upon reaching the target cells, leading to increased rates of membrane destabilization, transport of the loaded cargo inside the cells, and release from the endosome. pH sensitive lipids composed of PEG, an acid-labile linker, and a hydrophobic tail can be used to construct fusogenic liposomes<sup>128</sup>, or one can conjugate PEG and polycations with acid-sensitive linkers followed by compacting nucleic acids into pH-triggered deshielding lipoplexes/polyplexes<sup>129</sup>. Enzyme-sensitive linkers can also be applied to conjugate PEG and lipids, followed by entrapping nucleic acids in liposome-like vehicles, so that the PEG moiety can be cleaved off in tumor sites where the specific enzyme is widespread<sup>130-133</sup>.

Besides the external stimuli-triggered PEG shedding, conjugates of lipids and hydrophilic polymers are generally able to diffuse off of membranes depending on the strength of the anchorage or the anchor chain composition<sup>133</sup>. When particles (liposomes or lipoplexes) are coated with sheddable stealth PEG-lipid<sup>133</sup>, the spontaneous shedding of the PEG-lipid from particles (de-PEGylation)<sup>123,134</sup> will continuously happen when particles circulate in blood, which eventually exposes the shielded cationic lipids and allows

membrane fusion for nanoparticle uptake and endosome release<sup>123</sup>. In this case, the shedding rate is a crucial parameter that has to be addressed when designing sheddable PEG coating. If shedding occurs too quickly, the unprotected carrier will be rapidly cleared from circulation by the RES. In other words, RES competes with tumor for the uptake of nanoparticles<sup>123</sup>. However, if shedding is incomplete or occurs too slowly, the therapeutic efficacy of the loaded cargo might be compromised.

Targeting ligands are also frequently modified on the nanoparticle surface for enhanced cellular uptake by receptor-mediated endocytosis. Commonly used targeting ligands include aptamers<sup>135</sup>, cell penetrating peptides (CPPs)<sup>136</sup>, antibodies<sup>137</sup>, peptides or proteins<sup>138</sup>, and small molecule ligands<sup>139</sup>. Shixian Huang et al<sup>140</sup> conjugated the LRP1 ligand Angiopep-2 to a PAMAM dendrimer using bifunctional PEG, and complexed it with plasmid DNA (pORF-TRAIL) to treat brain glioma. Significant apoptosis induction and prolonged survival time after systemic administration indicated that the Angiopep-2 peptide could be exploited as a specific ligand to cross the BBB and target glial tumors. Sonsoles Diez et al<sup>141</sup> constructed an Asialoglycoprotein receptor-targeted lipopolymeric vector using the asialofetuin ligand for IL-12 gene transfer in hepatocellular carcinoma *in vivo*.

### **2.2.8 Endosome escape**

The delivery of nonviral gene vehicles almost invariably involves endocytosis, and escaping from endosomes before they traffic into lysosomes is an essential step for nanovectors to avoid enzymatic degradation.



Cationic lipid complexes can bind to anionic lipids on the endosome membrane and form neutral ion pairs. These ion-pairs destabilize the endosome membrane and promote de-assembly of the lipoplex through the formation of the inverted hexagonal ( $H_{II}$ ) phase<sup>142</sup>, and finally release nucleic acids to cytoplasm.

Some protonable groups that are charged at acidic pH but less charged at neutral pH could be an alternative choice to designing ionizable cationic lipids that condense nucleic acids and promote endosome release<sup>122, 143, 144</sup>. The rational design lies in the pKa of the ionizable cationic lipid and the abilities of these lipids to induce the hexagonal  $H_{II}$  phase structure with anionic lipids of the endosomal membrane when protonated in the acidic endosome.

Acid-responsive mechanisms have been widely used to design delivery carriers in order to promote endosome release. Polymers and peptides with high buffer capacity between pH 7.2 and 5.0, such as polyethylenimine (PEI)<sup>145</sup>, or peptides containing the cationic amino group lysine, arginine, and imidazole group histidine<sup>146</sup>, could buffer the endosome. This would cause more protons to enter into the endosomes, followed by chloride ions, leading to increased osmotic pressure and endosome rupture, releasing payloads into cytoplasm. This process is called the ‘proton sponge effect’.

Stimuli other than pH have been used to destabilize endosome membranes as well. Lipid or polymer derivatives which are sensitive to sulfhydryl reduction<sup>147-149</sup> and enzymatic cleavage<sup>132, 150</sup> have been used to construct non-viral gene vectors. Upon exposure to the intracellular reducing agents or selective enzymes at the target sites, the vectors become destabilized and fuse with the endosome membrane, and finally release the entrapped

cargo. Some fusogenic peptides can also be combined with nanoparticles to induce membrane fusion in endosomes through their structural changes in acidic conditions as compared to physiological pH.<sup>151,152</sup>

Li and Huang<sup>153</sup> developed a Lipid-calcium-phosphate nanoparticle (LCP) for efficient siRNA delivery. The LCP entraps siRNA in a biodegradable nano-sized calcium phosphate precipitate (CaP) core. The LCP de-assembles in endosomes due to the CaP core dissolving in acidic conditions, which increases the osmotic pressure, causing the endosome to swell and burst to release the entrapped siRNA.

### **2.2.9 Nuclear entry**

The final target destination of antisense oligonucleotides, siRNA/miRNA and mRNA, is the cytoplasm, whereas pDNA must be transported into the nucleus for gene expression. Nuclear transport generally occurs through nuclear pore complexes (NPCs), however, nucleic acid condensates are impermeable through NPCs due to their large size.<sup>154</sup> In dividing cells, the nuclear envelope disassembles during mitosis; pDNA transfection can only occur at this stage of the cell cycle due to elimination of the permeability barrier. The amount of DNA that reaches the nucleus is made lower due to the cytoplasmic nuclease that can degrade DNA, such that the majority of DNA that enters the cytoplasm never arrives in the nucleus. For non-dividing cells, the mechanisms of DNA nuclear transport are of critical importance.

To facilitate nuclear targeting, many nuclear localization signal (NLS) peptides have been developed to allow DNA nuclear entry through NPCs by active transport. NLSs are short clusters of amino acids that can bind to cytoplasmic receptors known as importins. NLS

peptides can bind to DNA either through non-covalent electrostatic interaction or by covalent attachment. The most well-known and popularly used NLS is from the large tumor antigen of simian virus 40 (SV40).<sup>155</sup> Some DNA sequences themselves have nuclear import activity based on their ability to bind to cell-specific transcription factors, such as the SMGA promoter and flk-1 promoter.<sup>156</sup>

In summary, in order to elicit superior *in vivo* therapeutic response to correct genetic defects, the non-viral vector must be able to tightly condense and protect nucleic acids to avoid enzymatic degradation, accumulate at tumor sites with little RES uptake, target specific cells, disrupt the endosomal membrane and release the therapeutic cargo to cytoplasm, and translocate the DNA cargo to the nucleus.<sup>154</sup> **(Fig 2.1)**

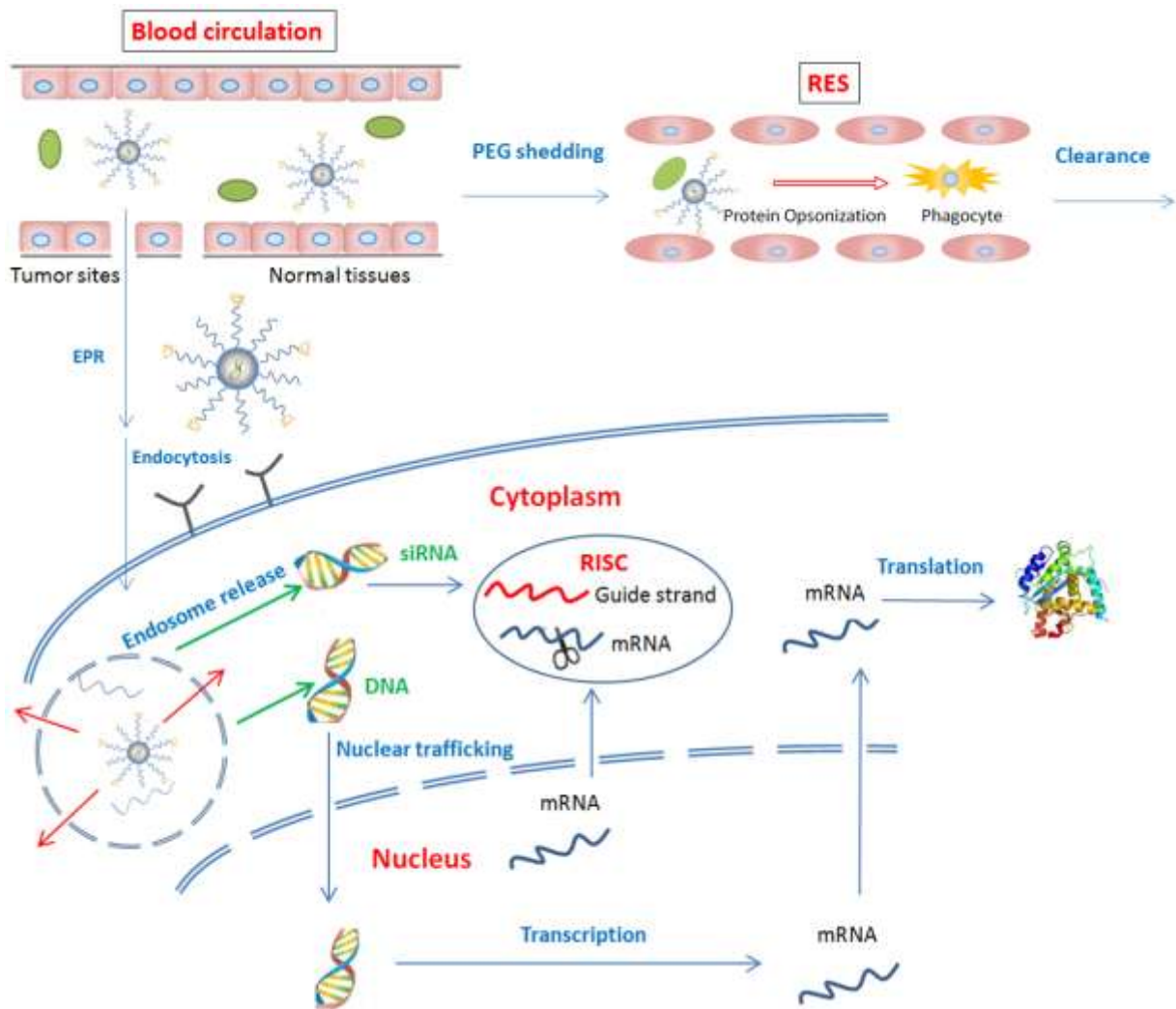


**Figure 2.1 Representative scheme of *in vivo* gene delivery barriers.** EPR, enhanced permeability and retention; mRNA, messenger RNA; PEG, polyethylene glycol; RES, reticuloendothelial system; RISC, RNA-induced silencing complex; siRNA, small interfering RNA.

## 2.3 NON-VIRAL VECTOR DESIGN FOR *IN VIVO* GENE DELIVERY

### 2.3.1 Lipoplex/Polyplex

Nucleic acids are easily complexed with cationic lipids (e.g. DOTAP), cationic polymers (e.g. PEI), biodegradable cationic polysaccharides (e.g. chitosan), and cationic

polypeptides (e.g. polylysine, protamine), via electrostatic interactions. By changing the charge ratio associated with nucleic acids and condensing agents, the transfection efficiency of condensates can be optimized<sup>122</sup>. Cationic polymers and lipids have shown superior gene transfection efficiency, but they have dose-dependent toxicity upon systemic administration. Among cationic polymers, the polymer chain length and the presence or absence of hydroxyl groups play a role in polyplex size and charge in addition to transfection efficiency and toxicity. The high gene transfection usually correlates with the high cytotoxicity.<sup>157</sup> Grandinetti et al<sup>158</sup> reported that direct interaction between (PEI-pDNA) polyplexes and mitochondria during PEI transfection causes impaired mitochondrial function through membrane depolarization and could be the reason for high cytotoxicity in the PEI-based vehicles. This toxicity can be ameliorated by conjugation with biocompatible, hydrophilic polymers such as PEG<sup>159, 160</sup>, and some pH and enzyme-sensitive linkers are widely used. For example, Walker et al designed pH-triggered deshielding polyplexes to enhance endosome release, and Yin et al entrapped RNA in poly ( $\beta$ -amine esters) complex nanoparticles that are degradable in the reductive environment due to the cleavage of disulfide bonds<sup>129, 161</sup>. Furthermore, some synthetic polymers have been optimized using combinatorial chemistry and library screening in order to mimic viral functional delivery domains, such as surface ligands for cell entry, evasion from endolysosomal compartment, and entry into the cytoplasm of target cells. Many defined, precise sequences have been found to perform potent pDNA and siRNA delivery by using solid-phase synthesis.<sup>162</sup> Since different topologies of the defined synthetic polymer structures can influence the complexation and biological properties of transfection agents, Schaffert et al<sup>163</sup> explored the gene delivery efficiency

and cytotoxicity of linear polycations with modifications in different areas and found that these changes could cause robust differences in biological function.

### 2.3.2 Lipopolyplex

In order to increase serum stability, avoid RES uptake and increase tumor accumulation, Li et al<sup>164</sup> designed a liposome-polycation-DNA nanoparticle (LPD) for siRNA delivery. siRNAs were mixed with calf thymus DNA before being condensed with protamine. Protamine is a natural arginine-rich cationic polypeptide which is biocompatible, biodegradable and nontoxic, so it is more desirable than synthetic polymers. The condensed particles were wrapped by cationic liposomes, followed by grafting PEG-lipid conjugate (DSPE-PEG) with or without a targeting ligand using a postinsertion method. The LPD can deliver a significant fraction of injected siRNA into the tumor after i.v. injection with little RES uptake. siRNA formulated in the targeted LPD completely silenced oncogenes in tumors, induced tumor cell apoptosis, and achieved superior tumor growth inhibition<sup>165,166</sup>. By adjusting the siRNA to protamine ratio, a positively charged LPD core can also be attained. LPD-II was formed by wrapping an anionic liposome composed of DOPA around this LPD core, followed by grafting DSPE-PEG<sup>167</sup>. Based on the LPD formulation, Chono et al<sup>168</sup> developed a liposome-polycation-hyaluronic acid (or heparin) nanoparticle (LPH). A remarkable advantage for LPH is that it showed very little immunotoxicity in a wide dose range compared to LPD. Chen et al<sup>169</sup> used the scFv ligand targeted LPH to effectively deliver siRNAs (c-Myc/MDM2/VEGF) and miRNA-34a to a B16F10 lung metastasis model. **Fig 2.2** shows the structure and preparation scheme of LPD (LPD-II)/LPH nanoparticles.

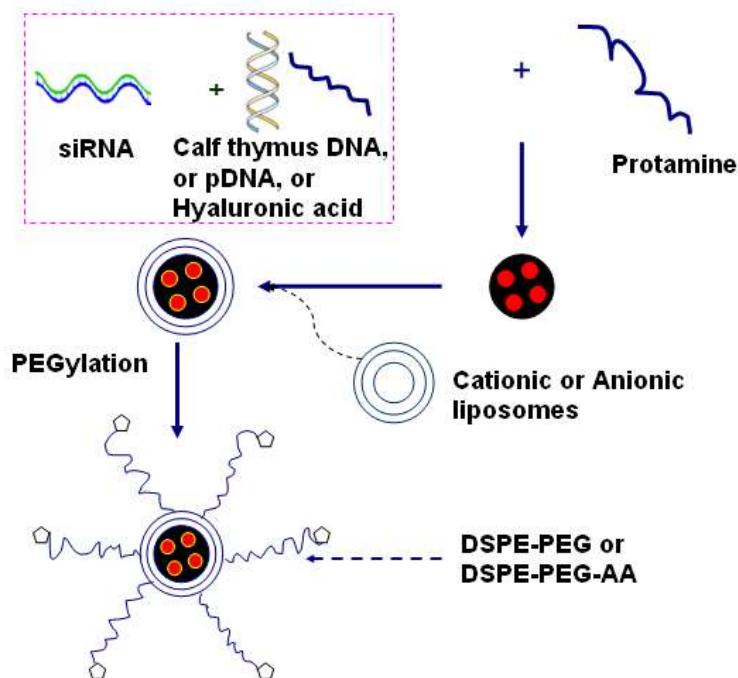


**Figure 2.2 The structure and preparation scheme of LPD (LPD-II)/LPH nanoparticles.** LPD, liposome-polycation-DNA; LPH, liposome-polycation-hyaluronic acid (or heparin); pDNA, plasmid DNA; PEG, polyethylene glycol; siRNA, small interfering RNA.

mRNA can be loaded in lipopolyplexes (termed LPRs, lipid-polymer-RNA) using the similar method of LPDs. Perche et al<sup>170</sup> reported that MART-1 mRNA lipopolyplexes with mannosylated liposomes (Man11-LPR100) targeting dendritic cells can be used as an efficient system for anti-B16F10 melanoma mRNA-based vaccines. A great inhibition of B16F10 melanoma growth was obtained after mice were intravenously immunized with MART-1 Man11-LPR100, indicating that tumor antigen mRNA-loaded Man11-LPR100 is an efficient system to induce an anticancer immune response. Although mRNA serves as a potential therapy in various medical indications, like other nucleic acid molecules, its strong immunogenicity and limited stability hamper clinical

applications. To solve these limitations, Kormann et al<sup>171</sup> designed a combination of nucleotide modifications. They found that replacement of only 25% of uridine and cytidine with 2-thiouridine and 5-methyl-cytidine synergistically abrogated mRNA interaction with TLR3, TLR7, TLR8 and retinoid-inducible gene I (RIG-I), thus substantially decreasing activation of the innate immune system. High expression of therapeutic proteins were detected in mice after intramuscular administration of double-modified mRNA, as well as in a congenital surfactant protein B (SP-B) deficiency disease model after two intratracheal doses of modified SP-B mRNA.

Although LPD nanoparticles are successful in the systemic delivery of siRNA, the delivered siRNA does not completely dissociate from the nanoparticles, such that most of the encapsulated siRNA is not bioavailable. In order to solve the problem regarding the inefficient release of siRNA from LPD, Li et al<sup>153</sup> developed a Lipid-Calcium-Phosphate nanoparticle (LCP). The LPD's DNA-protamine complex core was replaced by a biodegradable nano-sized calcium phosphate (CaP) precipitate prepared by water-in-oil microemulsions, and siRNA was entrapped in the CaP core. The rationale for the LCP design is that the CaP precipitate in the LCP core would dissolve and de-assemble at low pH in the endosome, increase the osmotic pressure, and cause endosome swelling and bursting to release the entrapped siRNA. The LCP can be further optimized by changing the precipitate core and the coating lipids.

Harashima et al developed a liposomal gene carrier known as multi-functional nano device (MEND) for systemic gene delivery. Similar to LPD, MEND consists of a nucleotide core condensed with polycations and covered with lipid membranes. The surface of the lipid envelope can be modified with various functional devices, such as



PEG for prolonged circulation, specific ligands for targeting, or fusogenic peptides for endosomal escape.<sup>172</sup> In order to avoid the PEG dilemma, an enzyme-cleavable PEG system, PEG-peptide-DOPE conjugate (PPD), was used to modify MEND<sup>132</sup>. In this strategy, the PEG is removed from MEND via the cleavage by a matrix metalloproteinase (MMP), which is specifically expressed in tumor tissues.

Harashima et al<sup>151, 152</sup> further modified a fusogenic peptide GALA (WEAALAEALAEALAEHLAEALAEALEALAA) on MEND for the sake of promoting endosome release. The 30 amino acid GALA contains a glutamic acid-alanine-leucine-alanine sequence that is repeated 4 times. Since the carboxyl groups of glutamic acid are negatively charged at physiological pH, electric repulsion between these groups forces GALA to be a random coil structure. In contrast, at acidic endosomal pH, protonation of the carboxyl group side chains of the glutamic acids dissipates electric repulsion, so the GALA structure changes into an  $\alpha$ -helix, a structure that tends to induce membrane fusion. To avoid the recognition by biomacromolecules *in vivo*, a shorter version of GALA (shGALA) was developed, which was masked by the PEG layer of the MEND. The shGALA-modified MEND showed significant gene silencing in the tumor and inhibition of tumor growth.

### **2.3.3 Aptamer-siRNA chimeras**

Aptamers are three-dimensional single-chain nucleic acid molecules that bind to a specific target molecule with high affinity and specificity.<sup>173</sup> They are selected from a combinatorial library of randomized sequences through repeated rounds of selection, known as “systematic evolution of ligands by exponential enrichment” (SELEX)<sup>174</sup>, and the target molecules can be small molecules, nucleic acids, proteins, carbohydrates,

whole cells, and even organisms. Aptamers have high diversity and those possessing very high affinities to the target molecules can be isolated. In addition, they are relatively stable in storage and elicit little immunogenicity in therapeutic applications.

Most aptamer-siRNA targeted chimeras for cancer therapy are against PSMA, a cell-surface receptor over-expressed in prostate cancer cells and tumor vascular endothelium. McNamara et al<sup>175</sup> developed aptamer-siRNA chimeric RNAs. The aptamer portion of the chimeras mediated binding to PSMA, whereas the siRNA portion targeted the expression of tumor survival gene Plk1 and Bcl-2. The chimera effectively delivered siRNAs to LNCaP prostate cancer cells expressing PSMA, and triggered apoptosis and cell death both in cultured cells and in a prostate tumor xenograft model<sup>175</sup>. In order to enhance silencing activity and specificity of siRNA, Dassie et al<sup>176</sup> incorporated modifications, including adding 2-nucleotide 3'-overhangs and optimizing the thermodynamic profile and structure of the duplex, which enabled more efficient processing of the siRNA guide strand and reduced the effective concentration of siRNA portion. The optimized chimeras resulted in pronounced regression of PSMA-expressing tumors after systemic administration. Anti-tumor activity was further enhanced by grafting a 20 kDa PEG moiety to the 5'-terminus of the RNA strand, which increased the chimeras' circulating half-life and bioavailability without affecting chimera targeting and silencing. The aptamer portion of the chimeras can also be truncated from 71nt to 39nt without loss of function, so that large-scale chemical synthesis can be facilitated. In principle, the aptamer-siRNA chimera approach can be applied to target reagents to many different cell types, provided that a cell-specific receptor exists and that an aptamer against the receptor can be selected<sup>176</sup>.

## **2.4 LOCAL GENE DELIVERY**

Local delivery by external stimulations can avoid or delay RES uptake, reduce systemic toxicity, provide organ specificity, and help the delivery system reach the target cells. These environment-sensitive nanoparticles have been designed to release their contents based on the environmental changes leading to controlled drug release, such as temperature, light, ultrasound response, or magnetic stimulus.

### **2.4.1 Bubble liposomes by ultrasound exposure**

Ultrasound technology provides an easy, safe, minimally-invasive, and tissue-specific method for gene delivery into tumors<sup>177</sup>. The bubble liposome (BL) is one of the most favorable ultrasound-aided delivery methods. BLs entrap the ultrasound imaging gas perfluoropropane, exploiting the cavitation bubbles produced by the pressure oscillations of ultrasound. This not only transiently enhances the permeability of a tissue or a cell membrane, reducing the thickness of the unstirred layer of the cell surface and aiding DNA entry into cells<sup>177</sup>, but also affects the intracellular vesicles and trafficking after ultrasound exposure, thus enhancing the escape of gene cargo from the endosome to the cytoplasm and further transfer to the nucleus<sup>178</sup>. Negishi et al<sup>178</sup> have used BLs and ultrasound exposure to enhance targeted liposome-mediated pDNA gene transfection, while Clumakova et al<sup>179</sup> have demonstrated that their PLGA nanoparticle gene vector produced a significantly higher expression of the reporter gene in the tumor after a five-minute ultrasonic treatment than that without ultrasound.

### **2.4.2 Heat and irradiation**

Au nanoparticles (AuNPs) possess vivid optical properties with strong optical resonances associated with their surface plasmons. The optical absorption of AuNPs can be tuned

from 690nm to 900nm in the near-infrared spectral range by varying the relative geometry and size of the core and shell. The plasmon-based optical properties of AuNPs assist in the photothermal ablation of solid tumors, providing a light-triggered release of short DNA strands conjugated to the surface of AuNPs.<sup>180, 129</sup> Ni et al<sup>181</sup> delivered DNAPK shRNAs by PSMA-targeting A10-3 RNA aptamers that selectively sensitized PSMA-positive cells to ionizing radiation, so that the toxicities to normal tissues were reduced.

### **2.4.3 Magnetofection**

Liposomal magnetofection potentiates gene transfection by applying a magnetic field. Wang et al<sup>182</sup> constructed magnetic lipoplexes, which are self-assembling complexes of cationic lipids with plasmid DNA associated with superparamagnetic iron oxide nanoparticles (SPIONs). Liposomal magnetofection provided a threefold improvement in transgene expression over lipofection and knocked down the target protein *in vitro*. *In vivo*, the plasmid delivery efficiency into the tumor was significantly higher via liposomal magnetofection than lipofection.

## **2.5 CONCLUSION AND PERSPECTIVE**

Various strategies have been developed to deliver gene cargos efficiently into target cells by non-viral vectors, which have attracted much attention in recent years. Rationally designed non-viral vectors have exhibited improved *in vivo* stability and pharmacokinetics, little RES uptake, high tumor accumulation, target specificity, efficient endosome release, and nuclear transcription of the encapsulated therapeutic nucleic acids. Even so, we have no doubt that the development of safe, stable, effective, and tumor-

specific nanoparticles for systemic administration remains an unmet goal for successful clinical applications of cancer gene therapeutics.

This literature review leads to the project designs described in Chapter 4 and Chapter 5 of this thesis.

### **3.0 SYSTEMIC DELIVERY OF GEMCITABINE TRIPHOSPHATE VIA LCP NANOPARTICLES FOR NSCLC AND PANCREATIC CANCER THERAPY**

Nucleoside analogues are a significant class of anticancer agents. As prodrugs, they terminate the DNA synthesis upon transforming to their active triphosphate metabolites. However, several *in vivo* delivery hurdles compromise their application in clinical settings. To address these delivery problems, we encapsulated the biologically activate nucleotide analogue (i.e. gemcitabine triphosphate (GTP)), instead of any form of nucleoside (i.e. gemcitabine) derivatives, into a novel Lipid/Calcium/Phosphate nanoparticle (LCP) platform. The therapeutic efficacy of LCP-formulated GTP was evaluated in a panel of human non-small-cell lung cancer (NSCLC) and human pancreatic cancer models after systemic administrations. GTP-loaded LCPs induced cell death and arrested the cell cycle in the S phase. *In vivo* efficacy studies showed that intravenously injected GTP-loaded LCPs triggered effective apoptosis of tumor cells, significant reduction of tumor cell proliferation and cell cycle progression, leading to dramatic inhibition of tumor growth, with little *in vivo* toxicity. Broadly speaking, the current study offers preclinical proof-of-principle that many active nucleotide or phosphorylated nucleoside analogues could be encapsulated in the LCP nanoplatform and delivered systemically for a wide variety of therapeutic applications.

---

Reference: Yuan Zhang, William Y Kim, Leaf Huang. Systemic delivery of gemcitabine triphosphate via LCP nanoparticles for NSCLC and pancreatic cancer therapy. *Biomaterials*. 2013 Feb 1. doi: 10.1016/j.biomaterials.2013.01.063.

### 3.1 INTRODUCTION

Cytotoxic nucleoside analogues have received considerable attention as clinical cancer treatments, including treatments for hematological malignancies and solid tumors<sup>183</sup>. About 20% of small molecule therapeutics that have been approved by the FDA for cancer treatment are nucleoside analogues or related compounds<sup>184</sup>. These drugs act as antimetabolites by interfering with nucleic acid synthesis and enzymes of nucleotide metabolism<sup>185</sup>.

Gemcitabine (2', 2'-difluoro 2'-deoxycytidine) (Gem) is a nucleoside analogue widely used in chemotherapy as a first-line treatment of various carcinomas, including non-small cell lung cancer (NSCLC) and pancreatic cancer<sup>186</sup>. As a prodrug, Gem relies on nucleoside transporters to enter into cells. The overall drug uptake depends on the balance of the nucleoside transporters and drug efflux proteins presented on the cell membrane. Once in the cells, Gem undergoes sequential phosphorylation into 5'-triphosphates by deoxycytidine kinase (dCK) before it can be incorporated into DNA and cause DNA synthesis inhibition, which leads to DNA damage and cell apoptosis. Triphosphates are the active forms of nucleotides in biosynthesis and energy conversions. Nucleoside monophosphates are converted into nucleoside triphosphates by two steps. First, nucleoside monophosphates are converted into diphosphates by specific nucleoside monophosphate kinases that utilize ATP as the phosphoryl-group donor. Second, nucleoside diphosphates and triphosphates are interconverted by nucleoside diphosphate kinase which has broad specificity. However, processes of mutational resistance readily occur in the nucleoside activation process, which makes Gem less efficacious. Examples of mutational resistance include down-regulation of nucleoside influx transporters (e.g.

ENT1, ENT2, CNT1, CNT3), up-regulation of drug efflux proteins (e.g. MRP, BCRP), and inactivation of dCK<sup>187</sup>. In addition, Gem is rapidly metabolized to 2',2'-difluorodeoxyuridine by the deoxycytidine deaminase and quickly excreted by the kidney following *in vivo* administration. The overall *in vivo* delivery hurdles of Gem are shown in **Figure 3.1**.

### *In vivo* delivery hurdles of Gemcitabine

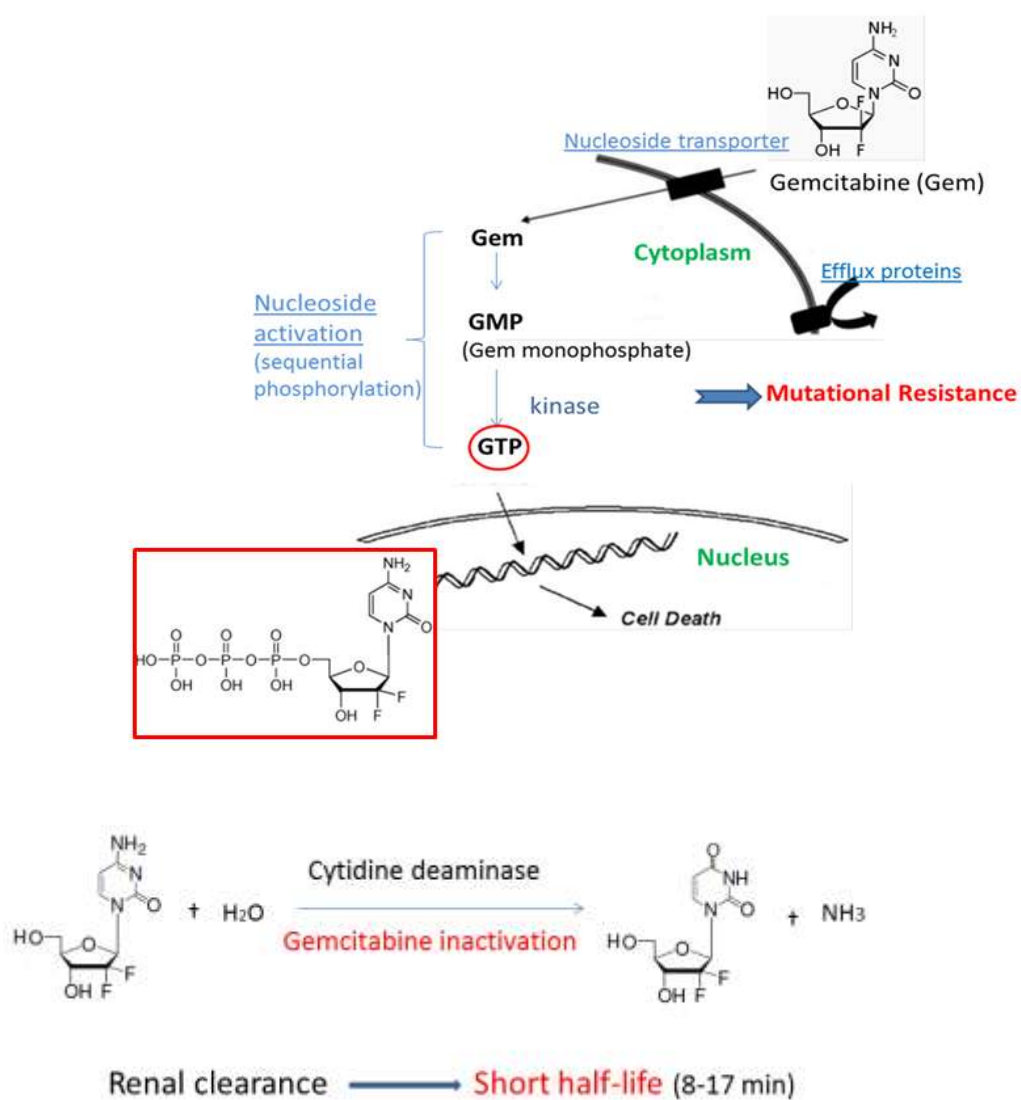


**Figure 3.1** *In vivo* delivery hurdles of Gemcitabine.



In order to enhance the *in vivo* delivery efficiency of Gem and overcome the aforementioned delivery challenges, our strategy is to entrap the bioactive form of Gem, gemcitabine triphosphate (GTP), into a cell-specific, targeted Lipid/Calcium/Phosphate nanoparticle (LCP). In this way, the metabolism mechanisms of Gem will be bypassed and the bioactive drug will be delivered directly into the cell through receptor-mediated endocytosis. Furthermore, LCPs can protect GTP from enzymatic breakdown, preventing inactivation within circulation and rapid excretion by the kidney.

Nanoparticles (NPs) are prone to lysosomal degradation after endocytosis. To avoid the degradation of entrapped drugs, NPs must be able to escape from endosomes before trafficking to lysosomes. In order to achieve this goal, we used calcium phosphate (CaP) precipitate to entrap GTP. The CaP core of the LCPs is dissolvable in endosomes due to its low pH<sup>188</sup>. Increase in osmotic pressure in the endosome leads to endosome swelling and rupture, releasing the entrapped GTP into the cytoplasm and allowing it to enter into the nucleus. A lipid bilayer membrane surrounds the GTP-entrapped CaP core and a high density of polyethylene glycol (PEG), either with or without a tethered targeting ligand anisamide (AA), was grafted onto the surface. These characteristics increased the tumor accumulation of the drug through the enhanced permeability and retention (EPR) effect<sup>189</sup>. They also allowed tumor specific targeting and reduced reticuloendothelial system (RES) uptake<sup>190</sup>.

In this study, the feasibility of using the novel LCPs as a nanocarrier for the delivery of biologically active GTP was evaluated on human NSCLC and pancreatic cancer models. The small molecule ligand anisamide (AA) was modified on the LCP for specific tumor targeting via the sigma receptors that are overexpressed in many human cancer cells.

Since cytidine triphosphate (CTP) has a similar structure to GTP and does not have any therapeutic activity, CTP-loaded LCPs were prepared as control nanoparticles. The cytotoxic activity of LCP-formulated GTP was compared with free GTP and its prodrug, Gem, both *in vitro* and *in vivo*.

## **3.2 MATERIALS AND METHODS**

### **3.2.1 Materials**

Gemcitabine triphosphate tris(triethylammonium) salt was synthesized by Bioduro company (Beijing, China). Gemcitabine was purchased from HDH Pharma, Inc. (Research Triangle Park, NC). 1, 2-Dioleoyl-3-trimethylammonium-propane chloride salt (DOTAP), dioleoyl phosphatidic acid (DOPA), and 1,2-distearoyl-sn-glycero-3-phosphoethanolamine-N-[methoxy(polyethyleneglycol-2000) ammonium salt (DSPE-PEG<sub>2000</sub>) were purchased from Avanti Polar Lipids, Inc. (Alabaster, AL). DSPE-PEG-anisamide (AA) was synthesized in our lab as described previously [9]. Other chemicals were obtained from Sigma-Aldrich (St. Louis, MO).

### **3.2.2 Cell culture**

H460 human NSCLC cells and BxPC-3 human pancreatic cancer cells, originally obtained from American Type Culture Collection (ATCC), were cultured in a RPMI-1640 medium (Invitrogen, Carlsbad, CA) supplemented with 10% fetal bovine serum, 100 U/mL penicillin, and 100 µg/mL streptomycin (Invitrogen). Cells were cultivated in a humidified incubator at 37°C and 5% CO<sub>2</sub>.

### 3.2.3 Experimental animals

Female nude mice that were 6-8 weeks of age were used in all studies. To establish the xenograft models,  $5 \times 10^6$  cells in 100  $\mu\text{L}$  of PBS were injected subcutaneously into the right flank of the mice. All work performed on animals was approved by the Institutional Animal Care and Use Committee at the University of North Carolina at Chapel Hill.

### 3.2.4 Preparation of GTP-loaded LCPs

The LCP cores were prepared by water-in-oil micro-emulsions in the oil phase containing cyclohexane/ Igepal CO-520 solution (71/29, v/v)<sup>192</sup>. One hundred and eighty  $\mu\text{L}$  of 20 mM GTP was mixed with 12.5 mM  $\text{Na}_2\text{HPO}_4$  (pH=9.0) to the total volume of 600  $\mu\text{L}$  before the addition of a 20 mL oil phase with continuous stirring. The calcium micro-emulsion was prepared by adding 600  $\mu\text{L}$  of 2.5 M  $\text{CaCl}_2$  to a separate 20 mL oil phase. Four hundred  $\mu\text{L}$  of 20 mM DOPA in chloroform was added to the phosphate phase and then the two separate micro-emulsions were mixed. After stirring for 5 min, another 400  $\mu\text{L}$  of 20 mM DOPA was added into the emulsion. The emulsion was stirred continuously for 20 min before 40 mL of absolute ethanol was added. The ethanol emulsion mixture was centrifuged at 9,000 g for 15 min to pellet the LCP core and the supernatant was discarded. The LCP core was washed twice with absolute ethanol and dried under  $\text{N}_2$ . The LCP core pellets were dissolved in 2 mL chloroform and stored in a glass vial at  $-20^\circ\text{C}$  for future use. To prepare the final GTP-loaded LCPs (GTP-LCP-PEG) with an outer lipid coating, 330  $\mu\text{L}$  LCP core in chloroform was mixed with 38.7  $\mu\text{L}$  of 10 mg/ml cholesterol, 28  $\mu\text{L}$  of 25 mg/ml DOTAP, 96  $\mu\text{L}$  of 25 mg/ml DSPE-PEG. After evaporating the chloroform, the residual lipids were dissolved in 30  $\mu\text{L}$  THF followed by 50  $\mu\text{L}$  absolute ethanol, and then suspended in 160  $\mu\text{L}$  water. After brief sonication, the

solution was dialyzed in distilled water to remove THF and ethanol. The AA-targeted GTP-loaded LCPs (GTP-LCP-PEG-AA) were prepared in the same way, except that 20% DSPE-PEG was replaced by an equal molar amount of DSPE-PEG-AA.

### **3.2.5 Characterization of GTP-loaded LCPs**

The particle size and zeta potential of LCPs were determined by Dynamic light scattering (DLS) using a Malvern ZetaSizer Nano series (Westborough, MA). GTP encapsulation efficiency was measured by a UV spectrophotometer (Beckman Coulter Inc., DU 800 spectrophotometer). Transmission electron microscope (TEM) images of GTP-loaded LCPs were acquired through the use of JEOL 100CX II TEM (Tokyo, Japan). Briefly, 4  $\mu$ l of LCP solution was dropped onto a 300 mesh carbon coated copper grid (Ted Pella, Inc., Redding, CA) for 2 min. Excess fluid was removed with filter paper, and the copper grid was dried before observation with TEM. To determine the release kinetics of GTP-loaded LCP nanoparticles, 250  $\mu$ L of GTP-loaded nontargeted or targeted particle solution was placed in a dialysis bag (MWCO 10,000 Da), and dialysis against 10 mL PBS buffer at 37°C with gentle shaking (50 rpm). Aliquots of release medium were withdrawn at designated time points, and equal amount of fresh PBS buffer was replenished. The GTP concentration was then measured by HPLC, with mobile phase containing 10% MeOH/90% 20 mM  $\text{NH}_4\text{OAc}$ . The flow rate was 1 mL/min at 20°C and the UV detection wavelength was set at 254 nm.

### **3.2.6 *In vitro* cellular uptake**

In the preparation of LCPs, small amount of NBD-labeled phosphatidic acid was used to label the LCP cores. H460 cells were seeded in 24-well plates (Corning Inc., Corning, NY) with cover glass. Twenty-four h later, cells were treated with NBD labeled LCP

formulations at 37°C for 1 h. After washing twice with PBS, cells were fixed with 4% paraformaldehyde at room temperature for 10 min, and stained the nuclei with DAPI (Vector Lab, Burlingame, CA) before imaging with a Leica SP2 Confocal Laser Scanning Microscope (Germany). In the receptor competitive inhibition experiment, cells were pre-incubated with 50  $\mu$ M haloperidol (a sigma receptor agonist) for 1 h prior to the incubation with NBD labeled GTP-LCP-PEG-AA for 1 h. To quantify the cellular uptake efficiency, H460 cells were seeded in 6-well plates 24 h before the treatment of NBD labeled LCPs for 1 h. Then cells were harvested and washed with PBS, and the NBD fluorescence intensity in the cells was detected by a FACS Canto flow cytometry (BD Biosciences). A total of 10,000 events were acquired for each sample and the mean fluorescence intensity of NBD in the cells was analyzed with FACS Diva software (BD Biosciences).

### **3.2.7 *In vitro* cytotoxicity assay**

*In vitro* cytotoxicity of GTP-loaded LCPs and free drugs (GTP, Gem) was determined using the 3-[4, 5-dimethylthiazol-2-yl]-2, 5-diphenyltetrazolium bromide (MTT) assay. Cells were seeded in 96-well plates. When cells reached 30% confluence, different concentrations of GTP-LCP-PEG-AA, GTP-LCP-PEG, GTP, Gem, and CTP-LCP-PEG-AA were added to the medium. After 48 h exposure to the LCPs and free drugs at 37°C, MTT (Biosynth Inc.) was added to each well with a final concentration of 0.5 mg/mL, and incubated with cells at 37°C for 4 h. The absorbance at a wavelength of 570 nm was measured with a microplate reader. Cell viability was calculated as the percentage of the absorbance of the treated cells to that of untreated cells.

### 3.2.8 Cell cycle analysis

Cells ( $2 \times 10^5$ ) were seeded in 6-well plates, and GTP-LCP-PEG-AA, GTP-LCP-PEG, GTP, Gem, and CTP-LCP-PEG-AA were added the following day resulting in a final concentration of  $1.8 \mu\text{M}$ . After 24 h incubation, cells were trypsinized and washed with PBS followed by fixation in pre-cooled 70% ethanol at  $-20^\circ\text{C}$  for at least 1 h. Fixed cells were washed with PBS staining buffer (BD Pharmingen, San Diego, CA) and incubated with RNAase (final concentration  $75 \mu\text{g/mL}$ ) at  $37^\circ\text{C}$  for 30 min, followed by incubation with  $10 \mu\text{g}$  propidium iodide (PI) at room temperature for 30 min. Finally, cells were washed and suspended in PBS, and analyzed with a FACS Canto flow cytometry (BD Biosciences) to measure the PI intensity, which correlates with the DNA content in the cell cycle. A total of 10,000 events were acquired for each sample and data were analyzed with FACS Diva software (BD Biosciences).

### 3.2.9 Caspase activation

Cells ( $2 \times 10^5$ ) were seeded in 6-well plates, and treated with GTP-LCP-PEG-AA, GTP-LCP-PEG, CTP-LCP-PEG-AA, GTP, and Gem with a dose of  $1.8 \mu\text{M}$  for 48 h. For the *in vivo* caspase activation study, H460 and BxPC-3 tumor-bearing mice were given 3 daily intravenous (IV) injections of GTP-LCP-PEG-AA, GTP-LCP-PEG, CTP-LCP-PEG-AA, GTP, and Gem with a dose of  $7.5 \mu\text{mol/Kg}$  ( $1.98 \text{ mg/Kg}$  in terms of Gem). Twenty-four hours after the last injection, mice were sacrificed and tumors were harvested. The cells and tumor tissues were lysed with a radioimmunoprecipitation assay (RIPA) buffer that was supplemented with a protease inhibitor cocktail (Promega, Madison, WI). Protein concentrations were determined using the BCA assay kit (Pierce Biotechnology) following the manufacturer's recommendations. Forty  $\mu\text{g}$  protein of each sample was

used to detect caspase-3/7 activity of the cell or tumor lysates according to the manufacturer's instructions (Promega).

### **3.2.10 Western blot analysis**

Twenty-four h after 3 daily IV injections, H460 and BxPC-3 tumor-bearing mice were sacrificed and tumor lysates were prepared as previously described. Forty  $\mu$ g of protein per lane was separated by 4%-12% SDS-PAGE electrophoresis (Invitrogen) before being transferred to polyvinylidene difluoride (PVDF) membranes (Bio-Rad). The membranes were blocked for 1h with 5% silk milk at room temperature and then incubated with mouse monoclonal poly(ADP-ribose) polymerase-1 (PARP-1) antibodies and rabbit polyclonal cyclin D1 antibodies (1:500 dilution; Santa Cruz biotechnology, Inc.) overnight at 4°C.  $\beta$ -actin antibody (1:4000 dilution; Santa Cruz biotechnology, Inc.) was probed as the loading control. The membranes were washed 3 times and then incubated with a secondary antibody (1:4000 dilution; Santa Cruz biotechnology, Inc.) at room temperature for 1 h. Finally, the membranes were washed 4 times and developed by an enhanced chemiluminescence system according to the manufacturer's instructions (Thermo scientific).

To confirm sigma receptor expressions on NSCLC and pancreatic cell lines, forty  $\mu$ g protein in different cell lysates were probed with sigma receptor antibody (1:500 dilution; Santa Cruz biotechnology, Inc.) and  $\beta$ -actin antibody (1:4000 dilution; Santa Cruz biotechnology, Inc.) overnight at 4°C. Goat anti-mouse secondary antibody was used to detect sigma receptor and  $\beta$ -actin primary antibody.

### 3.2.11 Immunostaining

*In vivo* tumor cell apoptosis after systemic administration was determined by the TdT-mediated dUTP Nick-End Labeling (TUNEL) assay. H460 and BxPC-3 tumor-bearing mice were given 3 daily IV injections of GTP-LCP-PEG-AA, GTP-LCP-PEG, CTP-LCP-PEG-AA, GTP, and Gem with a GTP dose of 7.5  $\mu\text{mol/Kg}$ . Twenty-four h after the final injection, mice were sacrificed and tumors were fixed in 10% formalin for 24 h before being embedded in paraffin and sectioned at a thickness of 5  $\mu\text{m}$ . The TUNEL staining was performed as recommended by the manufacturer (Promega). DAPI mounting medium was dropped on the sections for nucleus staining. Images of TUNEL-stained tumor sections were captured with a fluorescence microscope (Nikon Corp., Tokyo, Japan). The percentage of apoptotic cells was obtained by dividing the number of apoptotic cells (TUNEL positive cells shown as green dots in **Fig. 5**) from the number of total cells (blue nuclei stained by DAPI, not shown) in each microscopic field, and 10 representative microscopic fields were randomly selected in each treatment group ( $n=3$ ) for this analysis.

Proliferation of tumor cells after the aforementioned treatments and dosing schedule was detected by immunohistochemistry, using an antibody against proliferating cell nuclear antigen (PCNA) (1:200 dilution, Santa Cruz). The immunohistochemistry was performed using a mouse-specific HRP/DAB detection IHC kit as recommended by the manufacturer (Abcam, Cambridge, MA). The percentage of proliferation cells was obtained by dividing the number of PCNA positive cells (shown as brown dots) from the number of total cells (blue nuclei stained by hematoxylin) in each microscopic field, and



10 representative microscopic fields were randomly selected in each treatment group (n=3) for counting.

In addition to H460 and BxPC-3 xenograft models, we also tested the therapeutic response of GTP-LCP-PEG-AA on a NSCLC A549 xenograft model and a panel of pancreatic xenograft models, including Mia PaCa-2, AsPC-1, Capan-1, CFPAC-1, PANC-1 and SW1990 *in vivo*. Results were measured by TUNEL assay and PCNA immunohistochemistry.

### **3.2.12 Pharmacokinetic profile of GTP-loaded LCPs**

In the preparation of GTP-loaded LCPs, we mixed a trace amount of radioactive cytidine 5' triphosphate (CTP) [ $5\text{-}^3\text{H}$ ] disodium salt (American Radiolabeled Chemicals, Inc., 1mCi/mL) with GTP. Tritium labeled CTP served as a marker for the entrapped GTP. Thus, by measuring the tritium radioactivity, the percentage of GTP-loaded LCPs or free GTP circulating in the blood can be calculated. Nude mice bearing H460 tumors were IV injected with tritium-labeled, GTP-loaded LCPs or free GTP. At 20 min, 1 h, 2 h, 4 h, 8 h, 24 h post injection time point, 30  $\mu\text{L}$  blood was drawn from the venous plexus of the eyes of the mice, and was mixed with 4 mL scintillation cocktail (Thermo Fisher Scientific Inc.). In order to avoid color interference with the scintillation counting, 120  $\mu\text{L}$  of hydrogen peroxide (30% in water) was added to samples and vortexed to bleach the blood color before measurement. The tritium radioactivity in blood samples was counted using a liquid scintillation analyzer (Packard BioScience Co. TRI-CARB 2900TR). The percentage of the injected dose (%ID) in the blood was calculated based on the tritium DPM (Disintegrations per minute) values using an established standard curve. The initial concentration was set as 100% of the injected dose (ID). The post injection time (t)

and %ID were fitted with a non-compartment model using the WinNonlin program and the key PK parameters were calculated.

### **3.2.13 Tumor growth inhibition and toxicity study**

A tumor growth inhibition study was completed on H460 and BxPC-3 subcutaneous xenograft mouse models. When the tumor volumes reached about 150-200 mm<sup>3</sup>, the mice were randomly assigned into 6 treatment groups (n=5), and intravenously injected different formulations, including GTP-LCP-PEG-AA, GTP-LCP-PEG, CTP-LCP-PEG-AA, GTP, and Gem. IV injections were performed every other day for a total of four injections at a GTP dose of 7.5 µmol/Kg. Tumor sizes were measured every other day with calipers across their two perpendicular diameters, and the tumor volume was calculated using the following formula:

$V=0.5 \times (W^2 \times L)$ , where V = tumor volume, W = the smaller perpendicular diameter and L = the larger perpendicular diameter. Body weight of each mouse was recorded every other day. Humane sacrifice of mice was performed when tumors reached 20 mm in one dimension.

To test whether GTP-loaded LCPs would induce hepatic and renal dysfunction after frequent multiple dosing, mice were given three daily IV injections, and 24 h after the final injection, blood was drawn from the venous plexus of the eyes of the mice. Blood samples were immediately centrifuged at 3,000 g for 5 min at 4°C, and the supernatant blood serums were collected for hematological analysis. Blood urine nitrogen (BUN), creatinine, aspartate aminotransferase (AST), alanine aminotransferase (ALT) values were recorded, as indications of hepatic and renal functions.

### 3.2.14 Statistical analysis

Results were expressed as a mean  $\pm$  standard deviation (SD). Student's t-test and one-way analysis of variance (ANOVA) test were used to evaluate statistical significance. A  $p$  value of  $p < 0.05$  was considered to indicate statistical significance.

## 3.3 RESULTS

### 3.3.1 Characterization of GTP-loaded LCPs

The GTP used in this study is gemcitabine triphosphate tris(triethylammonium) salt (**Fig 3.2A**) which is synthesized as previously reported<sup>193</sup>. The particle sizes and zeta potentials of different LCP formulations were shown in **Table 3.1**. The GTP-loaded LCPs were homogeneous and spherical in shape, as shown in the TEM micrograph (**Fig 3.2B**). The encapsulation efficiency of GTP in LCPs was around 25%, as measured by UV spectrometry at a wavelength of 288 nm (data not shown). The GTP release profile from LCP nanoparticles were shown in **Fig 3.2D**. About 70-80% GTP was released from the particles in 48 h.

**Table 3.1 Particle size and zeta potential of LCPs.**

	Size (nm)	Zeta potential (mV)
GTP-LCP-PEG-AA	42.0 $\pm$ 9.0	25.4 $\pm$ 5.7
GTP-LCP-PEG	37.7 $\pm$ 7.2	7.2 $\pm$ 3.1
CTP-LCP-PEG-AA	33.4 $\pm$ 7.7	18.9 $\pm$ 5.4

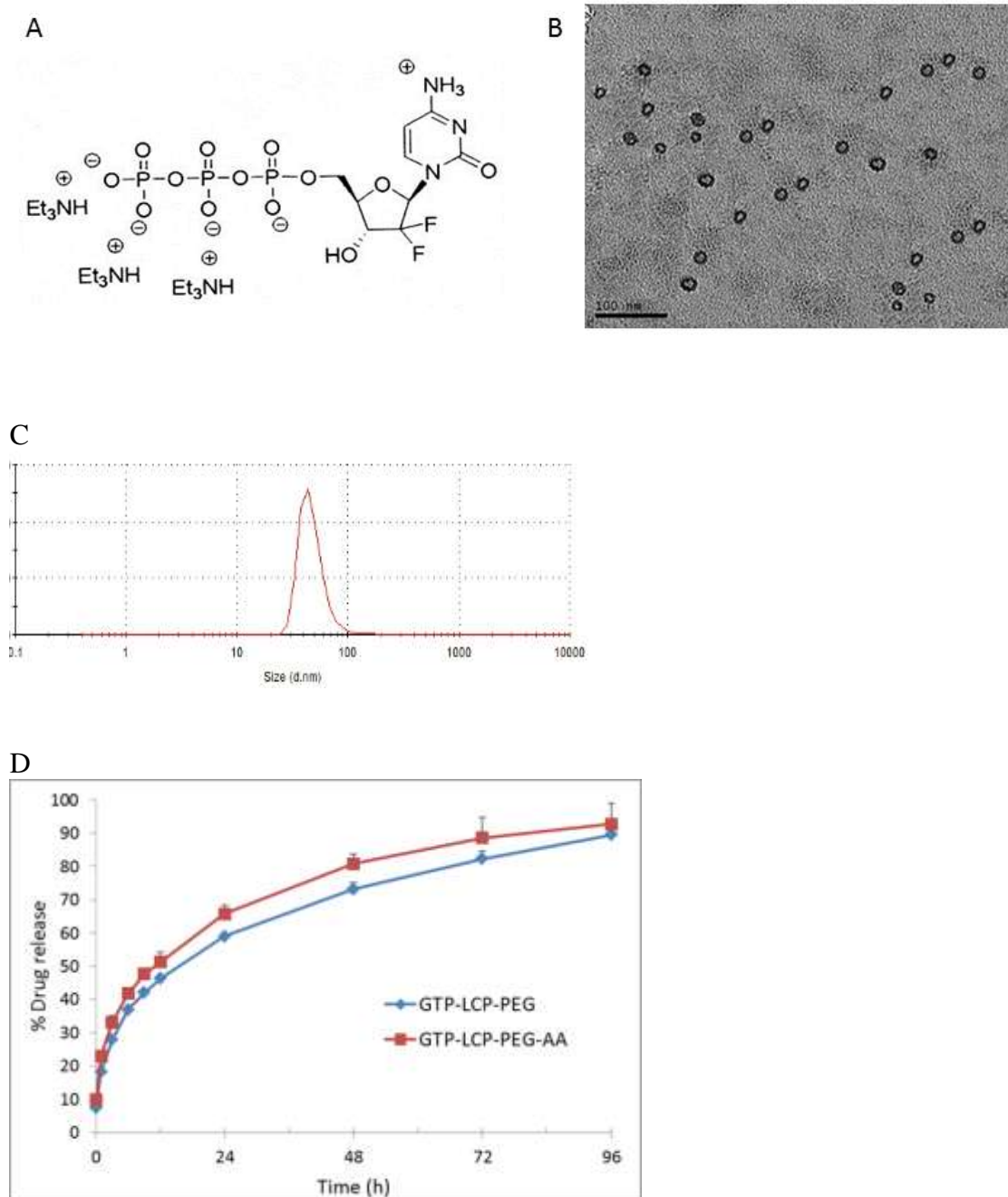


**Figure 3.2 Physiochemical characterization of GTP-loaded LCPs.** (A) The chemical structure of GTP (Gemcitabine triphosphate tris(triethylammonium) salt) used in this study. (B) TEM image of GTP-loaded LCPs. (C) Particle size distribution measured by DLS. (D) *In vitro* drug release of GTP from LCP nanoparticles in PBS buffer at 37 °C. The error bars were obtained from triplicate samples. Data are shown as mean  $\pm$  SD.

### 3.3.2 *In vitro* specific tumor cell targeting

The cellular uptake of GTP-LCP-PEG-AA and GTP-LCP-PEG at 37°C is shown in **Fig 3.3**. It is clear that the cellular endocytosis of AA-modified LCP was higher than that of untargeted LCP as shown by confocal images (**Fig 3.3A**). The addition of haloperidol, a known agonist for sigma receptors, significantly reduced the cellular uptake of AA-modified LCP, suggesting AA modification on the LCP induce sigma receptor-mediated endocytosis. The quantitative flow cytometry also confirmed that the AA ligand increased the intracellular uptake of LCPs (**Fig 3.3B-3.3C**).

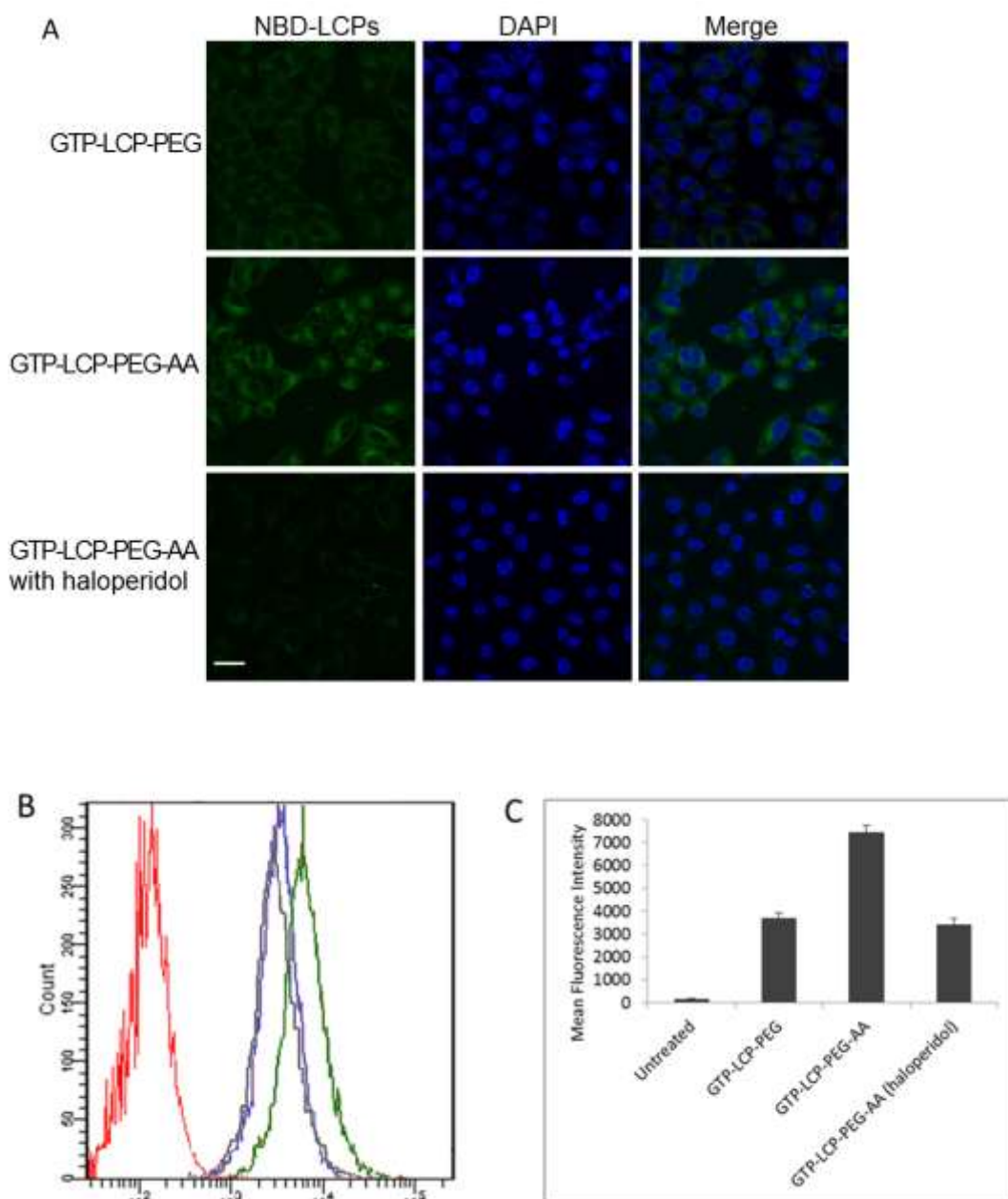
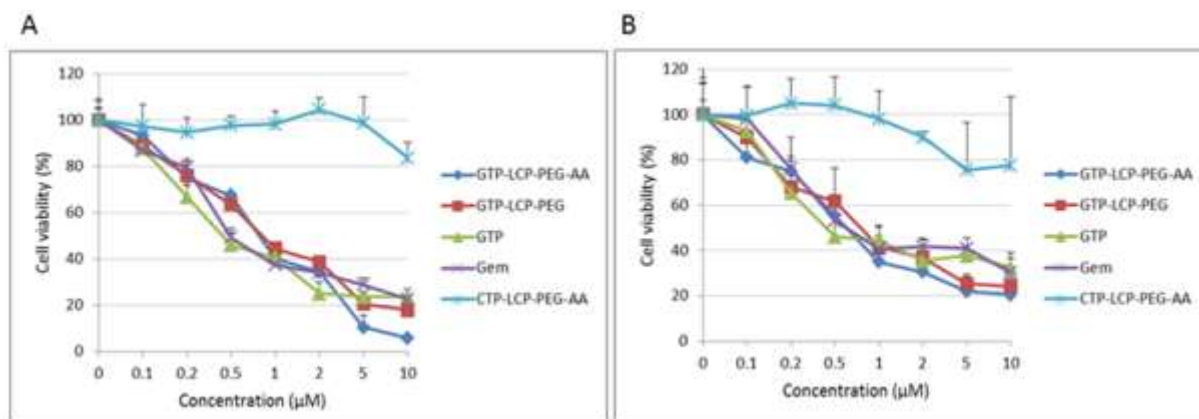


**Figure 3.3 The cellular uptake of GTP-LCP-PEG and GTP-LCP-PEG-AA at 37°C for 1 h on H460 cells.** (A) Confocal images for intracellular uptake. Green: NBD labeled LCP nanoparticles; Blue: DAPI stained nuclei. Scale bar, 15  $\mu$ m. (B) Flow cytometry study of cellular uptake. Red: untreated control cells; Blue: GTP-LCP-PEG; Green: GTP-LCP-PEG-AA. Gray: GTP-LCP-PEG-AA after haloperidol (50  $\mu$ M) incubation. (C) Quantitative results from flow cytometry by measuring intracellular mean fluorescence intensity. Data are shown as mean  $\pm$  SD.

### 3.3.3 GTP-loaded LCPs reduced the cell viability

The MTT assay was carried out to determine the cell viabilities after the treatment of GTP-loaded LCPs and free drugs. After 48 h incubation, the GTP-loaded LCPs caused dramatic reduction of viable H460 (**Fig 3.4A**) and BxPC-3 (**Fig 3.4B**) cells in a dose-dependent manner. Free Gem and GTP also decreased the cell viability *in vitro*. This observation is explained by the facts that Gem can be taken up into cells through nucleoside transporters and GTP can be metabolized to Gem by the alkaline phosphatase on the cell surface before entering into cells<sup>194</sup>. CTP-loaded LCPs had little effect on cell viability. The IC<sub>50</sub> concentrations for each of the treatments (GTP-LCP-PEG-AA, GTP-LCP-PEG, GTP, Gem, CTP-LCP-PEG-AA) were listed in **Table 3.2**.



The figure legend of Figure 3.4 A and B is on the next page.

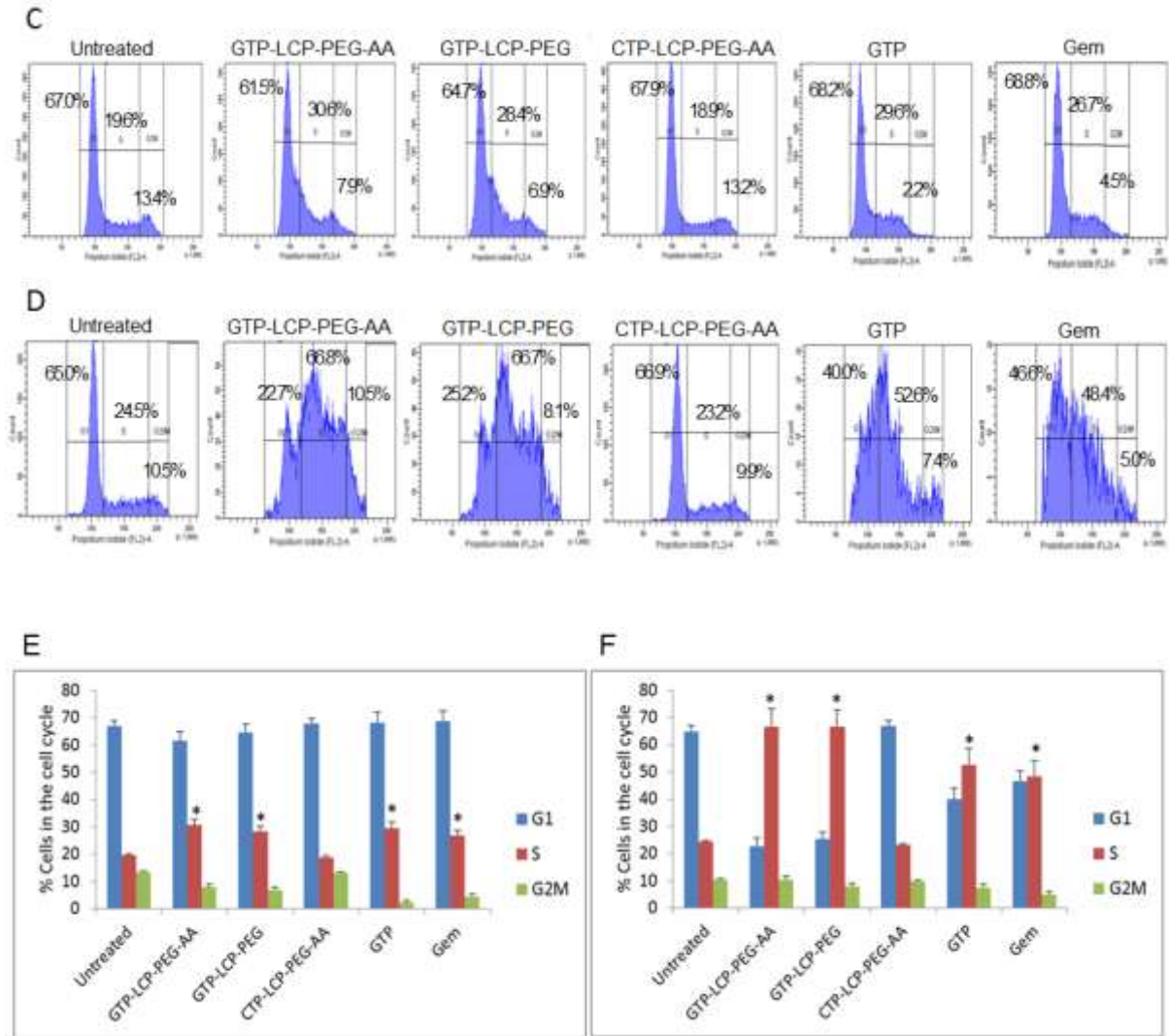


**Figure 3.4** *In vitro* cell viability and cell cycle arrest of GTP-loaded LCPs. (A-B) GTP-loaded LCPs induced potent cytotoxicity *in vitro* on H460 (A) and BxPC-3 (B) cells. The cell viabilities of H460 (A) and BxPC-3 (B) cells were measured by MTT assay after 48 h exposure to GTP-loaded LCPs, CTP-loaded LCPs and free drugs (GTP, Gem). Data are mean  $\pm$  S.D. (n=3). (C-D) Cell cycle arrest on H460 (C) and BxPC-3 (D) cells after 24 h treatment with different formulations and free drugs were analyzed by flow cytometry. The cell population of each sample was gated into three cell cycle phases: G1, S, G2/M. The percentage of H460 or BxPC-3 cells in different cell cycle phases of each sample was shown in the graph, based on the results from FACS software. Statistical analysis of cell cycle on (E) H460 and (F) BxPC-3 cells (n=3). \* $p < 0.05$ , vs Untreated. Data are shown as mean  $\pm$  SD.



**Table 3.2 IC<sub>50</sub> values in each treatment group in MTT assay on H460 and BxPC-3 cells** (concentration unit:  $\mu\text{M}$ , n=3). Data are shown as mean  $\pm$  SD.

IC <sub>50</sub> , $\mu\text{M}$	GTP-LCP- PEG-AA	GTP-LCP- PEG	GTP	Gem
H460	0.80 $\pm$ 0.11	0.85 $\pm$ 0.10	0.45 $\pm$ 0.08	0.50 $\pm$ 0.09
BxPC-3	0.63 $\pm$ 0.08	0.79 $\pm$ 0.09	0.43 $\pm$ 0.06	0.62 $\pm$ 0.07

### 3.3.4 GTP-loaded LCPs arrested the cell cycle in the S phase

We next evaluated the effect of GTP-loaded LCPs on the cell cycle progression. The mechanism of GTP cell-killing is its competition with cytidine triphosphate during DNA replication, which results in the inhibition of chain elongation. The termination of DNA synthesis impedes the cell cycle progression, leading to cell death. After 24 h incubation with GTP-loaded LCPs, the percentage of cells in the S phase increases in H460 and BxPC-3 cells (**Fig 3.4C-3.4D**), indicating the cell cycles were arrested in the S phase. GTP-loaded LCPs inhibited DNA synthesis by interfering with the progress toward the completion of S-phase in the cell cycle<sup>195</sup> because the process of incorporating nucleotides generally occurs during DNA replication in the S phase of the cell cycle<sup>196</sup>. CTP-loaded LCPs had no effect on cell cycle alteration in both cell lines (**Fig 3.4C-3.4D**). The statistical analysis of the cell cycle result was listed in **Fig 3.4E-3.4F**.

### 3.3.5 GTP-loaded LCPs induced caspase activation *in vitro* and *in vivo*

Caspases are activated in cells when cells undergo the apoptotic process. Among them, caspase-3 and caspase-7 are primarily responsible for the proteolytic cleavage of a large number of substrates during apoptosis<sup>197</sup>. As shown in **Fig 3.5**, the *in vitro* caspase-3/7 activities of GTP-loaded LCPs and free drug (GTP, Gem) treatments were significantly

higher than the control in H460 (**Fig 3.5A**) and BxPC-3 (**Fig 3.5B**) cells. *In vivo* caspase activation was tested on H460 and BxPC-3 xenograft models. Twenty-four h after 3 daily IV injections, the caspase-3/7 activity in tumors after the treatment of GTP-loaded LCPs was significantly higher than that of free drugs in H460 (**Fig 3.5C**) and BxPC-3 (**Fig 3.5D**) xenografts, indicating that the LCPs greatly improved the *in vivo* delivery efficiency of GTP to the tumors. Our data suggests that free GTP and Gem were able to activate caspase signaling events only *in vitro* and did not elicit caspase activity *in vivo*.

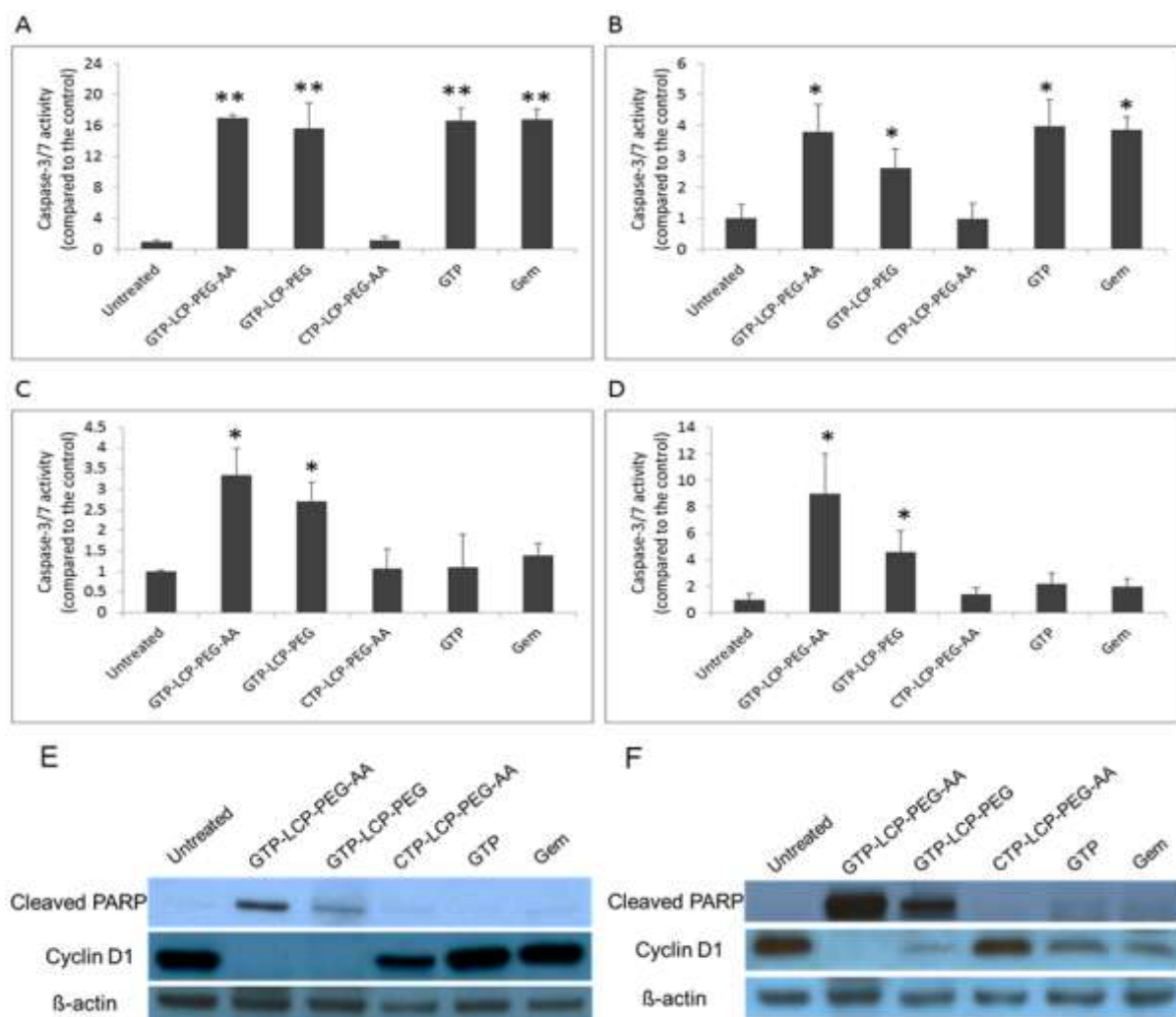


**Figure 3.5 Caspase activation and western blot analysis after different treatments.** (A-D) GTP-loaded LCPs induced caspase activation *in vitro* (A, B) and *in vivo* (C, D). (A-B) *In vitro* caspase activation in H460 (A) and BxPC-3 (B) cells after 48 h incubation with different formulations. (C-D) *In vivo* caspase activation in tumors in H460 (C) and BxPC-3 (D) xenografts after 3 daily IV injections. Statistics were as follows (n=3): \*\* $p < 0.005$  vs. Untreated, \* $p < 0.01$  vs. Untreated. Data are shown as mean  $\pm$  SD. (E—F) GTP-loaded LCPs induced PARP cleavage and reduced cyclin D1 expression level in tumors after 3 daily IV injections in H460 (E) and BxPC-3 (F) xenografts. Twenty-four h after the last injection, tumor lysates were extracted and analyzed by western blots for cleaved PARP, cyclin D1 and  $\beta$ -actin (loading control).

### 3.3.6 GTP-loaded LCPs triggered PARP cleavage and inhibited cell cycle

#### progression *in vivo*

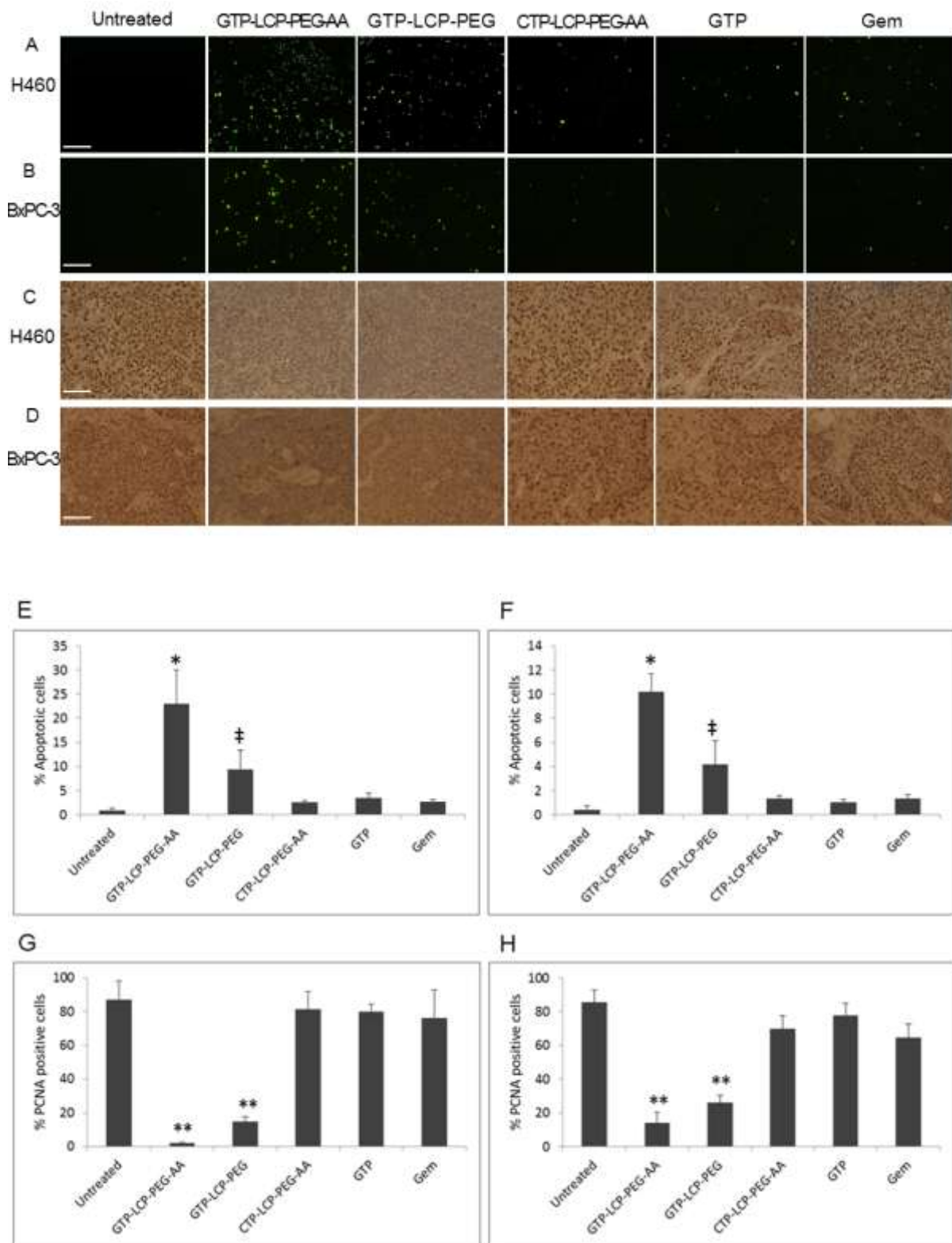
PARP is mainly involved in DNA repair induction and apoptosis. During the execution phase of apoptosis, intact PARP (116 kDa) is cleaved to its significant segment (85 kDa) by members of the caspase family, mainly caspase-3 and caspase-7<sup>197</sup>, reflecting an immediate cellular response to DNA damage. Therefore, the cleavage of PARP serves as a reliable marker of apoptosis<sup>198</sup>. From the western blots data (**Fig 3.5E and 3.5F**), the cleaved PARP was significantly elevated after the treatment of GTP-loaded LCPs in NSCLC and pancreatic tumors. The cleaved PARP expression level of AA-targeted GTP-loaded LCPs was higher than that of non-targeted LCPs, due to the specific targeting of tumor cells. Free GTP and Gem did not induce PARP elevation and did not trigger apoptosis *in vivo*. This was most likely due to the rapid inactivation and excretion of free GTP and Gem after systemic administration, which results in little cellular apoptotic response. The high expression level of the cleaved PARP coincided with the high caspase-3/7 activity after the treatment of GTP-loaded LCPs *in vivo*, suggesting that the induction of apoptosis by GTP-loaded LCPs was due to the activation of the caspase-dependent pathway<sup>199</sup>.

Cyclin D1 is involved in regulating cell cycle progression. GTP-loaded LCPs dramatically reduced the cyclin D1 expression (**Fig 3.5E and 3.5F**), while free drugs did not show any cell cycle alteration after *in vivo* treatment. CTP-loaded LCPs did not elicit any cellular response in apoptosis induction or cell cycle alteration.

### **3.3.7 GTP-loaded LCPs triggered tumor cell apoptosis and inhibited tumor cell proliferation *in vivo***

Apoptotic signaling cascades result in DNA fragmentation (DNA damage) that can be detected by TUNEL assay. After 3 daily injections, AA-targeted GTP-loaded LCPs elicited the most effective killing effects *in vivo* and triggered a dramatic increase in apoptotic cells in H460 (**Fig. 3.6A and 3.6E**) and BxPC-3 (**Fig 3.6B and 3.6F**) xenograft tumors when compared with the control. Non-targeted GTP-loaded LCPs showed medium cell-killing effects. AA-targeted GTP-loaded LCPs displayed higher efficacy than the non-targeted group, suggesting that the receptor-mediated endocytosis was involved in the *in vivo* cellular uptake of LCPs. Free drugs caused few apoptotic cells *in vivo* after systemic administration, probably because the majority of the free drugs were metabolized and cleared before they encountered the tumor cells. These *in vivo* apoptosis results also agree with the caspase activation and PARP cleavage in tumors shown in **Fig 3.5**.

Next, we detected the inhibition of tumor cell proliferation following different treatments. PCNA is expressed in the cell nuclei during DNA synthesis and can be used as a marker for cell proliferation<sup>200</sup>. From the results, GTP-loaded LCPs significantly decreased the number of PCNA positive cells in H460 (**Fig 3.6C and 3.6G**) and BxPC-3 (**Fig 3.6D and 3.6H**) xenograft tumors compared to the control. However, free drugs and CTP-loaded control LCPs had few anti-proliferative effects. This dramatic reduction of the tumor cell proliferation also related to the reduced cell cycle progression as illustrated by the decreased cyclin D1 protein expression in tumors shown in **Fig 3.5E and 3.5F**.



The figure legend of Figure 3.6 is on the next page.

**Figure 3.6 GTP-loaded LCPs triggered tumor cell apoptosis and inhibited tumor cell proliferation effectively *in vivo* in H460 and BxPC-3 xenografts.** Mice were given 3 daily IV injections. Twenty-four h after the last injection, mice were sacrificed and tumor tissues were sectioned for TUNEL assay (A, B) and PCNA immunohistochemistry (C, D). The immunostaining results of H460 tumors (A, C), BxPC-3 tumors (B, D) were shown. (E-F) Percentage of apoptotic cells in H460 (E) and BxPC-3 (F) xenograft tumors after the treatment of different formulations. (G-H) Percentage of PCNA positive cells in H460 (G) and BxPC-3 (H) xenograft tumors after the treatment of different formulations. Statistics were as follows (n=10): (E)  $*p<0.01$ : GTP-LCP-PEG-AA *vs.* Untreated;  $\ddagger p<0.05$ : GTP-LCP-PEG *vs.* Untreated. (F)  $*p<0.01$ : GTP-LCP-PEG-AA *vs.* Untreated;  $\ddagger p<0.05$ : GTP-LCP-PEG *vs.* Untreated. (G)  $**p<0.0005$  *vs.* Untreated. (H)  $**p<0.0005$  *vs.* Untreated. Data are shown as mean  $\pm$  SD.

We also tested the anti-tumor potency of AA-targeted GTP-loaded LCPs on a panel of NSCLC (A549) and pancreatic cancer (Mia PaCa-2, AsPC-1, Capan-1, CFPAC-1, PANC-1 and SW1990) xenograft models by TUNEL assay and PCNA immunohistochemistry (**Fig 3.7**). These NSCLC and pancreatic cancer cells have been reported to overexpress sigma receptors<sup>201-203</sup>. Our data suggest that systemic treatment of GTP-LCP-PEG-AA induced a significantly higher fraction of apoptotic cells (~4% to 12%, **Fig 3.7B**) and decreased the number of proliferating cells (2 to 4 folds lower, **Fig 3.7C**) in tumors compared to the corresponding untreated tumors in all NSCLC and pancreatic cancer models tested. These data suggest that GTP-loaded LCP delivery platform was efficacious in many tumor malignancies.

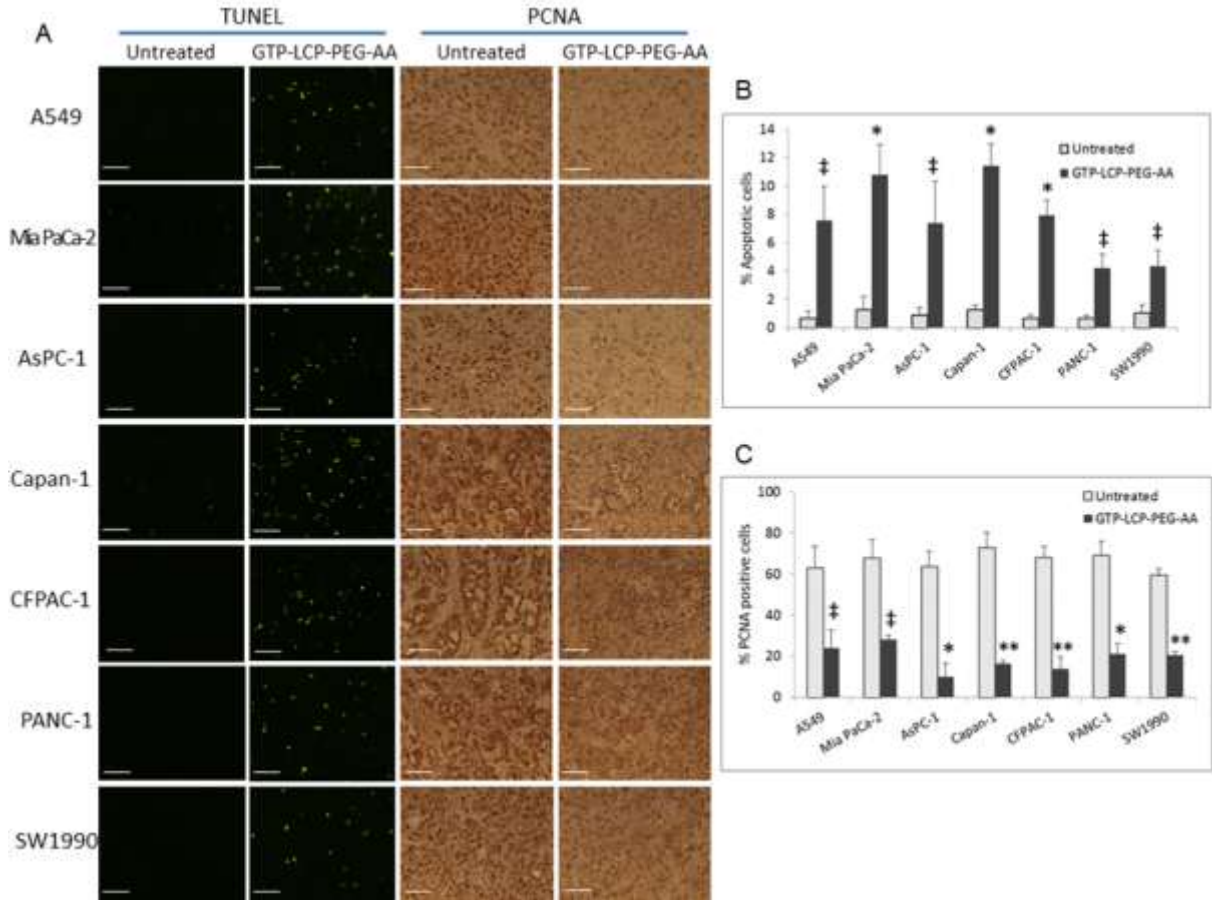


**Figure 3.7 AA-targeted and GTP-loaded LCPs triggered tumor cell apoptosis and inhibited tumor cell proliferation effectively *in vivo* in NSCLC A549 tumor and a panel of pancreatic tumor xenografts.** (A) Twenty-four h after 3 daily IV injections, mice were sacrificed and tumor tissues were sectioned for TUNEL assay and PCNA immunohistochemistry. Scale bar, 100  $\mu$ m. (B) Percentage of apoptotic cells in tumors after the treatment of GTP-LCP-PEG-AA. (C) Percentage of PCNA positive cells in tumors after the treatment of GTP-LCP-PEG-AA. Statistics were as follows (n=10): (B) \* $p$ <0.01 vs. Untreated; ‡ $p$ <0.05 vs. Untreated. (C) \*\* $p$ <0.0005 vs. Untreated; \* $p$ <0.001 vs. Untreated; ‡ $p$ <0.01 vs. Untreated. Data are shown as mean  $\pm$  SD.



### 3.3.8 GTP-loaded LCPs prolonged blood circulation time *in vivo*

The pharmacokinetics (PK) experiment (**Fig 3.8**) indicated that the GTP-loaded LCPs have prolonged blood circulation time compared to the free GTP. After bolus administration, about 35-40% of the LCPs were retained in the blood circulation after 2 h, while the free GTP was quickly excreted within 20 min. The PK data were fitted with a non-compartment model using the WinNonlin program and the key PK parameters were calculated (**Table 3.3**). There was no significant difference between the PK profiles of AA-targeted and non-targeted LCPs. The results indicated that GTP-loaded LCPs increased the area under the curve (AUC) more than 25 fold and decreased the clearance more than 25 fold compared to the free GTP. The mean residence time (MRT) increased about 7 fold, the steady state volume of distribution ( $V_{ss}$ ) decreased about 4 fold. Thus, compared to free GTP, LCP-formulated GTP had less chance to distribute into tissues, leading to an increase in plasma concentration profile. Taken together, incorporation GTP in LCPs increased the drug retention in the circulation, and reduced the drug distribution and clearance, which results in the effective therapeutic response occurring at a low dose.

The pharmacokinetic profile of prodrug gemcitabine is expected to be similar to that of GTP, because nucleoside analogs are primarily cleared by the kidney after intravenous administration. Nucleoside metabolism or phosphorylation does not contribute significantly to the total clearance of the prodrug.<sup>253</sup>

The systemic clearance of Gem in human is ranged from 29.2 L/h/m<sup>2</sup> to 92.2 L/h/m<sup>2</sup> depending on gender and age (renal clearance is 2-7 L/h/m<sup>2</sup>). Clearance appears to decrease with age, and clearance for women is lower than the values for men.<sup>254</sup>

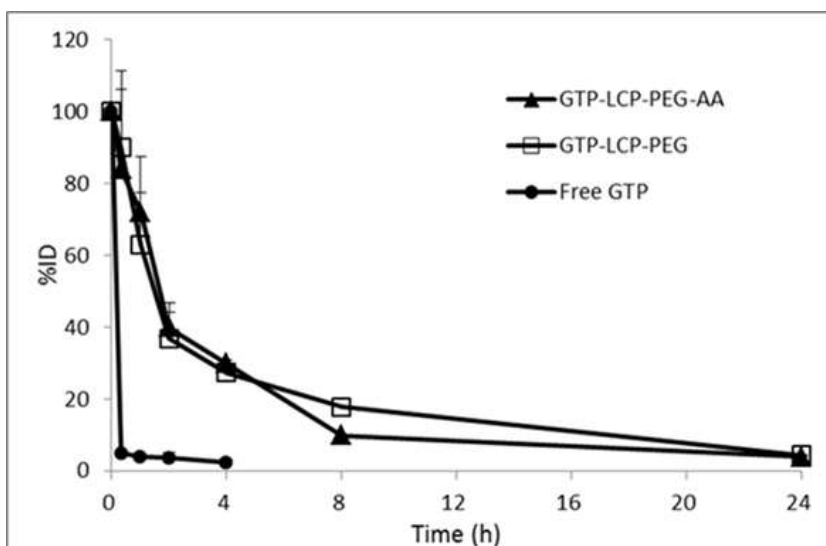


**Figure 3.8** Percentage of the GTP injected dose (%ID) in blood after intravenous bolus administration of GTP-loaded LCPs and free GTP in H460 tumor-bearing mice (n=3).

**Table 3.3** The key pharmacokinetic parameters of GTP-loaded LCPs and free GTP in H460 xenograft model. *Abbreviations:*  $t_{1/2}$ , elimination half-life; AUC: area under the curve; MRT: mean residence time; CL: clearance; Vss: steady state of volume distribution. Data are generated by using WinNonlin program. Three mice were used per group for this analysis.

	$t_{1/2}$ (h)	AUC (h·%)	AUMC (h <sup>2</sup> ·%)	MRT (h)	CL (L/h)	Vss (L)
GTP-LCP-PEG-AA	5.36	401	2120	5.30	0.25	1.33
GTP-LCP-PEG	7.75	468	2810	6.01	0.21	1.26
Free GTP	/	14.9	25.3	0.83	6.72	5.58

### 3.3.9 Tumor growth inhibition study

The tumor growth inhibition was evaluated in nude mice bearing either H460 or BxPC-3 subcutaneous tumors. As shown in **Fig 3.9A and 3.9B**, GTP-LCP-PEG-AA treatment

group exhibited the most efficient tumor growth inhibition after 4 systemic injections, and GTP-LCP-PEG also suppressed tumor growth effectively compared to the control and CTP-loaded LCPs. In GTP-LCP-PEG-AA treatment group, the final tumor loads were dramatically suppressed by 80% and 50% compared to the control group in H460 and BxPC-3 xenograft models, respectively. Free GTP and Gem showed limited therapeutic effects as compared to GTP-loaded LCPs. No serious toxicity, indicated by body weight changes, was observed (**Fig 3.9C and 3.9D**).

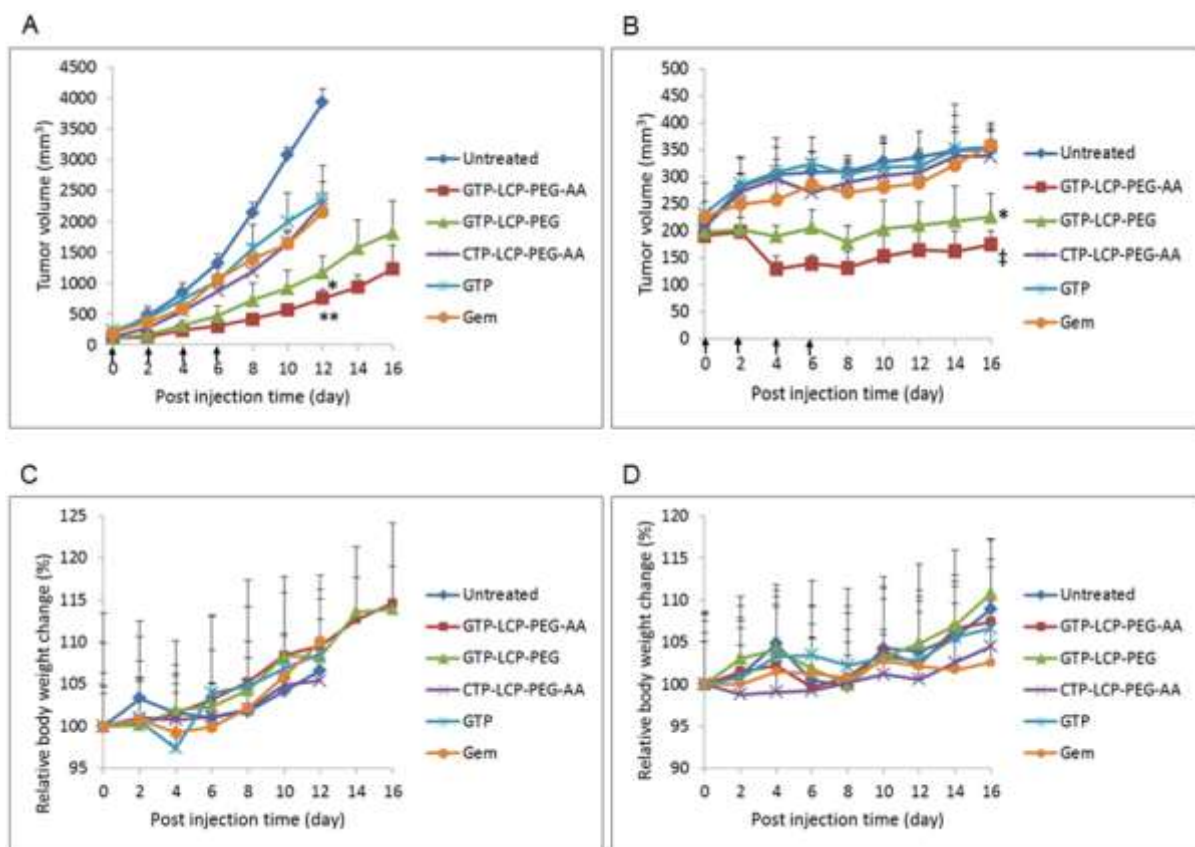


**Figure 3.9 GTP-loaded LCPs inhibited the tumor growth on H460 (A) and BxPC-3 (B) xenografts.** The relative body weight changes of H460 (C) and BxPC-3 (D) xenografts were calculated. Data are mean  $\pm$  S.D. (n=5). Statistics were as follows: \*\* $p < 0.0005$  vs. Untreated, ‡ $p < 0.001$  vs. Untreated, \* $p < 0.005$  vs. Untreated.

Hematological parameters were measured 24 h after 3 daily IV treatments (**Table 3.4**). There was little elevation of BUN, creatinine and liver enzymes (AST, ALT) in blood serum compared to the control, and all parameter values were in the normal range. Thus, GTP-loaded LCPs, at the therapeutic dose, did not elicit any toxicity in kidney and liver and there were no significant safety issues.

**Table 3.4 Serum levels of BUN, creatinine, AST, ALT after 3 daily IV injections (n=3).** Data are shown as mean  $\pm$  SD.

	BUN mg/dL	Creatinine mg/dL	AST U/L	ALT U/L
Control	24	0.3	111.0 $\pm$ 4.2	56.0 $\pm$ 2.8
GTP-LCP-PEG-AA	24.7 $\pm$ 1.2	0.3	144.7 $\pm$ 12.9	69.3 $\pm$ 22.0
GTP-LCP-PEG	27.0 $\pm$ 2.8	0.3	148.5 $\pm$ 82.0	74.2 $\pm$ 25.5
CTP-LCP-PEG-AA	27.0 $\pm$ 1.4	0.3	134.0 $\pm$ 8.5	73.0 $\pm$ 12.7
Normal Range	18--33.7	0.2--0.9	110.5--247	33.4--132

### 3.4 DISCUSSION

All nucleoside analogues require transport into the cell and phosphorylation to the triphosphate form to be biologically active. Specific nucleoside transporters are responsible for the cellular uptake of the principal therapeutic nucleosides (i.e. gemcitabine)<sup>196</sup>. Gem mainly works in rapidly dividing cells (i.e. cancer cells) that usually grow at uncontrollable rate. It is reported that high dose therapy with nucleoside analogs can overcome the mutational deficiency of nucleoside transporters and limiting rates of cellular entry by enhancing passive accumulation of the drug within the cell<sup>204</sup>. Additionally, due to the rapid enzyme deamination and renal clearance, Gem has a very short plasma half-life<sup>205</sup>. In order to achieve therapeutic drug levels, Gem has to be administered at a high dose (1,000 mg/m<sup>2</sup>) by intravenous infusion<sup>205</sup> which causes toxicity, particularly kidney and liver dysfunctions. The extensive usage of nucleoside analogs also results in the development of drug resistance<sup>185</sup>.

In order to improve the therapeutic efficiency of nucleoside analogues, some prodrug and drug delivery approaches have been developed. Liposomes were used to load nucleoside

drugs due to their biphasic (lipophilic/hydrophilic) character. But most nucleoside analogues are located exclusively in the aqueous compartment of liposomes because of their relatively high solubilities. However, they readily diffuse through the liposome bilayer, which limits their stability on storage and reduces the drug concentration accumulated inside the tumors<sup>206</sup>. The fabrication of lipophilic nucleoside derivatives increased the cell membrane permeability and was expected to bypass the barriers of nucleoside transporters<sup>207</sup>. Other studies focused on entrapping the modified lipophilic nucleoside derivatives into liposome's lipid bilayer<sup>208</sup> or micelle's hydrophobic inner core<sup>209</sup>. Though these nanocarriers can alleviate the entrapped nucleoside drugs from enzymatic degradation, their therapeutic potency is still dependent on the conversion of the lipophilic prodrug to the nucleoside drug inside the tumor cells. Besides, the lipophilic nucleosides cannot overcome the resistance mutations in the kinases<sup>210</sup>. Thus, there is an unmet medical need for the development of new technologies allowing a more effective systemic delivery of nucleoside analogues for the treatment of cancer patients.

In this study, we report a novel systemic delivery platform of nucleoside analogs. Gemcitabine triphosphate (GTP), the bioactive form of Gem, was encapsulated into a nanoparticle system containing a calcium phosphate precipitate core, i.e. LCP. Such that the cellular uptake deficiency and the following requirement of nucleoside kinase activation process of Gem can be avoided. Due to the triphosphate structure, GTP can be readily co-precipitated in the CaP core of LCP. A lipid bilayer was used to wrap around the LCP core to allow a high density of DSPE-PEG being grafted onto the surface. This nanoparticle design can protect the GTP from enzymatic degradation and renal clearance *in vivo*. The surface modification with PEG helps shield the cationic charge of the lipid

bilayer and may minimize the interaction with circulating blood components<sup>211</sup>. With AA as a tumor specific targeting ligand, LCPs can be more effectively taken up into tumor cells via sigma-receptor-mediated endocytosis. When LCPs are delivered to acidic endosomes, the CaP core of LCPs rapidly dissolves to increase osmotic pressure, eventually bursting the endosomes and enabling the entrapped GTP to escape<sup>188</sup>. The cationic lipid DOTAP wrapping the LCP core may also promote the release of GTP from endosomes to the cytosol by destabilizing the anionic endosome membrane<sup>212</sup>. Altogether, the selection of a right drug formulated in a “smart” delivery system is likely to decrease the therapeutic dose required and corresponding dose-dependent adverse effects.

NSCLC and pancreatic cancers are among the top 3 leading causes of cancer death worldwide, and pancreatic cancer is particularly deadly. AA-targeted GTP-loaded LCPs showed a potent anti-cancer efficacy in NSCLC H460 and pancreatic BxPC-3 models at a low dose. In order to further prove the potential therapeutic applications of GTP-loaded LCPs in extensive tumor malignancies, we randomly selected 6 additional human pancreatic adenocarcinoma cell lines, and established the xenograft tumor models in nude mice. All these pancreatic tumor xenografts responded well to systemic treatment with AA-targeted GTP-loaded LCPs (**Fig 3.6**). In addition, Gem is prone to elicit potent clinical efficacy in rapidly proliferating cancer cells with high metabolic activity due to its impediment of DNA replication<sup>185</sup>. This is probably the reason that H460 xenograft with fast growing tumor showed more significant apoptosis induction and proliferation inhibition than other cancer models. The different cell-killing effects may also be attributed to the extent of the tumors’ vascular abnormalities, which alter the EPR effect. The effectiveness of this LCP formulation to gemcitabine-resistant cancer models will

under further investigation. Based on our extensive study on multiple NSCLC and pancreatic cancer models, we conclude that the targeted GTP-loaded LCPs elicit significant anti-cancer efficacy *in vivo*. This targeted LCP-formulated GTP represents a new class of improved nucleoside anticancer drug which should be further investigated for potential clinical trials.

### 3.5 CONCLUSION

Encapsulating the bioactive GTP in LCPs holds the advantages of overcoming chemoresistance, targeting specifically to tumor, lowering dosages and toxicities. We have shown that AA-targeted GTP-loaded LCPs can induce effective cell death and enhanced S-phase cell cycle arrest in NSCLC and pancreatic cell lines *in vitro*. *In vivo*, AA-targeted GTP-loaded LCPs effectively delayed the tumor growth of human NSCLC H460 and pancreatic BxPC-3 cancer xenografts, with little toxicity. Molecular analysis indicated that this high efficacy of targeted GTP-loaded LCPs was associated with its ability to induce dramatic apoptosis of tumor cells, as shown in the TUNEL assay, caspase-3/7 activation and the cleaved PARP overexpression in tumor tissues; as well as significantly inhibit tumor cell proliferation and cell cycle progression, as indicated in the PCNA immunohistochemistry and the cyclin D1 down-regulation in tumor tissues. To the best of our knowledge, this is the first report using gemcitabine bioactive form, GTP, instead of any forms of gemcitabine prodrug as the delivery cargo for cancer therapy. Further, we predict that many chemotherapeutic drugs with phosphate group(s) could be entrapped into LCPs and delivered systemically, so that some of the drugs will no longer rely on the relative kinase phosphorylation to be bioactive.



#### **4.0 CO-DELIVERY OF VEGF SIRNA AND GEMCITABINE MONOPHOSPHATE IN A SINGLE NANOPARTICLE FORMULATION FOR EFFECTIVE TREATMENT OF NSCLC**

There is an urgent need for new therapeutics for the treatment of aggressive and metastatic refractory human non-small-cell-lung cancer (NSCLC). Anti-angiogenesis therapy and chemotherapy are the two major treatment options. Unfortunately, both types of therapy are prone to induce resistance. Integrating anti-angiogenesis therapy with chemotherapy is expected to target the tumor's vascular endothelial cells and the tumor cells simultaneously. In this study, we co-formulated VEGF siRNA targeting vascular endothelial growth factors and gemcitabine monophosphate (GMP) into a single cell-specific, targeted Lipid/Calcium/Phosphate (LCP) nanoparticle formulation. Anti-tumor effect of the combination therapy using LCP loaded with both VEGF siRNA and GMP was evaluated in a xenograft model of NSCLC with systemic administration. The improved therapeutic response, as compared to either VEGF siRNA or GMP therapy alone, was supported by the observation of effective induction of tumor cell apoptosis, significant reduction of tumor cell proliferation and tumor microvessel density. The combination therapy led to dramatic inhibition of tumor growth, with little *in vivo* toxicity. Additionally, the current studies demonstrated the possibility of incorporating multiple nucleic acid molecules and phosphorylated small molecule drugs, targeting to different pathways, into a single nanoparticle formulation for profound therapeutic effect.

## 4.1 INTRODUCTION

The combination of chemotherapy and gene therapy could greatly increase their therapeutic efficacy in the treatment of many human diseases. The drug resistance associated with standard chemotherapy regimens can be alleviated by the addition of gene therapy to the treatment plan<sup>216</sup>. Furthermore, the efficacy of gene therapy can be bolstered by chemo-agents whose effects are often more potent and widespread. This increase in efficacy could be particularly important in the treatment of aggressive human cancers whose progression and invasion involves a variety of physiological or pathological factors, such as NSCLC.

Anti-angiogenesis therapy and chemotherapy are important treatment regimens for NSCLC. VEGF is over-expressed in malignant tumors and is a major driver of tumor angiogenesis. Blocking the VEGF signaling pathway can reduce tumor-associated angiogenesis and blood-vessel-dependent metastasis.<sup>217, 218</sup> VEGF-receptor inhibitors, such as small-molecule inhibitors, anti-VEGF monoclonal antibodies, and aptamers that strongly antagonize the VEGF-VEGFR binding with high specificity, have been developed.<sup>219-221</sup> However, the efficacy of these inhibitors is often limited by unfavorable pharmacokinetics, low tumor accumulation and undesired interaction with the immune system. Additional adverse effects also compromise the therapeutic response in patients.<sup>222, 223</sup> siRNA specific to VEGF, if properly delivered to the tumor cells, may overcome some shortcomings of the traditional drugs, especially when it is co-delivered with an efficient chemodrug. Gemcitabine (2', 2'-difluoro 2'-deoxycytidine) (Gem) is a nucleoside analogue widely used as the first-line chemotherapy of advanced NSCLC. Gem relies on nucleoside transporters to enter into cells, sequentially phosphorylated by

deoxycytidine kinase (dCK) that forms mono-, di-, and triphosphate derivatives. The addition of the first phosphate group to become gemcitabine monophosphate (GMP) is the rate-limiting step.<sup>224</sup> 5'-Triphosphate derivative of Gem is then incorporated into the DNA strand where it inhibits replication by terminating the DNA chain elongation<sup>224</sup>. However, mutational drug resistance readily occurs at the steps of nucleoside transport and intracellular nucleoside activation.<sup>225</sup>

In order to combine the therapeutic advantages of VEGF siRNA and Gem, while also avoiding their delivery roadblocks, we entrapped both VEGF siRNA and GMP into a single Lipid/Calcium/Phosphate (LCP) nanoparticle formulation. Our aim was to apply multiple tumor-killing steps to programmatically inhibit tumor growth and eventually eradicate tumor progression. The small molecule ligand, anisamide (AA), was modified to the LCP surface to specifically target the sigma receptors that are over-expressed in many human cancer cells. The rational design of LCP nanoplatform lies in the fact that calcium ions can precipitate both siRNA and GMP. Thus, an anti-angiogenic and a chemo agents can be simultaneously delivered to the tumor cells to block different mechanisms of tumor cell proliferation (**Fig 4.1**).<sup>226</sup> LCPs entrapping only VEGF siRNA (VEGF-LCP-AA) and LCPs entrapping only GMP (GMP-LCP-AA) were prepared and tested separately to compare with the combination therapy. Cytidine monophosphate (CMP), having a chemical structure similar to GMP, but without any cytotoxic effect, serves as the surrogate for GMP. LCPs entrapping both CMP and control siRNA ((CMP+Con)-LCP-AA) were used as control nanoparticles.

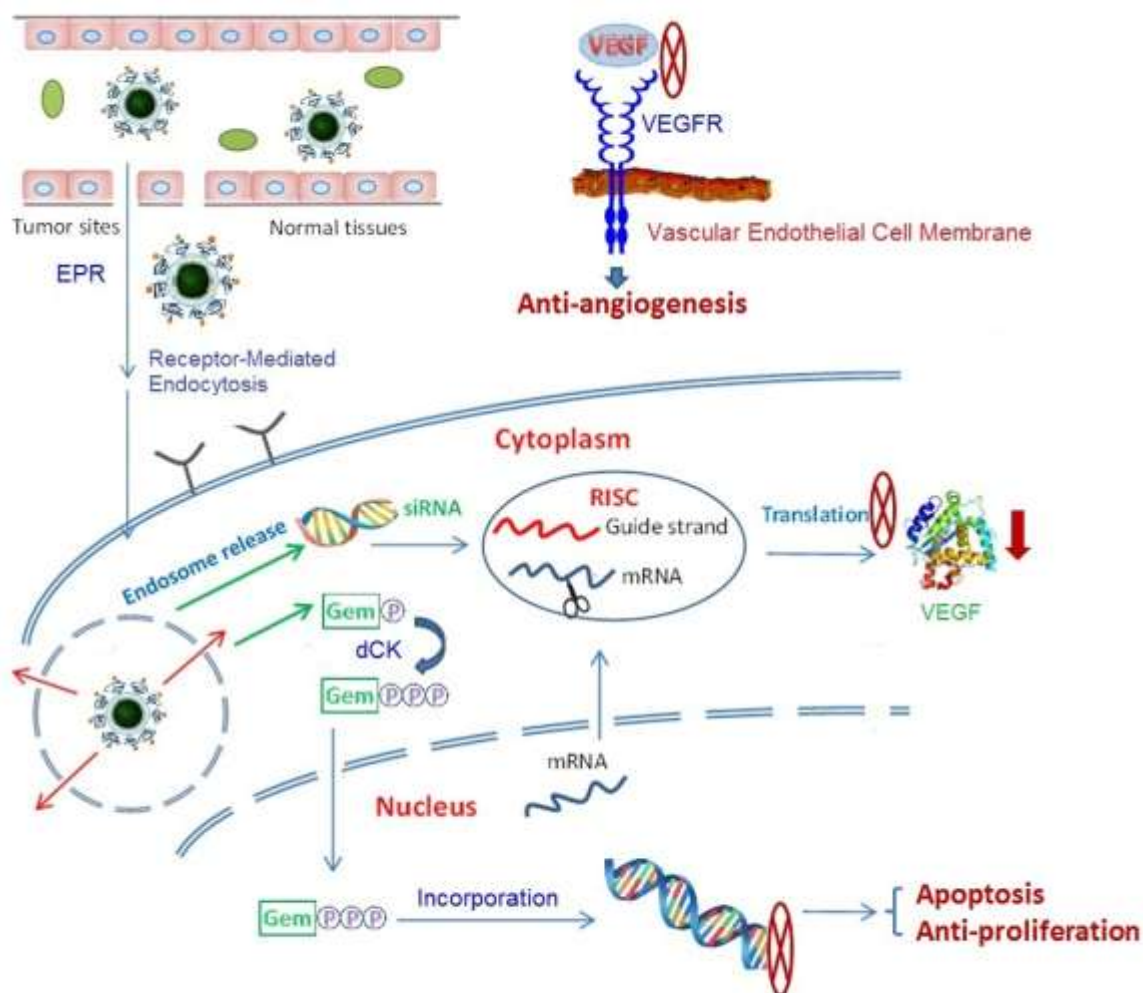


**Figure 4.1 Schematic illustration of the *in vivo* co-delivery mechanism**

## **4.2 MATERIALS AND METHODS**

### **4.2.1 Materials**

Gemcitabine monophosphate disodium salt (GMP) was synthesized by HDH Pharma, Inc. (Research Triangle Park, NC). VEGF siRNA (target sequence: 5'-ACC UCA CCA AGG CCA GCA C-3') and control siRNA (target sequence: 5'-AAU UCU CCG AAC GUG TCA CGU-3') were synthesized by Sigma-Aldrich (St. Louis, MO). 1, 2-Dioleoyl-3-

trimethylammonium-propane chloride salt (DOTAP), dioleoylphosphatidic acid (DOPA), and 1,2-distearoyl-sn-glycero-3-phosphoethanolamine-N-[methoxy(polyethyleneglycol-2000) ammonium salt (DSPE-PEG<sub>2000</sub>) were purchased from Avanti Polar Lipids, Inc. (Alabaster, AL). DSPE-PEG-AA was synthesized in our lab as described previously.<sup>240</sup> DeadEnd Fluorometric TUNEL assay kits and Apo-ONE Homogeneous Caspase-3/7 assay substrates were obtained from Promega Corporation (Madison, WI). Other chemicals were obtained from Sigma-Aldrich (St. Louis, MO).

#### **4.2.2 Cell culture**

H460 human NSCLC cells, originally obtained from American Type Culture Collection (ATCC) (Manassas, VA), were cultured in RPMI-1640 medium (Invitrogen, Carlsbad, CA) supplemented with 10% fetal bovine serum, 100 U/mL penicillin and 100 µg/mL streptomycin (Invitrogen). Cells were cultivated in a humidified incubator at 37°C and 5% CO<sub>2</sub>. Cells were harvested with 0.05% trypsin-EDTA before subculture.

#### **4.2.3 Experimental animals**

Female nude mice 6-8 weeks of age were used in all studies. To establish the xenograft models,  $5 \times 10^6$  H460 cells in 100 µL of PBS were injected subcutaneously into the right flank of mice. All work performed on animals was approved by the Institutional Animal Care and Use Committee at University of North Carolina at Chapel Hill.

#### **4.2.4 Preparation of VEGF-LCP-AA, GMP-LCP-AA and (GMP+VEGF)-LCP-AA**

LCP cores were prepared using water-in-oil micro-emulsions, with the oil phase containing cyclohexane/ Igepal CO-520 solution (71/29, v/v).<sup>241</sup> To prepare the VEGF-LCP cores, 48 µg VEGF siRNA was mixed with 600 µL 2.5 M CaCl<sub>2</sub> and added into 20

mL of oil phase, where the other emulsion contained 600  $\mu$ L 12.5 mM  $\text{Na}_2\text{HPO}_4$  (pH=9.0). The GMP-LCP core was formulated using 180  $\mu$ L of 60 mM GMP mixed with 12.5 mM  $\text{Na}_2\text{HPO}_4$  (pH=9.0) (final concentration) to reach a total volume of 600  $\mu$ L. This solution was then added into 20 mL of oil phase. Six-hundred  $\mu$ L 2.5 M  $\text{CaCl}_2$  was added to a separate the 20 mL oil phase. To prepare the (GMP+VEGF)-LCP core, the phosphate phase met the same specifications outlined in the preparation of the GMP-LCP core. The calcium phase contained 600  $\mu$ L of 2.5 M  $\text{CaCl}_2$  mixed with 48  $\mu$ g of VEGF siRNA. Four-hundred  $\mu$ L of 20 mM DOPA in chloroform was added to the phosphate phase of the GMP-LCP and (GMP+VEGF)-LCP, whereas only 200  $\mu$ L of 20 mM DOPA was added to the phosphate phase during the preparation of the VEGF-LCP.

The two separate micro-emulsions were then mixed. After stirring for 5 min, another 400  $\mu$ L of 20 mM DOPA was added into the emulsion of GMP-LCP and (GMP+VEGF)-LCP; for VEGF-LCP, 200  $\mu$ L of 20 mM DOPA was added. The emulsion was allowed to continually stir for another 20 min before 40 mL of absolute ethanol was added. The ethanol emulsion mixture was centrifuged at 10,000 g for 15 min to pellet the LCP core and the supernatant was then discarded. The LCP core was washed twice with absolute ethanol and dried under  $\text{N}_2$ . The LCP core pellets were suspended in 2 mL chloroform and stored in a glass vial at  $-20^\circ\text{C}$  for further use.

To prepare the final VEGF-LCP-AA, GMP-LCP-AA and (GMP+VEGF)-LCP-AA with outer lipid outting, 330  $\mu$ L LCP core in chloroform was mixed with 38.7  $\mu$ L of 10 mg/ml Cholesterol, 28  $\mu$ L of 25 mg/ml DOTAP, 76.8  $\mu$ L of 25 mg/ml DSPE-PEG and 19.2  $\mu$ L of 25 mg/ml DSPE-PEG-AA. After evaporating the chloroform, the residual lipids were dissolved in 30  $\mu$ L THF followed by 50  $\mu$ L absolute ethanol, and then suspended in 160

$\mu$ L water. After brief sonication, the solution was dialyzed in distilled water to remove the THF and ethanol. The preparation procedure of (CMP+Con)-LCP-AA was identical to that of (GMP+VEGF)-LCP-AA, except that GMP and VEGF siRNA were replaced by equal molar amount of CMP and control siRNA.

#### **4.2.5 Characterization of VEGF-LCP-AA, GMP-LCP-AA and (GMP+VEGF)-LCP-AA**

The particle size and zeta potential of LCPs were determined by dynamic light scattering using a Malvern ZetaSizer Nano series (Westborough, MA). The EE% of GMP or siRNA was measured after lysing the LCPs with a THF/1 M HCl (v/v= 70/30) solution. GMP EE% was measured using a UV spectrophotometer (Beckman Coulter Inc., DU 800 spectrophotometer) at a wavelength of 275 nm. The EE% of siRNA was measured by mixing a small amount of Texas-red labeled siRNA with VEGF siRNA in LCP cores, and the fluorescence intensity of Texas-red was detected at the wavelength of Ex=589 nm and Em=615 nm. TEM images of LCP formulations were acquired through the use of JEOL 100CX II TEM (Tokyo, Japan). Briefly, 4  $\mu$ L of LCP solution was dropped onto a 300 mesh carbon coated copper grid (Ted Pella, Inc., Redding, CA) for 2 min. Excess fluid was then removed with filter paper, and the copper grid was dried before observation using the TEM.

#### **4.2.6 Western blot analysis**

Twenty-four h after the third injection, mice were sacrificed and tumor lysates were prepared with radioimmunoprecipitation assay (RIPA) buffer, supplemented with a protease inhibitor cocktail (Promega, Madison, WI). Protein concentrations were determined using a BCA assay kit (Pierce Biotechnology) following the manufacturer's

recommendations. Forty  $\mu\text{g}$  of protein per lane was separated by 4%-12% SDS-PAGE electrophoresis (Invitrogen) before being transferred into polyvinylidene difluoride (PVDF) membranes. The membranes were blocked for 1 h with 5% silk milk at room temperature and then incubated with rabbit polyclonal VEGF antibody and mouse monoclonal poly(ADP-ribose) polymerase-1 (PARP-1) antibody (1:500 dilution; Santa Cruz Biotechnology) overnight at 4°C.  $\beta$ -actin antibodies (1:4000 dilution; Santa Cruz Biotechnology) served as the loading control. The membranes were washed 3 times and then incubated with secondary antibodies (1:4000 dilution; Santa Cruz Biotechnology) at room temperature for 1 h. Finally, the membranes were washed 4 times and developed by an enhanced chemiluminescence system according to the manufacturer's instructions (Thermo Scientific).

#### **4.2.7 Caspase activation**

Twenty-four h after 3 daily IV injections, forty  $\mu\text{g}$  protein of each tumor lysate was used to detect caspase-3/7 activity in tumors according to the manufacturer's instructions (Invitrogen, NY). Briefly, 25  $\mu\text{L}$  sample solution containing 40  $\mu\text{g}$  of protein was added to a 96-well plate, and 25  $\mu\text{L}$  caspase-3/7 reagent was added to each sample well. The contents of the wells were gently mixed at 400 rpm for at least 1 h at room temperature. Their fluorescence was measured using a microplate reader at a wavelength of  $\text{Ex}=485$  nm and  $\text{Em}=535$  nm. The fluorescence intensity of treatment groups was normalized to that of the control group to indicate the extent of caspase activation.

#### **4.2.8 TUNEL assay**

After predetermined dosing schedule, H460 tumor-bearing mice were sacrificed and tumors were fixed in 10% formalin for 24 h before embedded in paraffin and sectioned at



a thickness of 5  $\mu\text{m}$ . The TUNEL staining was performed as recommended by the manufacturer (Promega, Madison, WI). Then DAPI mounting medium was dropped on the sections for nucleus staining. Images of TUNEL-stained tumor sections were captured with a fluorescence microscope (Nikon Corp., Tokyo, Japan). The percentage of apoptotic cells was obtained by dividing the number of apoptotic cells (TUNEL positive cells shown as green dots) from the number of total cells (blue nuclei stained by DAPI, not shown) in each microscopic field, and 10 representative microscopic fields were randomly selected in each treatment group (n=3) for this analysis.

#### **4.2.9 Immunohistochemistry**

Paraffin-embedded tumor sections were obtained as mentioned above. The CD31 (1:50 dilution, Abcam) and PCNA (1:200 dilution, Santa Cruz) immunohistochemistry was performed using the HRP/DAB detection IHC kit as recommended by the manufacturer (Abcam, Cambridge, MA). Immunostaining images were observed under a light microscope (Nikon Corp., Tokyo, Japan). The percentage of proliferation cells was obtained by dividing the number of PCNA positive cells (shown as brown dots) from the number of total cells (blue nuclei stained by hematoxylin) in each microscopic field, and 10 representative microscopic fields were randomly selected in each treatment group (n=3) for counting.

#### **4.2.10 Tumor growth inhibition**

Tumor growth inhibition of the nanoparticles system was evaluated in an H460 subcutaneous xenograft mouse model. When the tumor volumes reached about 150-200  $\text{mm}^3$ , the mice were randomly assigned into 6 treatment groups, and intravenously injected different LCPs, including VEGF-LCP-AA, GMP-LCP-AA, (GMP+VEGF)-

LCP-AA, (CMP+Con)-LCP-AA and free GMP. The IV injections were performed every other day for a total of 4 injections with a dose of 50.4  $\mu\text{mol/Kg}$  GMP and/or 0.2 mg/Kg VEGF siRNA. Tumor sizes were measured every other day with calipers across their two perpendicular diameters, and the tumor volume was calculated using the following formula:  $V=0.5 \times (W^2 \times L)$ , where  $V$  = tumor volume,  $W$  = the smaller perpendicular diameter and  $L$  = the larger perpendicular diameter. Two days after the final injection, the mice were sacrificed and the tumors were stripped off. Some tumors were fixed in 10% formalin and cut into paraffin-embedded tissue sections for TUNEL assay, immunohistochemistry analysis and an H&E stain. Other tumors were arranged and the photographs of tumors were taken as a visual comparison of the representative tumor sizes in each treatment group.

#### **4.2.11 *In vivo* toxicity**

Twenty-four h after 3 daily IV injections, blood was drawn from the venous plexus of the eyes of the mice. Blood samples were immediately centrifuged at 3,000 g for 5 min at 4°C, and the supernatant blood serums were collected for hematological analysis. BUN, creatinine, AST, ALT values were recorded, as indications of hepatic and renal functions. Organs (heart, liver, spleen, lung, kidney) of mice in different treatment groups were fixed and sectioned for H&E stain.

#### **4.2.12 Statistical analysis**

Results were expressed as a mean  $\pm$  standard deviation (SD). Student t-tests were used to evaluate statistical significance. A result of  $p < 0.05$  was considered to be statistically significant.

## 4.3 RESULTS

### 4.3.1 Characterization of drug-loaded LCPs

LCP is a membrane/core type nanoparticle. It is composed of a solid calcium phosphate precipitate core coated with a single lipid bilayer. The lipid membrane wrapping around the core is modified by grafting a high density of polyethylene glycol (PEG) chains, with a tethered targeting ligand AA. The preparation scheme of LCP is illustrated in **Fig 4.2**.

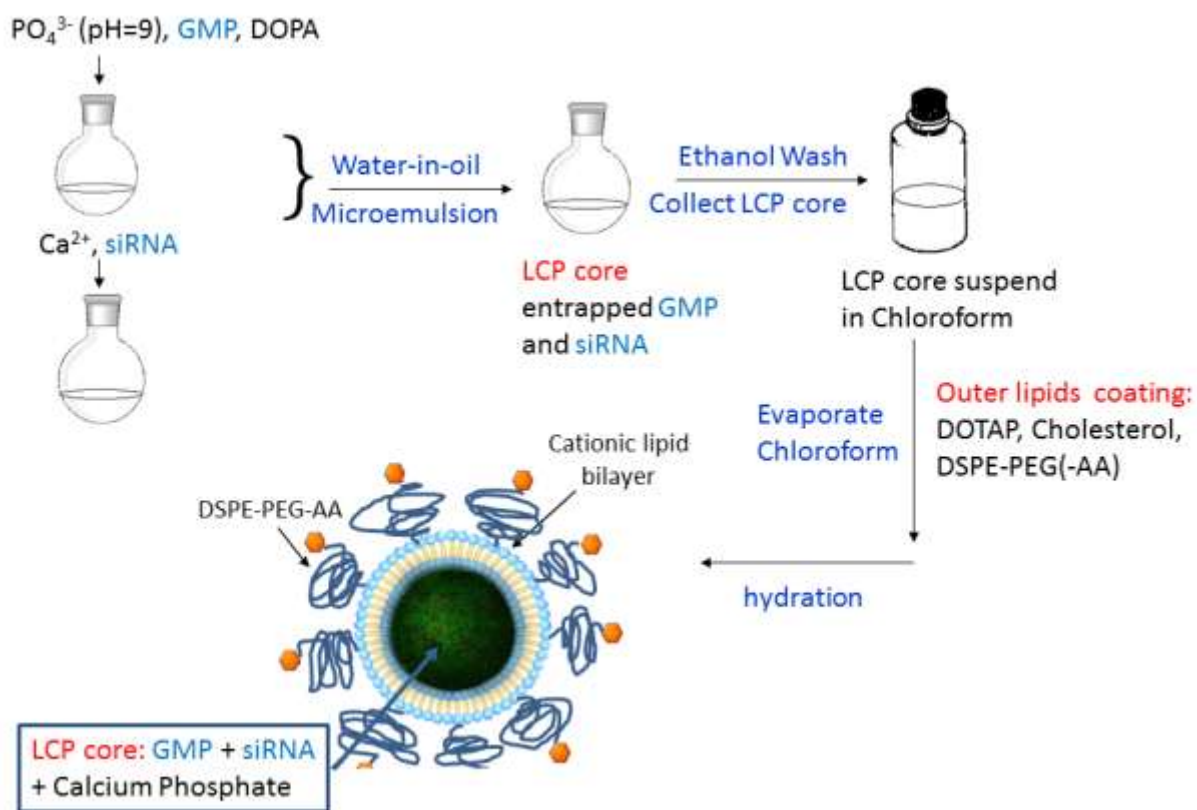


**Figure 4.2** Schematic illustration of the preparation procedure of GMP- and/or VEGF siRNA- loaded LCP formulations.

The Transmission electron microscope (TEM) photographs showed that all drug-loaded LCP-AAs had a spherical shape and were monodispersed, with a particle size of around

20 nm (**Fig 4.3**). The relatively small size of LCPs renders them better tumor penetration capability over large size nanoparticles.<sup>12</sup> The zeta potentials of VEGF-LCP-AA, GMP-LCP-AA and (GMP+VEGF)-LCP-AA were  $30.2 \pm 14.1$  mV,  $3.4 \pm 3.1$  mV, and  $10.0 \pm 4.0$  mV, respectively. The encapsulation efficiency (EE%) of VEGF siRNA and GMP in LCP-AA was around 55% and 75%, respectively. The EE% of VEGF siRNA and GMP in co-formulated LCP-AA was almost the same as that of the VEGF-LCP-AA or GMP-LCP-AA single formulation, which indicates that VEGF siRNA and GMP did not interfere with each other in the process of co-precipitation with calcium ions within the LCP core.

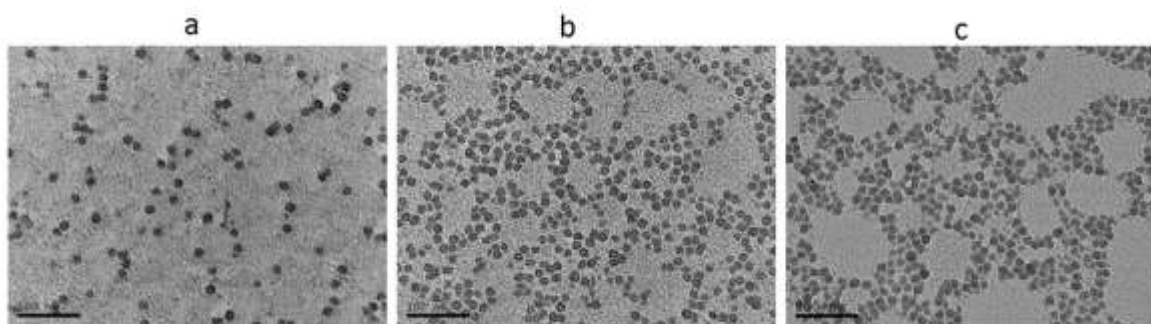


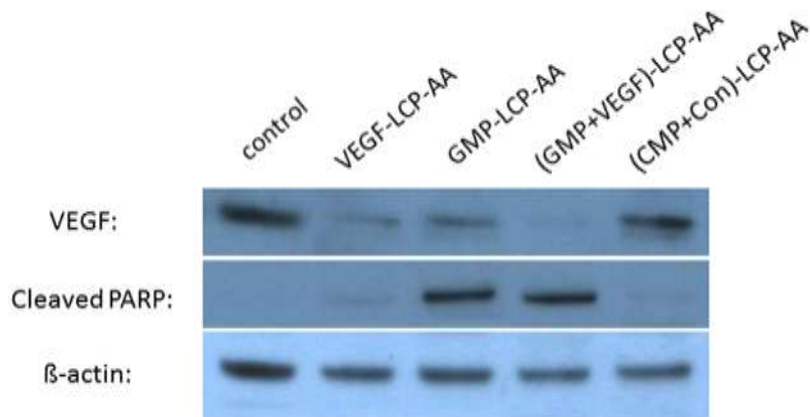
**Figure 4.3 TEM pictures of drug-loaded LCPs.** (a) VEGF-LCPs, (b) GMP-LCPs and (c) (GMP+VEGF)-LCPs. Scale bar = 100 nm.

#### **4.3.2 Drug-loaded LCPs induced VEGF down-regulation and apoptosis *in vivo***

Human NSCLC H460 tumor bearing mice were given three daily IV injections of different LCP formulations with a dose of  $50.4 \mu\text{mol/Kg}$  GMP ( $19.5 \text{ mg/Kg}$  GMP, or  $13.2 \text{ mg/Kg}$  in terms of Gem) and/or  $0.2 \text{ mg/Kg}$  VEGF siRNA. Twenty-four h after the third injection, mice were sacrificed and tumor lysates were prepared for western blot. VEGF-VEGFR signaling in the endothelial cells of tumor blood vessels can be prevented by silencing VEGF, which should induce tumor cell apoptosis. PARP is a nuclear protein

that performs central roles in the repair of damaged DNA. Cleavage of PARP by caspases is considered to be a hallmark of apoptosis.<sup>228</sup> As shown in **Fig 4.4**, (GMP+VEGF)-LCP-AA showed significant knockdown of VEGF, and stimulated the over-expression of cleaved PARP. GMP-LCP-AA also activated the cleaved PARP over-expression, but had only a minor effect on the VEGF expression level. VEGF-LCP-AA clearly reduced the VEGF expression, but had limited effect on PARP cleavage. Compared to the control, (CMP+Con)-LCP-AA had no measurable effect on the protein expression level of VEGF, and was not able to cleave PARP. VEGF mRNA levels coincided with the VEGF western blot results.

A



B

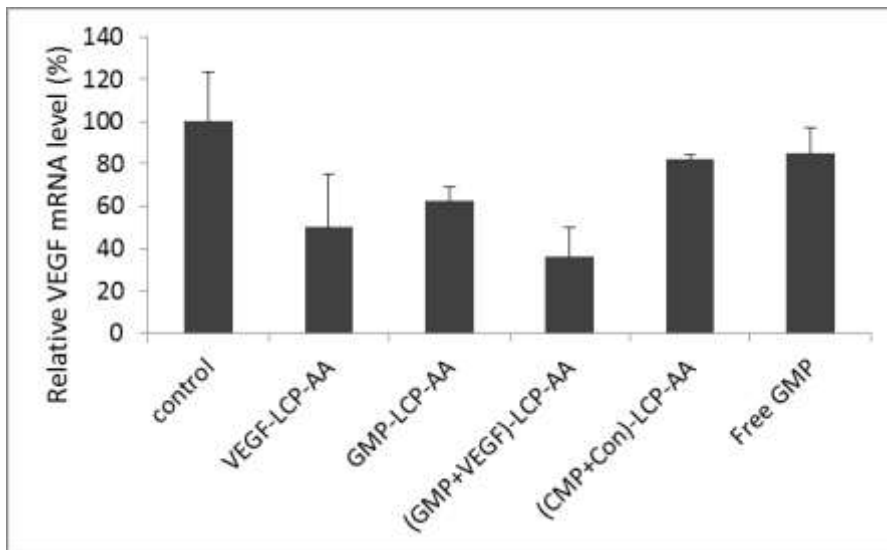


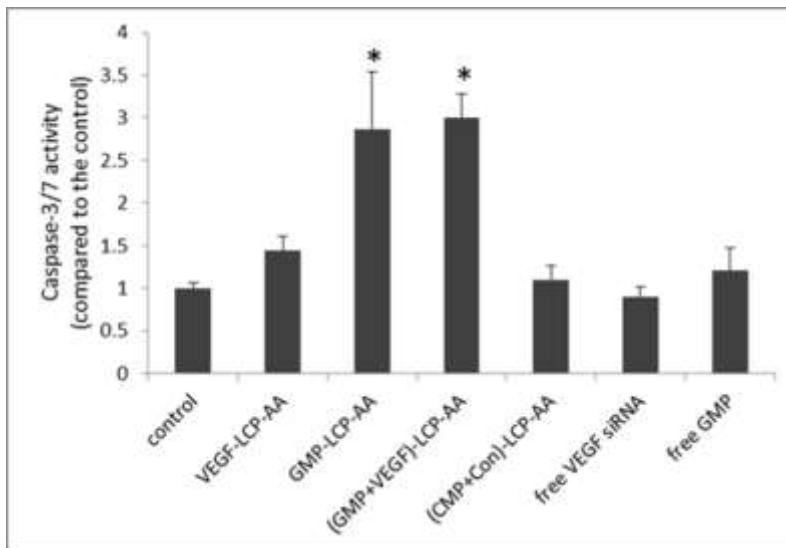
**Figure 4.4 Western blot analysis and VEGF mRNA level after systemic treatments.** (A) Western blots analysis for VEGF and cleaved PARP expressions in vivo after systemic treatment of different LCP formulations. (B) H460-tumor bearing mice were given 4 every other day IV injections, and mice were sacrificed two days after the final injection. Tumor VEGF mRNA levels in different treatment groups (n=3) were measured by RT-PCR. Data are shown as mean  $\pm$  SD.

### 4.3.3 Drug-loaded LCPs triggered caspase activation and tumor cell apoptosis *in vivo*

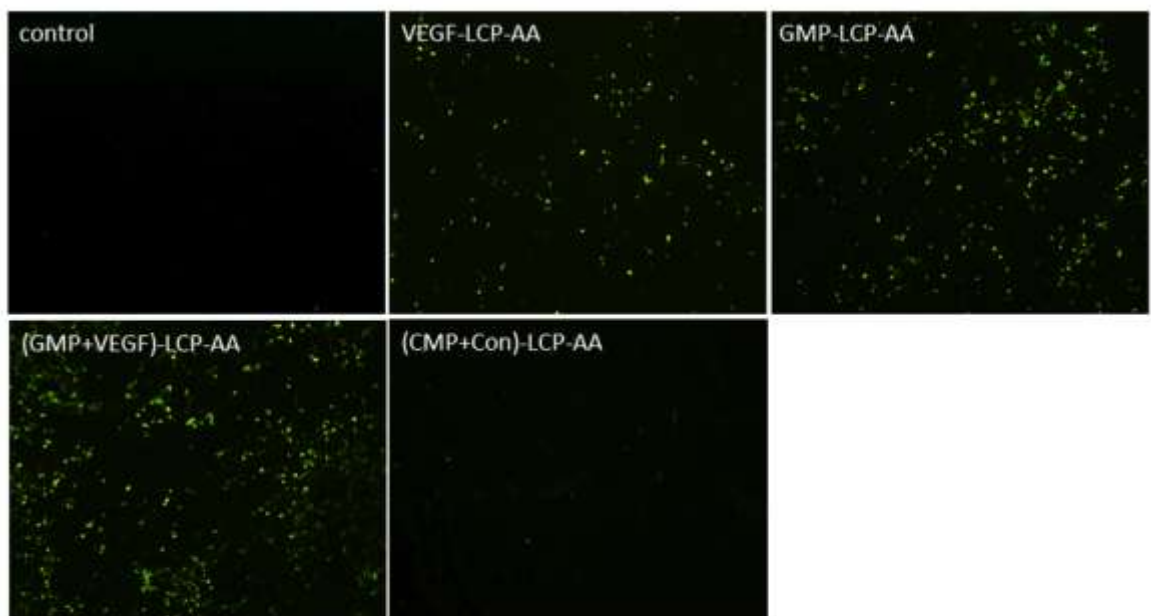
Caspases are proteolytic enzymes and play an important role in apoptosis as effector molecules. Among the caspase enzymes, caspase-3 and caspase-7 are especially important, and they are responsible for the proteolytic cleavage of a large number of substrates during apoptosis.<sup>229</sup> Twenty-four h after three daily IV injections, caspase-3/7 activity in tumors was increased 3-fold in mice injected with (GMP+VEGF)-LCP-AA and GMP-LCP-AA and 1.5-fold in mice injected with VEGF-LCP-AA, as compared to the control (**Fig 4.5A**). (CMP+Con)-LCP-AA, free VEGF siRNA, and free GMP displayed little caspases elevation (**Fig 4.5A**). The results indicated that the LCPs greatly improved the *in vivo* delivery efficiency of VEGF siRNA and GMP, and the caspase activation was predominantly triggered by GMP rather than VEGF siRNA.

We also measured the apoptotic induction in tumor tissues using the TdT-mediated dUTP Nick-End Labeling (TUNEL) assay. Twenty-four h after 3 daily IV injections, (GMP+VEGF)-LCP-AA triggered a dramatic killing effect, inducing 40% apoptotic cells in tumors. GMP-LCP-AA and VEGF-LCP-AA led to 22% and 5% apoptotic tumor cells, respectively. (CMP+Con)-LCP-AA did not elicit tumor cell apoptosis (**Fig 4.5B**). The tumor cell apoptotic induction of (GMP+VEGF)-LCP-AA was significantly higher than GMP-LCP-AA and VEGF-LCP-AA, indicating a profound therapeutic effect of the combined LCP. GMP-loaded LCPs were more potent than VEGF-loaded LCP in terms of tumor-cell killing effect.

A



B



The figure legend of Figure 4.5 A and B is on the next page.



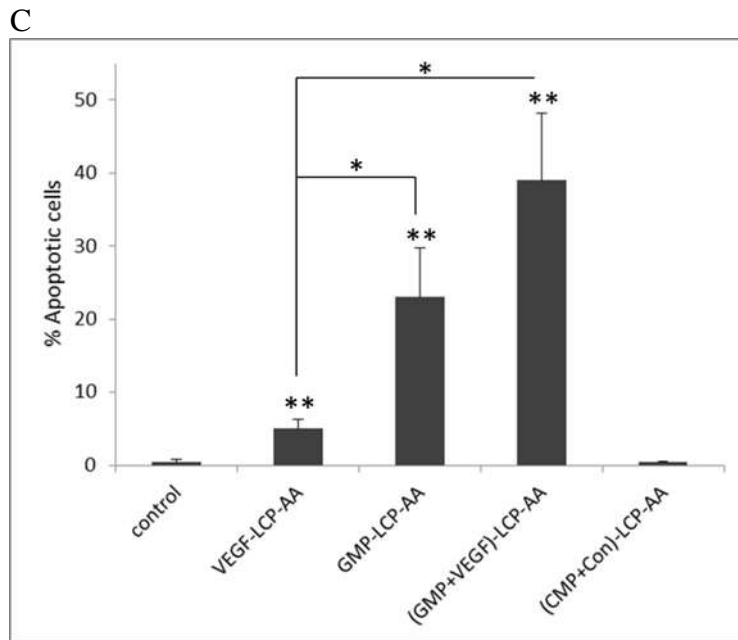


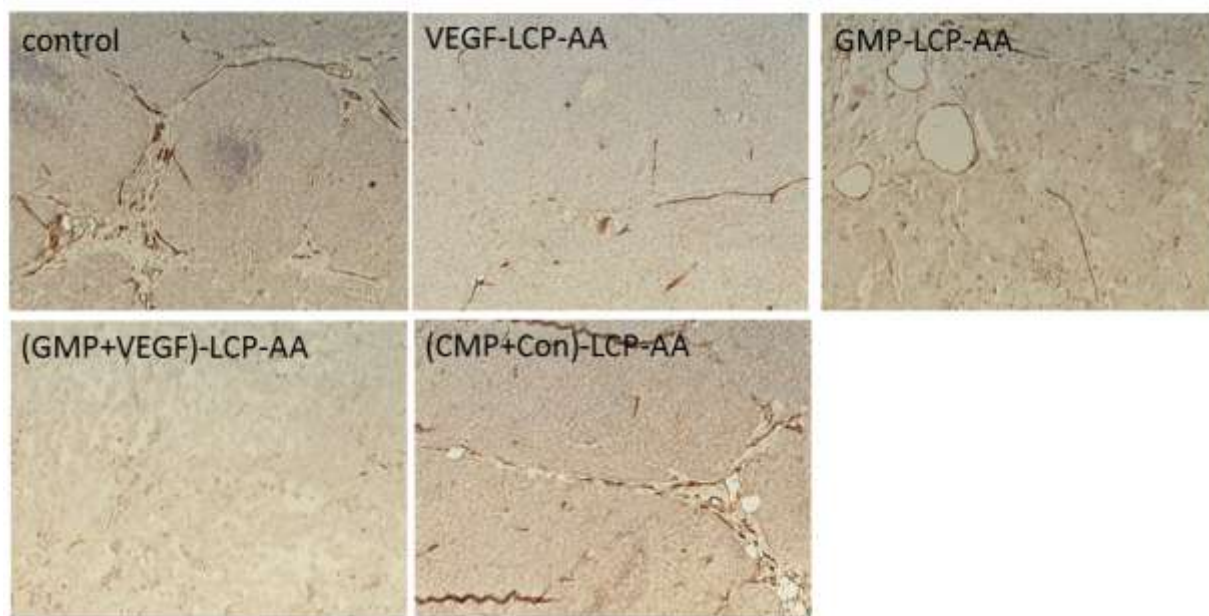
**Figure 4.5 The caspase activation and induction of apoptosis after the systemic administration of different LCPs in H460 exnografts.** (A) In vivo caspase-3/7 activity in tumors (n=3). \* $p<0.01$ , GMP-LCP-AA vs. control, (GMP+VEGF)-LCP-AA vs. control, GMP-LCP-AA vs. VEGF-LCP-AA, (GMP+VEGF)-LCP-AA vs. VEGF-LCP-AA. (B) In vivo tumor apoptosis by TUNEL assay. (C) The percentage (%) of apoptotic cells in the TUNEL assay. Statistics of the TUNEL assay in H460 xenografts (n=10): \*\* $p<0.005$ , VEGF-LCP-AA vs. control, GMP-LCP-AA vs. control, (GMP+VEGF)-LCP-AA vs. control; \* $p<0.01$ , GMP-LCP-AA vs. VEGF-LCP-AA, (GMP+VEGF)-LCP-AA vs. VEGF-LCP-AA. Data are shown as mean  $\pm$  SD.

#### 4.3.4 Drug-loaded LCPs inhibited the formation of tumor vasculature

Next, we evaluated the effect of different LCP formulations on the formation of tumor vasculature. We compared two treatment regimens: a short-term, frequent treatment schedule and a long-term, infrequent treatment schedule. The short-term treatment was characterized by daily IV injections over 3 consecutive days; the mice were sacrificed 24

h after the final injection. The long-term treatment was characterized by IV injections given every other day over 8 days, totaling 4 injections. Mice treated with this regimen were sacrificed two days after the final injection. **Fig 4.6** shows the results of staining CD31 antigen, an endothelial cell-specific surface marker. Control tumor showed thick, elongated, and disorganized layers of the vascular endothelium. (GMP+VEGF)-LCP-AA caused a significant reduction in tumor vasculature in both short-term and long-term treatments, indicating an immediate and lasting effect of tumor angiogenesis inhibition. VEGF-LCP-AA dramatically shut down the tumor vasculature after long-term treatment, but only displayed partial anti-angiogenesis effects with sparsely dispersed microvessels after short-term treatments, indicating that VEGF-LCP-AA needs more time to effectively impair the tumor vasculature. It seems that GMP co-delivered in the combined LCPs sensitized the tumor vasculature for anti-angiogenesis therapy. Indeed, Gem can induce apoptosis in tumor-associated endothelial cells, leading to a decrease in microvessel density.<sup>230, 231</sup> GMP-LCP-AA caused minor, partial reduction of tumor vessel formation after multiple doses. (CMP+Con)-LCP-AA and free GMP had little effect on the alteration of the endothelial cells compared to the control.

A



B

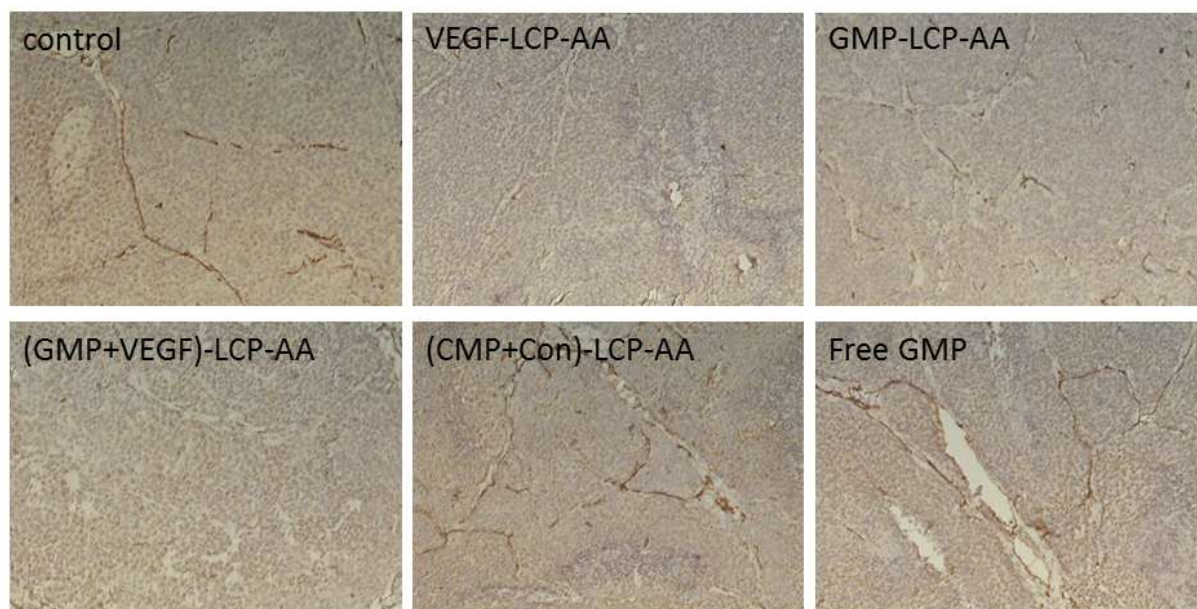


**Figure 4.6 CD31 immunohistochemistry staining of H460 xenograft tumors after (A) short term treatment and (B) long term treatment of different LCP formulations.**

#### 4.3.5 Drug-loaded LCPs triggered tumor cell apoptosis and inhibited tumor cell proliferation *in vivo*

The H460 tumor-bearing mice were given IV injections of different LCP formulations every other day for a total of 4 injections. Two days after the final injection, the mice were sacrificed and the tumors were sectioned for TUNEL assay, PCNA immunohistochemistry and H&E stain. In the TUNEL assay (**Fig 4.7A**), (GMP+VEGF)-LCP-AA elicited the most effective killing effects and triggered a significant amount (~30%) of apoptotic cells in the tumor, more potent than GMP-LCP-AA which induced 12% apoptotic cells. The results indicates antiangiogenesis-induced tumor cell starvation may augment the intrinsic cytotoxicity and duration of antitumor effects of the co-formulated GMP.<sup>232</sup> Treatment with VEGF-LCP-AA was less efficient than with GMP-LCP-AA, only 3% of tumor cells underwent apoptosis. (CMP+Con)-LCP-AA and free GMP had limited ability to induce apoptosis in tumor cells.

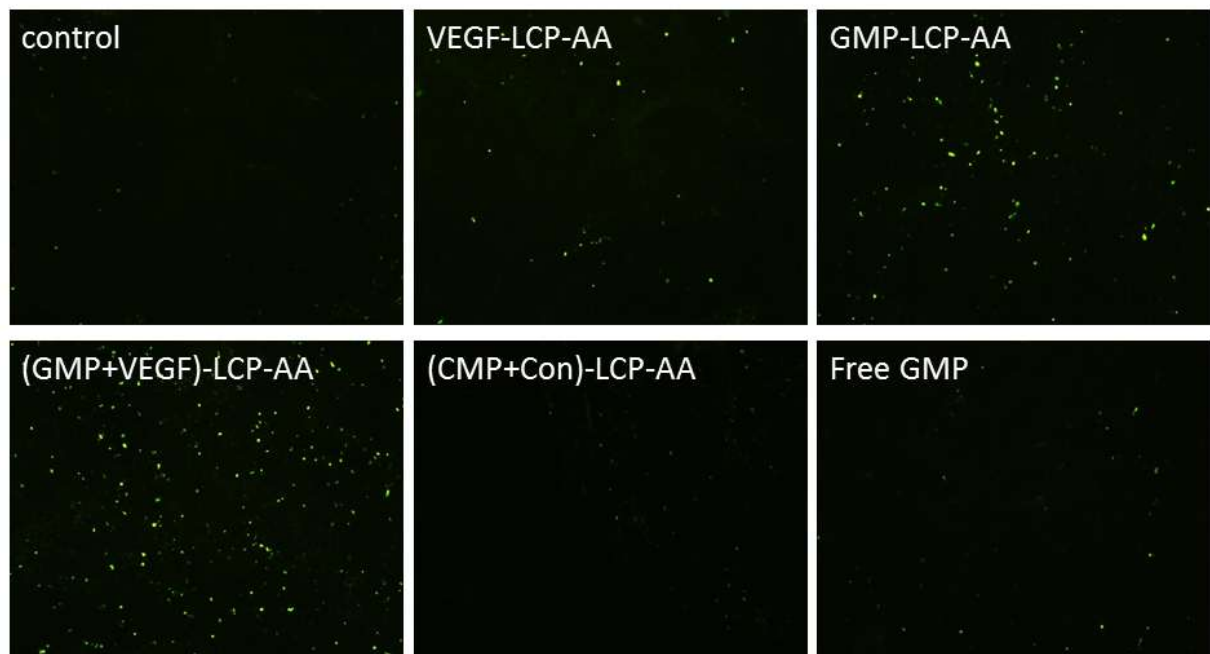
We also evaluated the anti-proliferation effect of different LCP formulations. PCNA is expressed in the cell nuclei during DNA synthesis and can be used as a marker for cell proliferation. As shown in **Fig 4.7C**, (GMP+VEGF)-LCP-AA significantly decreased the number of PCNA positive cells in H460 xenograft tumors. VEGF-LCP-AA and GMP-LCP-AA also caused reductions in the proliferation of tumor cells. The anti-proliferation effect of VEGF-LCP-AA indicates that VEGF not only acts as an endothelial-specific growth factor, it can also promote proliferation of tumor cells.<sup>233</sup> However, (CMP+Con)-LCP-AA and free GMP showed little anti-proliferative effect. From this relatively long-term and infrequent dosing treatment, we had observed additive tumor-cell-killing and

anti-proliferation effects of (GMP+VEGF)-LCP-AA compared to the mono-therapy of GMP-LCP-AA or VEGF-LCP-AA.

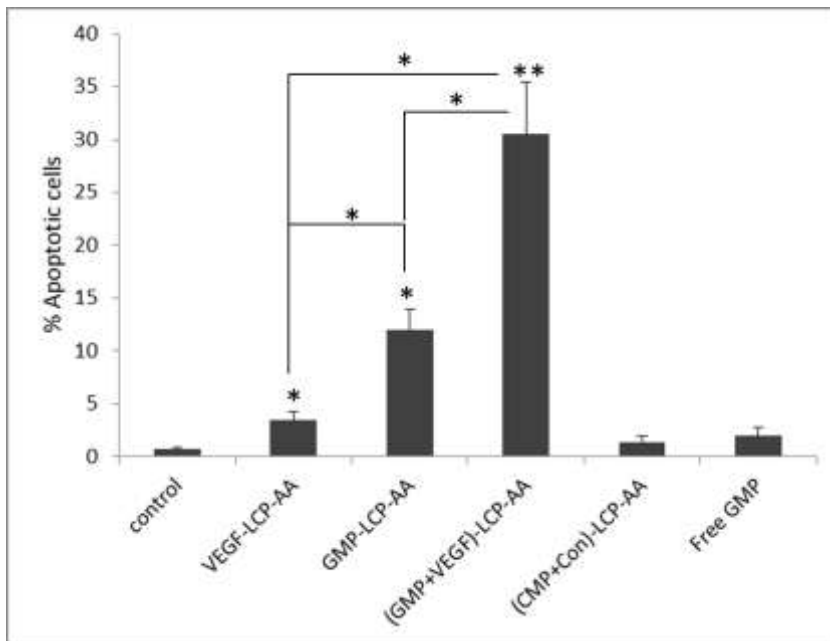
#### **4.3.6 Drug-loaded LCPs inhibited mitotic figures in tumors**

As shown in the H&E stain (**Fig 4.7E**), after long term treatment, the control tumor had many mitotic figures, showing a high mitotic activity of tumor cells. Some typical mitotic figures were shown by arrows in blue. The chromosomes of the mitotic figures are visible as tangled, dark-staining threads or spots. Counting mitotic figures serves as a tool for differentiating benign tumors from malignant ones.<sup>234</sup> The control tumor displayed various cell morphologies with dark clumped chromatin, indicating uncontrollable tumor growth and poor differentiation, otherwise known as malignancy. Cellular and nuclear features also correlated with proliferative activity, with untreated tumors exhibiting marked anisocytosis and anisokaryosis (variation in cell and nuclear size), polyploidy, and open vesicular nuclei with dispersed chromatin and prominent nucleoli. Tumors that were treated with (GMP+VEGF)-LCP-AA experienced a dramatic decrease in mitotic figures and exhibited more basophilic and uniform nuclei. However, some chromosome condensation remained due to the cytotoxicity induced by the combined therapy. The decrease in mitotic figures supported the aforementioned PCNA staining, indicating the anti-proliferation effects of (GMP+VEGF)-LCP-AA partially results from the inhibition of cell mitosis in tumors. VEGF-LCP-AA and GMP-LCP-AA also triggered a decrease in mitotic figures compared to the control. The mitotic figures of tumors in each group are shown quantitatively in **Fig 4.7F**.

A

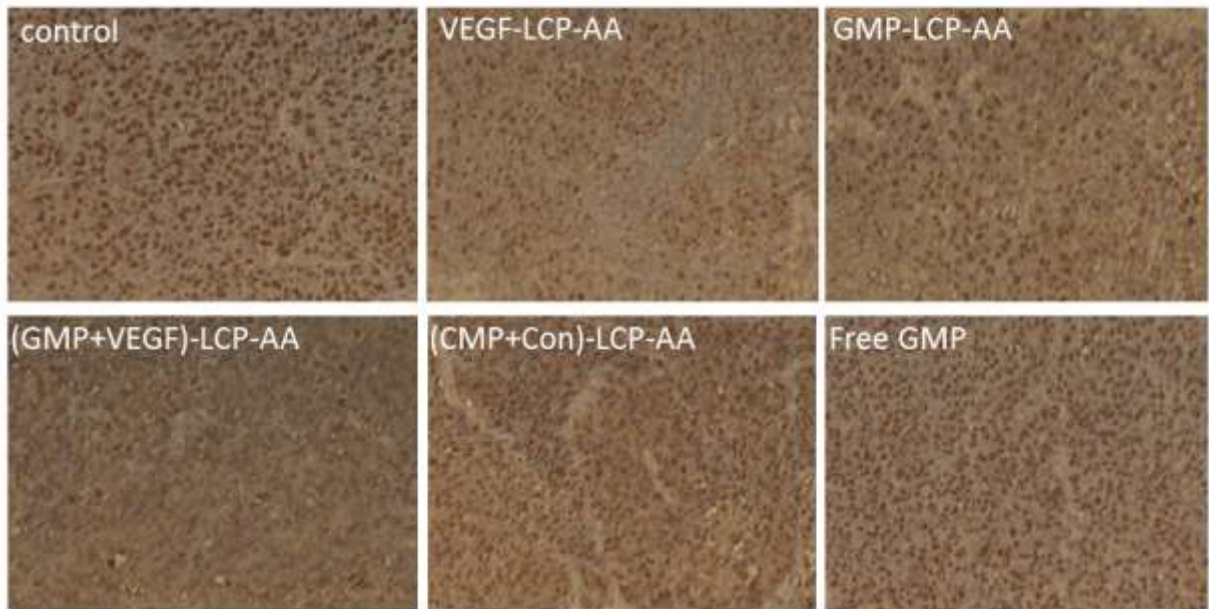


B

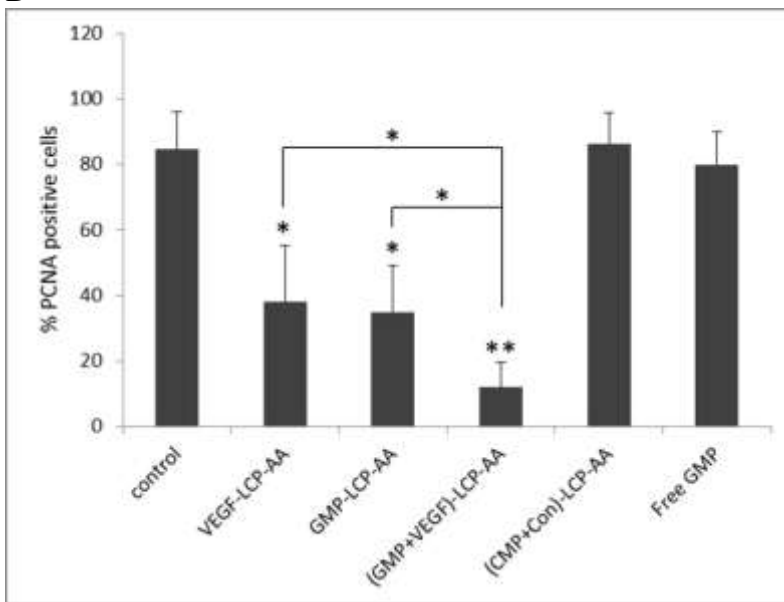


The figure legend of Figure 4.7A and B is on page 124.

C



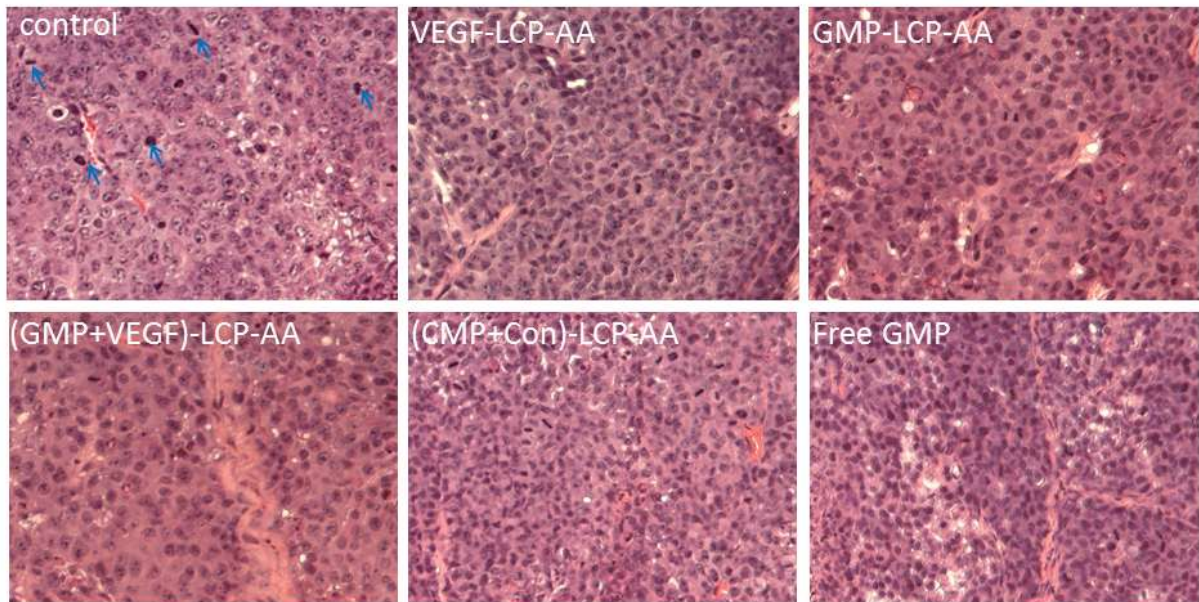
D



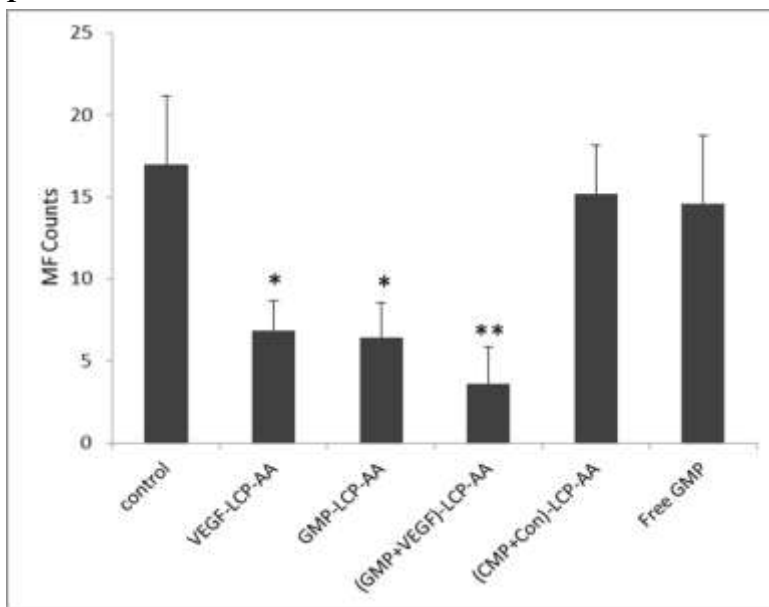
The figure legend of Figure 4.7C and D is on page 124.



E



F



The figure legend of Figure 4.7E and F is on page 124.



#### **Figure 4.7 Immunostaining and mitotic figures after long term treatments.**

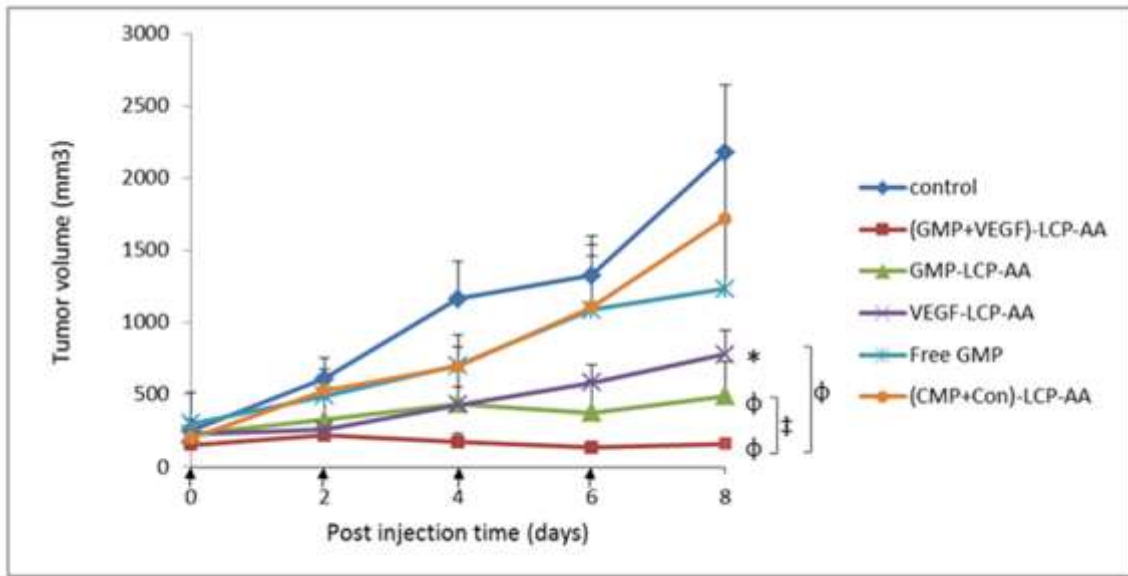
VEGF-LCP-AA, GMP-LCP-AA, (GMP+VEGF)-LCP-AA, (GMP+Con)-LCP-AA and free GMP were administered intravenously every other day for total 4 injections. Two days after the last injection, mice were sacrificed and tumor tissues were sectioned for (A, B) TUNEL assay and (C, D) PCNA immunohistochemistry. (E) Mitotic figures (MF) in tumors were evaluated by H&E stain. (B) Statistics of the TUNEL assay in H460 xenografts:  $*p < 0.005$ , VEGF-LCP-AA vs. control, GMP-LCP-AA vs. control, VEGF-LCP-AA vs. GMP-LCP-AA, VEGF-LCP-AA vs. (GMP+VEGF)-LCP-AA, GMP-LCP-AA vs. (GMP+VEGF)-LCP-AA;  $**p < 0.001$ , (GMP+VEGF)-LCP-AA vs. control. (D) Statistics of the PCNA immunohistochemistry in H460 xenografts:  $*p < 0.05$ , VEGF-LCP-AA vs. control, GMP-LCP-AA vs. control, (GMP+VEGF)-LCP-AA vs. VEGF-LCP-AA, (GMP+VEGF)-LCP-AA vs. GMP-LCP-AA;  $**p < 0.01$ , (GMP+VEGF)-LCP-AA vs. control. (F) Statistics of mitotic figures in tumors:  $*p < 0.001$ , VEGF-LCP-AA vs. control, GMP-LCP-AA vs. control;  $**p < 0.0001$ , (GMP+VEGF)-LCP-AA vs. control.

#### **4.3.7 Tumor growth inhibition**

The tumor growth inhibition was evaluated in nude mice bearing H460 subcutaneous tumors. Mice were treated every other day for a total of 4 IV injections with a dose of 50.4  $\mu\text{mol/Kg}$  GMP and/or 0.2 mg/Kg VEGF siRNA. As shown in **Fig 4.8**, (GMP+VEGF)-LCP-AA exhibited the most effective tumor growth inhibition; growth was almost completely arrested during the combined therapeutic regimen. GMP-LCP-AA also suppressed tumor growth effectively, but not as potently as the combined nanoparticle treatment. Anti-angiogenic monotherapy with VEGF-LCP-AA was not sufficient to obtain long-term tumor suppression. VEGF-LCP-AA stabilized the tumor

growth at early stages of treatment, but unfortunately, was associated with insufficient anti-cancer activity and tumor progression at later stages. The (CMP+Con)-LCP-AA and free GMP had little effect on tumor growth inhibition compared to the control. At the treatment end point, representative tumors in each treatment group were harvested (**Fig 4.8B**) for visual comparison. Tumors treated with (GMP+VEGF)-LCP-AA were smaller than tumors in other treatment groups. Thus, the combined treatment with (GMP+VEGF)-LCP-AA was significantly more effective than treatment with GMP-LCP-AA and VEGF-LCP-AA individually.

A



The figure legend of Figure 4.8A is on the next page.

B

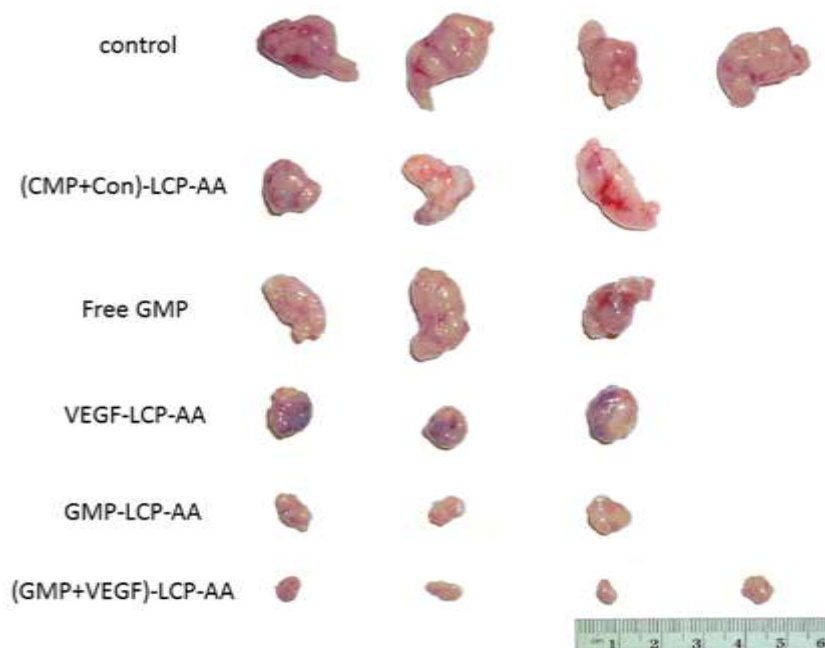


**Figure 4.8 Tumor growth inhibition of different LCPs after systemic treatments.** (A) Tumor growth inhibition effects of different LCP formulations on H460-tumor bearing mice. VEGF-LCP-AA, GMP-LCP-AA, (GMP+VEGF)-LCP-AA, (CMP+Con)-LCP-AA and free GMP were administered intravenously every other day for total 4 injections. Tumor volume was measured every other day. Data are mean  $\pm$  S.D. Statistics are as follows:  $*p < 0.01$ , VEGF-LCP-AA vs. control;  $\phi p < 0.001$ , GMP-LCP-AA vs. control, (GMP+VEGF)-LCP-AA vs. control, (GMP+VEGF)-LCP-AA vs. VEGF-LCP-AA;  $\ddagger p < 0.05$ , (GMP+VEGF)-LCP-AA vs. GMP-LCP-AA. (B) Visual observations of the tumor sizes in each treatment group at the end time point. (Scale unit: cm)

#### 4.3.8 (GMP+VEGF)-LCP-AA reduced the *in vivo* toxicity

To test whether GMP and VEGF siRNA loaded LCPs would induce *in vivo* toxicity, especially hepatic and renal dysfunction after frequent multiple dosing, mice were given

three daily IV injections. Twenty-four h after the final injection, blood samples were obtained for hematological analysis and histopathology of different organs were evaluated by H&E stain. As shown in **Table 4.1**, VEGF-LCP-AA induced a relatively high level of blood urine nitrogen (BUN). GMP-LCP-AA led to higher aspartate aminotransferase (AST) and alanine aminotransferase (ALT) compared to the control. However, treatment with (GMP+VEGF)-LCP-AA alleviated the elevations of BUN, AST and ALT and kept the parameters of kidney and liver functions within the normal range. The administration of chemotherapy to patients with liver impairment may result in complicated safety issues, a treatment regimen using the nanoparticles formulated with both GMP and VEGF can help alleviate the potential liver toxicity as well as enhance the therapeutic response, compared to treatment with a single agent. From the H&E-stained tissue sections of heart, liver, spleen, lung and kidney (**Fig 4.9**), there were no noticeable histological changes between the control and (GMP+VEGF)-LCP-AA treatment group, which showed no evidence of organ toxicity.

**Table 4.1 Serum levels of BUN, creatinine, AST, ALT after 3 daily IV injections in H460 xenograft model.** Data are shown as mean  $\pm$  SD.

	BUN mg/dL	Creatinine mg/dL	AST U/L	ALT U/L
control	15.0 $\pm$ 3.0	0.4 $\pm$ 0.1	129.5 $\pm$ 2.5	45.0 $\pm$ 1.0
VEGF-LCP-AA	33.0 $\pm$ 1.0	0.4	158.5 $\pm$ 3.5	30.5 $\pm$ 8.5
GMP-LCP-AA	11.0 $\pm$ 1.0	0.4 $\pm$ 0.1	371.5 $\pm$ 31.5	81.0 $\pm$ 15.0
(GMP+VEGF)-LCP-AA	15.0 $\pm$ 1.0	0.5	213 $\pm$ 95.1	35.0 $\pm$ 10.0
Reference Range	8--33	0.2--0.9	54--298	17--132

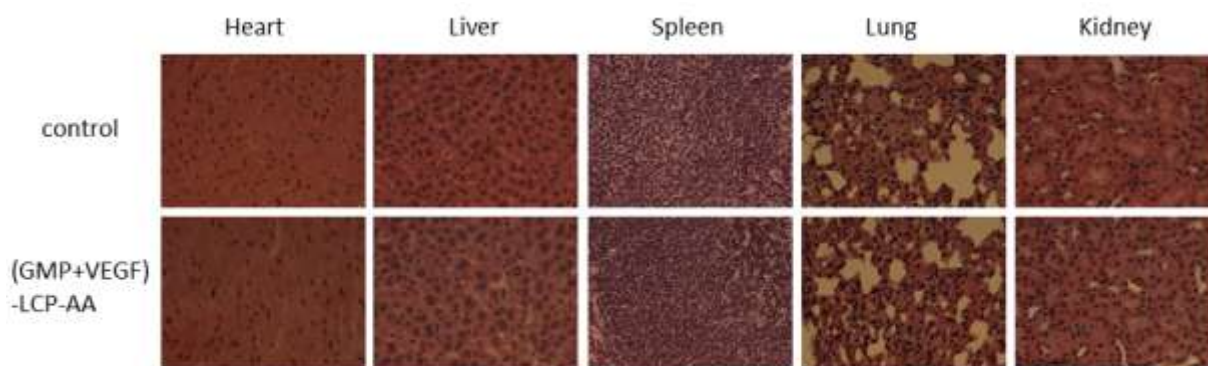


**Figure 4.9 Histopathology of different organs evaluated by H&E stain.**

#### **4.4 DISCUSSION**

In this study, we report a novel systemic delivery platform consisting of the co-formulation of nucleic acid molecules and phosphorylated, small-molecule drugs in a single LCP nanoparticle. GMP and VEGF siRNA were co-formulated using LCP nanotechnology in order to target two therapeutic pathways of an aggressive human cancer malignancy (i.e. NSCLC). Specifically, our delivery system aimed to induce apoptosis through GMP chemotherapy and to shut down the tumor neovasculature by blocking the VEGF-VEGFR signaling cascade with VEGF RNAi.

Phosphate groups on the molecules can interact with calcium in a microemulsion, enabling the encapsulation of GMP and VEGF siRNA in the nanoparticle system containing a calcium phosphate precipitate (CaP) core (i.e. LCP). A lipid bilayer surrounds the CaP core to allow a high density of DSPE-PEG to be grafted onto the surface. The surface modification with PEG helps shield the cationic charge of the lipid bilayer and may minimize the interaction with circulating blood components to prolong circulation time of the particle. The prolonged circulation half-life is a prerequisite for

enhanced tumor targeting and increases the probability that the LCPs will encounter the 'leaky' tumor vasculature and be exposed to the EPR effect.<sup>235</sup> The LCP's high density PEG and small size allow it to evade RES surveillance, which may promote tumor accumulation and decrease toxicity in the liver and kidney. With AA as a tumor-specific targeting ligand, LCPs can be more effectively taken up into tumor cells via sigma-receptor-mediated endocytosis. In addition, the design of the CaP core also promotes endosomal release of the cargo while preventing lysosomal degradation of the entrapped VEGF siRNA and GMP. When LCPs are delivered into acidic endosomes, the CaP core of the LCPs rapidly dissolves to increase the osmotic pressure in the endosome, eventually bursting the endosomes and enabling the entrapped GMP and VEGF siRNA to escape (Fig. 1a).<sup>236</sup> The cationic lipid, DOTAP, surrounding the LCP core may also promote the release of the entrapped cargo by destabilizing the anionic endosome membrane.<sup>237</sup>

Loading Gem derivatives in LCPs can potentially avoid drug efflux proteins (e.g. MRP, BCRP) and the deficiency of cellular uptake caused by the mutations of nucleoside transporters (e.g. ENT1, ENT2, CNT1, CNT3) in the cell membrane. In our previous study, we have validated that the nucleotide analogue Gem triphosphate (GTP)-loaded LCP nanoparticle showed significant anti-tumor efficacy on lung and pancreatic xenograft models (unpublished data). We later found that comparing to GTP which was synthesized in an big organic salt form, GMP (disodium salt form) gave us higher EE% and drug loading, such that similar anti-tumor efficacy were attained. So GMP was used in the current study. The monophosphate modification on GMP allows it to bypass the first rate-limiting phosphorylation step, greatly increasing the conversion rate to

biologically active Gem triphosphate derivatives. On the other hand, the down-regulation of VEGF expression in tumors leads to blockage of the sequential survival signaling initiated by dimerization and autophosphorylation of VEGFR molecules. Blocking VEGF/VEGFR signaling by down-regulating VEGF potentially inhibits aberrant angiogenesis (**Fig 4.1**). Additionally, LCPs can potentially protect VEGF siRNA and GMP from enzymatic degradation (i.e. nuclease and deoxycytidine deaminase, respectively) and renal clearance *in vivo*.

This study indicates that combining anti-angiogenesis treatment with chemotherapy through systemic administrations of LCP nanoparticles containing both VEGF siRNA and phosphorylated Gem results in an additive anti-tumor effect. The co-delivered VEGF siRNA that can damage existing blood vessels in tumors might influence response to the concurrent chemotherapy. Combination therapies are most likely successful because damaging the established tumor endothelium has been shown to increase vessel permeability and facilitate the delivery of subsequently administered LCPs and the co-formulated GMP.<sup>238</sup> The significant knockdown of the pro-angiogenic protein, VEGF, caused by the systemic administrations of (GMP+VEGF)-LCP-AA illustrates that this treatment regime can lead to decreased tumor angiogenesis (**Fig 4.4**). Furthermore, microvessel density is reduced through the reduction of VEGF/VEGFR interactions and the resulting signaling cascades, as indicated by the expression of CD31 antigen in vascular endothelial cells (**Fig 4.6**). These effects of (GMP+VEGF)-LCP-AA modify the tumor microenvironment to potentiate the delivery of the chemodrug. GMP entrapped in the combined LCP subsequently inhibits the pro-survival program as evidenced by

elevated PARP cleavage and caspase activation (**Fig 4.4, 4.5**), significant induction of tumor cell apoptosis and reduction of tumor cell proliferation (**Fig 4.4, 4.7**).

The advantages of nanoparticles containing multiple drugs are that they can offer the unique features of vehicle uniformity, ratiometric drug loading and temporal drug release, while maintaining the ability to unify the pharmacokinetics of different drugs they encapsulate. These nanoparticles are thereby able to simultaneously deliver multiple gene- and/or chemo- therapeutic agents to the target site.<sup>239</sup> We have done some preliminary work on the comparison of (GMP+VEGF)-LCP-AA and the co-administered mixture of GMP-LCP-AA and VEGF-LCP-AA on the anti-tumor therapeutic response. The results indicated the combined (GMP+VEGF)-LCP-AA had more potency in inducing cell-killing effects compared to the administration of separate LCPs loaded with each individual agent (unpublished data). The pharmacokinetic profiles and the therapeutic effects of the drug loading ratio are now under investigation. The strategy of co-formulating multiple gene therapeutics and phosphorylated chemodrugs in a single vector via LCP nanotechnology is expected to lead to superior therapeutic improvement in many human diseases, and to modulate multiple therapeutic pathways simultaneously.



## **5.0 CO-DELIVERY OF C-MYC siRNA AND GEMCITABINE MONOPHOSPHATE VIA LCP NANOPARTICLES TO NSCLC SUBCUTANEOUS AND ORTHOTOPIC MOUSE MODELS.**

There is an urgent need for new therapeutics for the treatment of aggressive and metastatic refractory human non-small-lung-cell cancer (NSCLC). In this study, we developed a Lipid/Calcium/Phosphate (LCP) nanoparticle-based lung cancer therapeutic regimen which combines the anti-tumor efficacy of a chemodrug gemcitabine monophosphate (GMP) with siRNA that is specific for an undruggable oncogene c-Myc, while overcoming the *in vivo* delivery challenges that currently limit their clinical application. The combination therapy using LCP loaded with both c-Myc siRNA and GMP showed a potent activity in inducing apoptosis and reducing proliferation in both a subcutaneous tumor model and an orthotopic model of NSCLC in nude mice with systemic administration. The improved therapeutic response, as compared to either c-Myc siRNA or GMP therapy alone, was supported by the observation of effective induction of tumor cell apoptosis, significant reduction of tumor cell proliferation. The combination therapy led to dramatic inhibition of tumor growth with little *in vivo* toxicity. Additionally, the current studies demonstrated the possibility of incorporating multiple nucleic acid molecules and phosphorylated small molecule drugs, targeting to different pathways, into a single nanoparticle formulation. Co-encapsulation of an oncogene-modulating siRNA and a chemotherapeutic agent will allow simultaneous interruption of

diverse anti-cancer pathways, leading to increased therapeutic efficacy and reduced toxicities.

## 5.1 INTRODUCTION

Lung cancer continues to be the leading cause of cancer-related deaths both in the United States and throughout the world. Non-small-cell lung carcinoma (NSCLC) is the most aggressive type of lung cancer and accounts for up to 80-85% of all lung cancers, while SCLC and other more rare histologic subtypes make up the remainder. Many NSCLC tumors over-express c-Myc which is a pivotal transcription factor controlling the expressions of many proliferation genes. It is one of the most highly amplified downstream oncogenes that promote cell growth, proliferation, invasion, expansion and angiogenesis.<sup>242, 243</sup> Although the importance of c-Myc in oncogenesis and maintenance of the lung malignancy has long been recognized, no small molecule chemo drugs have been approved for clinical use. Thus, c-Myc remains to be an “undruggable” target to which alternative approaches must be developed. Myc oncogene family members are considered “undruggable” for two reasons. First, Myc genes encode basic helix-loop-helix transcription factors, which do not provide druggable domains. Second, Myc-encoded transcription factors carry out so many functions, so their persistent down-regulation would likely result in severe side effects for patients.<sup>250</sup> The advent of RNAi has brought about a fresh look in controlling any “undruggable” targets. siRNA, although very potent and specific in silencing an oncogenic target, has to be protected from degradation and efficiently delivered to the cytoplasm of the tumor cells. LCP contains a core consisted of amorphous calcium phosphate precipitation which can encapsulate

siRNA. The CaP core is further coated with a single lipid bilayer to which PEGylation and targeting ligand can be efficiently added for functionalization.

One of the salient features of LCP is the opportunity to co-encapsulate both siRNA and a phosphorylated chemo drug. Gemcitabine is a nucleoside prodrug which must be activated intracellularly by phosphorylation. GMP, the first activated species of gemcitabine, can be effectively encapsulated in LCP and delivered to tumor cells to induce apoptosis. The anticancer potency of GMP was shown in the previous study. In this study, GMP was co-encapsulated in LCP together with c-Myc siRNA. Tumor lesions were dissected for caspase 3/7 assay. They were tested for TUNEL and PCNA assays, for apoptosis and proliferation, respectively. Apoptosis marker PARP was also tested by western blot analysis. Hematological, hepatic and renal toxicities of the NP were evaluated in immune competent normal mice after repeated injection of NPs at therapeutic dose. LCP containing both therapeutic agents showed greater apoptosis induction and proliferation reduction activities than either agent alone in the subcutaneous and orthotopic xenograft model of human NSCLC.

## **5.2 MATERIALS AND METHODS**

### **5.2.1 Materials**

Gemcitabine monophosphate disodium salt (GMP) was synthesized by HDH Pharma, Inc. (Research Triangle Park, NC). c-Myc siRNA (target sequence: 5'- CAG AAA UGU CCU GAG CAA UUU-3') and control siRNA (target sequence: 5'-AAU UCU CCG AAC GUG TCA CGU-3') were synthesized by Sigma-Aldrich (St. Louis, MO). 1, 2-Dioleoyl-3-trimethylammonium-propane chloride salt (DOTAP), dioleoylphosphatidic acid (DOPA), and 1,2-distearoyl-sn-glycero-3-phosphoethanolamine-N-

[methoxy(polyethyleneglycol-2000) ammonium salt (DSPE-PEG<sub>2000</sub>) were purchased from Avanti Polar Lipids, Inc. (Alabaster, AL). DSPE-PEG-AA was synthesized in our lab as described previously.<sup>240</sup> DeadEnd Fluorometric TUNEL assay kits and Apo-ONE Homogeneous Caspase-3/7 assay substrates were obtained from Promega Corporation (Madison, WI). Other chemicals were obtained from Sigma-Aldrich (St. Louis, MO).

### **5.2.2 Cell culture**

H460 and A549 human NSCLC cells, originally obtained from American Type Culture Collection (ATCC) (Manassas, VA), were cultured in RPMI-1640 medium (Invitrogen, Carlsbad, CA) supplemented with 10% fetal bovine serum, 100 U/mL penicillin and 100 µg/mL streptomycin (Invitrogen). Cells were cultivated in a humidified incubator at 37°C and 5% CO<sub>2</sub>. Cells were harvested with 0.05% trypsin-EDTA before subculture.

### **5.2.3 Experimental animals**

Female nude mice 6-8 weeks of age were used in all studies. To establish the xenograft models,  $5 \times 10^6$  H460 cells in 100 µL of PBS were injected subcutaneously into the right flank of mice. All work performed on animals was approved by the Institutional Animal Care and Use Committee at University of North Carolina at Chapel Hill. With the orthotopic model (**Fig 5.1**), A549 cells were injected via a 28 g needle about 2 cm up from the bottom of the ribcage via the left dorsal side. Mice will be maintained under a surgical plane of anesthesia and receive lidocaine at the incision site preoperatively. These procedures were conducted by experienced full-time veterinarians at the Animal Facility of UNC-Chapel Hill.

## NSCLC (A549) Orthotopic model

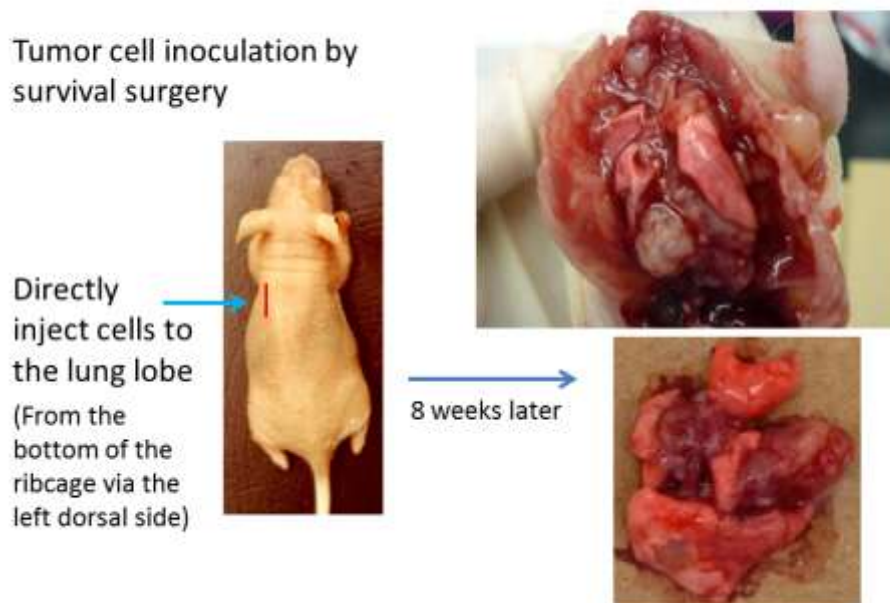


**Figure 5.1 Graphical illustration of the establishment of NSCLC (A549) orthotopic model.**

### **5.2.4 Preparation of cMyc-LCP-AA, GMP-LCP-AA and (GMP+cMyc)-LCP-AA**

LCP cores were prepared using water-in-oil micro-emulsions, with the oil phase containing cyclohexane/ Igepal CO-520 solution (71/29, v/v).<sup>241</sup> To prepare the cMyc-LCP cores, 48  $\mu\text{g}$  cMyc siRNA was mixed with 600  $\mu\text{L}$  2.5 M  $\text{CaCl}_2$  and added into 20 mL of oil phase, where the other emulsion contained 600  $\mu\text{L}$  12.5 mM  $\text{Na}_2\text{HPO}_4$  (pH=9.0). The GMP-LCP core was formulated using 180  $\mu\text{L}$  of 60 mM GMP mixed with 12.5 mM  $\text{Na}_2\text{HPO}_4$  (pH=9.0) (final concentration) to reach a total volume of 600  $\mu\text{L}$ . This solution was then added into 20 mL of oil phase. Six-hundred  $\mu\text{L}$  2.5 M  $\text{CaCl}_2$  was added to a separate the 20 mL oil phase. To prepare the (GMP+cMyc)-LCP core, the phosphate phase met the same specifications outlined in the preparation of the GMP-LCP

core. The calcium phase contained 600  $\mu\text{L}$  of 2.5 M  $\text{CaCl}_2$  mixed with 48  $\mu\text{g}$  of cMyc siRNA. Four-hundred  $\mu\text{L}$  of 20 mM DOPA in chloroform was added to the phosphate phase of the GMP-LCP and (GMP+cMyc)-LCP, whereas only 200  $\mu\text{L}$  of 20 mM DOPA was added to the phosphate phase during the preparation of the cMyc-LCP.

The two separate micro-emulsions were then mixed. After stirring for 5 min, another 400  $\mu\text{L}$  of 20 mM DOPA was added into the emulsion of GMP-LCP and (GMP+cMyc)-LCP; for cMyc-LCP, 200  $\mu\text{L}$  of 20 mM DOPA was added. The emulsion was allowed to continually stir for another 20 min before 40 mL of absolute ethanol was added. The ethanol emulsion mixture was centrifuged at 10,000 g for 15 min to pellet the LCP core and the supernatant was then discarded. The LCP core was washed twice with absolute ethanol and dried under  $\text{N}_2$ . The LCP core pellets were suspended in 2 mL chloroform and stored in a glass vial at  $-20^\circ\text{C}$  for further use.

To prepare the final cMyc-LCP-AA, GMP-LCP-AA and (GMP+cMyc)-LCP-AA with outer lipid coating, 330  $\mu\text{L}$  LCP core in chloroform was mixed with 38.7  $\mu\text{L}$  of 10 mg/mL Cholesterol, 28  $\mu\text{L}$  of 25 mg/mL DOTAP, 76.8  $\mu\text{L}$  of 25 mg/mL DSPE-PEG and 19.2  $\mu\text{L}$  of 25 mg/mL DSPE-PEG-AA. After evaporating the chloroform, the residual lipids were dissolved in 30  $\mu\text{L}$  THF followed by 50  $\mu\text{L}$  absolute ethanol, and then suspended in 160  $\mu\text{L}$  water. After brief sonication, the solution was dialyzed in distilled water to remove the THF and ethanol. The preparation procedure of (CMP+Con)-LCP-AA was identical to that of (GMP+cMyc)-LCP-AA, except that GMP and cMyc siRNA were replaced by equal molar amount of CMP and control siRNA.

### **5.2.5 Characterization of cMyc-LCP-AA, GMP-LCP-AA and (GMP+cMyc)-LCP-AA**

The particle size and zeta potential of LCPs were determined by dynamic light scattering using a Malvern ZetaSizer Nano series (Westborough, MA). The EE% of GMP or siRNA was measured after lysing the LCPs with a THF/1M HCl (v/v= 70/30) solution. GMP EE% was measured using a UV spectrophotometer (Beckman Coulter Inc., DU 800 spectrophotometer) at a wavelength of 275 nm. The EE% of siRNA was measured by mixing a small amount of Texas-red labeled siRNA with c-Myc siRNA in LCP cores, and the fluorescence intensity of Texas-red was detected at the wavelength of Ex=589 nm and Em=615 nm. TEM images of LCP formulations were acquired through the use of JEOL 100CX II TEM (Tokyo, Japan). Briefly, 4  $\mu$ l of LCP solution was dropped onto a 300 mesh carbon coated copper grid (Ted Pella, Inc., Redding, CA) for 2 min. Excess fluid was then removed with filter paper, and the copper grid was dried before observation using the TEM.

### **5.2.6 Western blot analysis**

Twenty-four h after the third injection, mice were sacrificed and tumor lysates were prepared with radioimmunoprecipitation assay (RIPA) buffer, supplemented with a protease inhibitor cocktail (Promega, Madison, WI). Protein concentrations were determined using a BCA assay kit (Pierce Biotechnology) following the manufacturer's recommendations. Forty  $\mu$ g of protein per lane was separated by 4%-12% SDS-PAGE electrophoresis (Invitrogen) before being transferred into polyvinylidene difluoride (PVDF) membranes. The membranes were blocked for 1 h with 5% silk milk at room temperature and then incubated with mouse monoclonal c-Myc antibody and mouse

monoclonal poly(ADP-ribose) polymerase-1 (PARP-1) antibody (1:500 dilution; Santa Cruz Biotechnology) overnight at 4°C.  $\beta$ -actin antibodies (1:4000 dilution; Santa Cruz Biotechnology) served as the loading control. The membranes were washed 3 times and then incubated with secondary antibodies (1:4000 dilution; Santa Cruz Biotechnology) at room temperature for 1 h. Finally, the membranes were washed 4 times and developed by an enhanced chemiluminescence system according to the manufacturer's instructions (Thermo Scientific).

### **5.2.7 Caspase activation**

Twenty-four h after 3 daily IV injections, forty  $\mu$ g protein of each tumor lysate was used to detect caspase-3/7 activity in tumors according to the manufacturer's instructions (Invitrogen, NY). Briefly, 25  $\mu$ L sample solution containing 40  $\mu$ g of protein was added to a 96-well plate, and 25  $\mu$ L caspase-3/7 reagent was added to each sample well. The contents of the wells were gently mixed at 400 rpm for at least 1 h at room temperature. Their fluorescence was measured using a microplate reader at a wavelength of Ex=485 nm and Em=535 nm. The fluorescence intensity of treatment groups was normalized to that of the control group to indicate the extent of caspase activation.

### **5.2.8 TUNEL assay**

After predetermined dosing schedule, H460 tumor-bearing mice were sacrificed and tumors were fixed in 10% formalin for 24 h before embedded in paraffin and sectioned at a thickness of 5  $\mu$ m. The TUNEL staining was performed as recommended by the manufacturer (Promega, Madison, WI). Then DAPI mounting medium was dropped on the sections for nucleus staining. Images of TUNEL-stained tumor sections were captured with a fluorescence microscope (Nikon Corp., Tokyo, Japan). The percentage of



apoptotic cells was obtained by dividing the number of apoptotic cells (TUNEL positive cells shown as green dots) from the number of total cells (blue nuclei stained by DAPI, not shown) in each microscopic field, and 10 representative microscopic fields were randomly selected in each treatment group (n=3) for this analysis.

#### **5.2.9 Immunohistochemistry**

Paraffin-embedded tumor sections were obtained as mentioned above. The PCNA (1:200 dilution, Santa Cruz) immunohistochemistry was performed using the HRP/DAB detection IHC kit as recommended by the manufacturer (Abcam, Cambridge, MA). Immunostaining images were observed under a light microscope (Nikon Corp., Tokyo, Japan). The percentage of proliferation cells was obtained by dividing the number of PCNA positive cells (shown as brown dots) from the number of total cells (blue nuclei stained by hematoxylin) in each microscopic field, and 10 representative microscopic fields were randomly selected in each treatment group (n=3) for counting.

#### **5.2.10 Tumor growth inhibition**

Tumor growth inhibition of the nanoparticles system was evaluated in an H460 subcutaneous xenograft mouse model. When the tumor volumes reached about 150-200 mm<sup>3</sup>, the mice were randomly assigned into 6 treatment groups, and intravenously injected different LCPs, including cMyc-LCP-AA, GMP-LCP-AA, (GMP+cMyc)-LCP-AA, (CMP+Con)-LCP-AA and (GMP-LCP-AA)+(cMyc-LCP-AA) mixture with each reagent half dose to maintain the same amount of nanoparticles. The IV injections were performed every other day for a total of 4 injections with a dose of 25.2 µmol/Kg GMP and/or 0.2 mg/Kg c-Myc siRNA. Tumor sizes were measured every other day with calipers across their two perpendicular diameters, and the tumor volume was calculated

using the following formula:  $V=0.5 \times (W^2 \times L)$ , where V = tumor volume, W = the smaller perpendicular diameter and L = the larger perpendicular diameter. The body weights in each treatment group were also measured during the study. Two days after the final injection, the mice were sacrificed and the tumor weights were measured.

#### **5.2.11 *In vivo* toxicity**

Mice were given every other day IV injections, total 4 injections. Two days after the last injection, blood was drawn from the venous plexus of the eyes of the mice. Blood samples were immediately centrifuged at 3,000 g for 5 min at 4°C, and the supernatant blood serums were collected for hematological analysis. BUN, creatinine, AST, ALT values were recorded, as indications of hepatic and renal functions.

#### **5.2.12 Statistical analysis**

Results were expressed as a mean  $\pm$  standard deviation (SD). Student t-tests were used to evaluate statistical significance. A result of  $p < 0.05$  was considered to be statistically significant.

### **5.3 RESULTS**

#### **5.3.1 Characterization of drug-loaded LCPs**

The Transmission electron microscope (TEM) photographs showed that all drug-loaded LCP-AAs had a spherical shape and were monodispersed, with a particle size of around 30 nm (**Fig 5.2**). The relatively small size of LCPs renders them better tumor penetration capability over large size nanoparticles.<sup>227</sup> The encapsulation efficiency (EE%) of c-Myc siRNA and GMP in LCP-AA was around 55% and 75%, respectively. The EE% of c-Myc siRNA and GMP in co-formulated LCP-AA was almost the same as that of the

cMyc-LCP-AA or GMP-LCP-AA single formulation, which indicates that c-Myc siRNA and GMP did not interfere with each other in the process of co-precipitation with calcium ions within the LCP core.

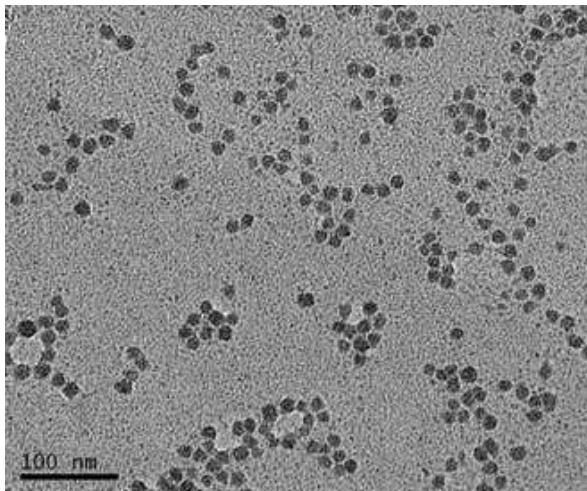


**Figure 5.2** TEM pictures of (GMP+cMyc)-LCPs. Scale bar = 100 nm.

### **5.3.2 Drug-loaded LCPs induced VEGF down-regulation and apoptosis *in vivo***

Human NSCLC H460 tumor bearing mice were given three daily IV injections of different LCP formulations with a dose of 25.2  $\mu\text{mol/Kg}$  GMP (9.3 mg/Kg GMP, or 6.6 mg/Kg in terms of Gem) and/or 0.2 mg/Kg c-Myc siRNA. Twenty-four h after the third injection, mice were sacrificed and tumor lysates were prepared for western blot. PARP is a nuclear protein that performs central roles in the repair of damaged DNA. Cleavage of PARP by caspases is considered to be a hallmark of apoptosis.<sup>228</sup> As shown in **Fig 5.3**, (GMP+cMyc)-LCP-AA showed significant knockdown of the c-Myc oncogene, and stimulated the over-expression of cleaved PARP. GMP-LCP-AA also activated the cleaved PARP over-expression, but had only a minor effect on the c-Myc expression level. cMyc-LCP-AA clearly reduced the c-Myc expression, but had limited effect on

PARP cleavage. (GMP-LCP-AA) and (cMyc-LCP-AA) mixture showed partial downregulation of the c-Myc oncogene.

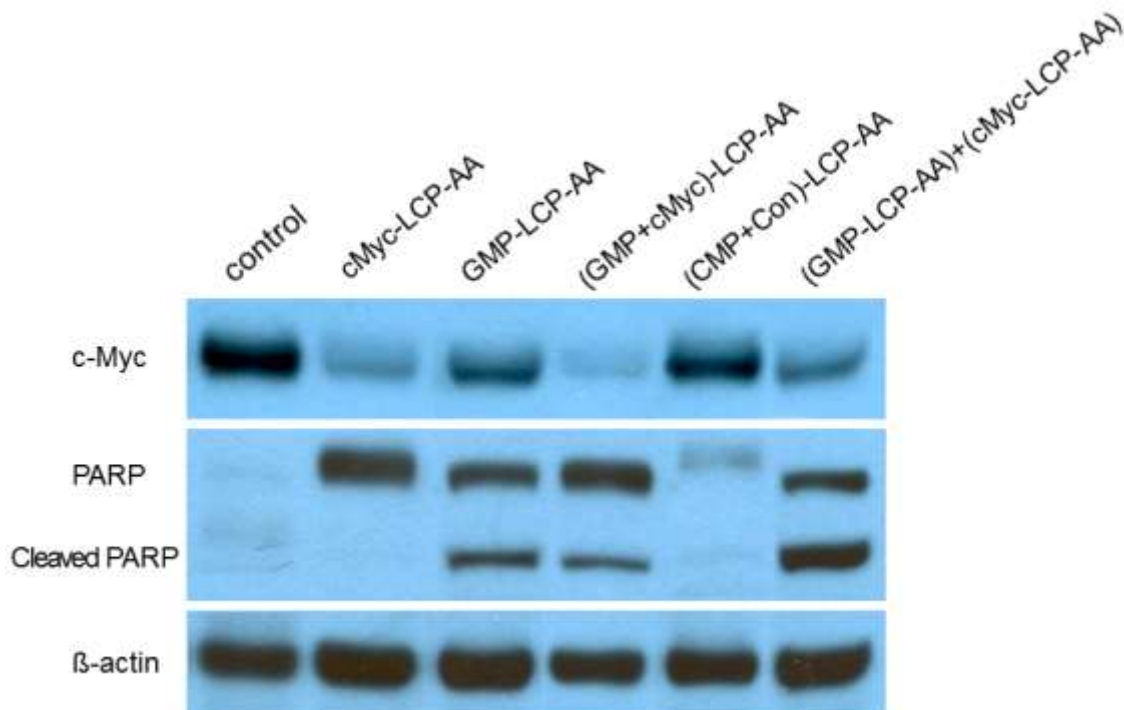


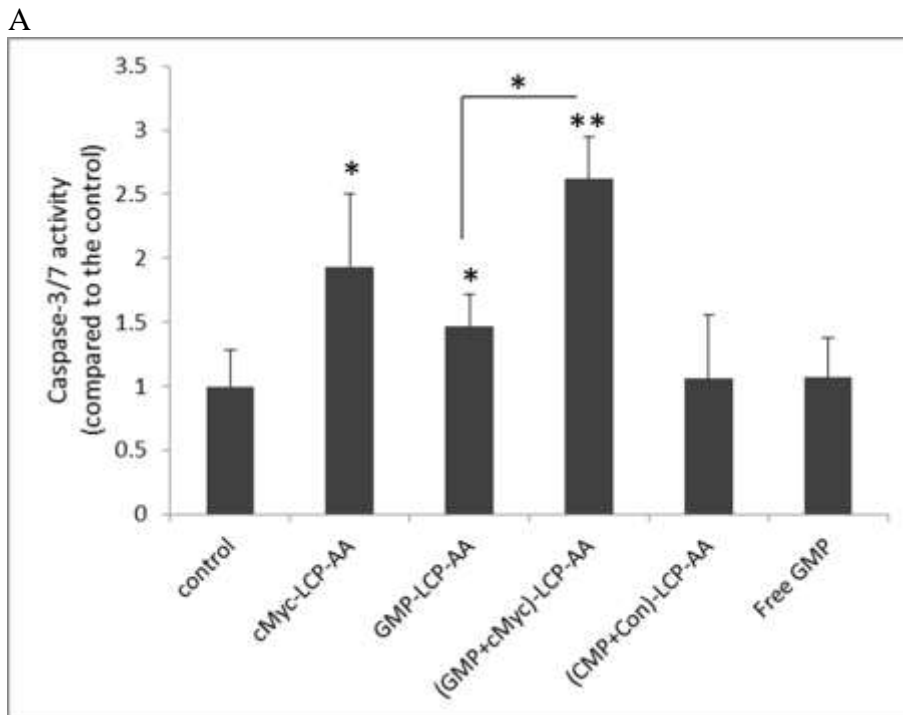
**Figure 5.3 Western blot analysis for VEGF and cleaved PARP expressions *in vivo* after systemic treatment of different LCP formulations on H460 subcutaneous xenograft model.**

### **5.3.3 Drug-loaded LCPs triggered caspase activation and tumor cell apoptosis *in vivo***

Caspases are proteolytic enzymes and play an important role in apoptosis as effector molecules. Among the caspase enzymes, caspase-3 and caspase-7 are especially important, and they are responsible for the proteolytic cleavage of a large number of substrates during apoptosis.<sup>229</sup> Twenty-four h after 3 daily IV injections, caspase-3/7 activity in A549 lung orthotopic tumor nodules was increased significantly in mice injected with (GMP+cMyc)-LCP-AA. The GMP-LCP-AA and cMyc-LCP-AA partially

increased the caspase activity (**Fig 5.4A**). (CMP+Con)-LCP-AA and free GMP displayed little caspases elevation (**Fig 5.4A**).

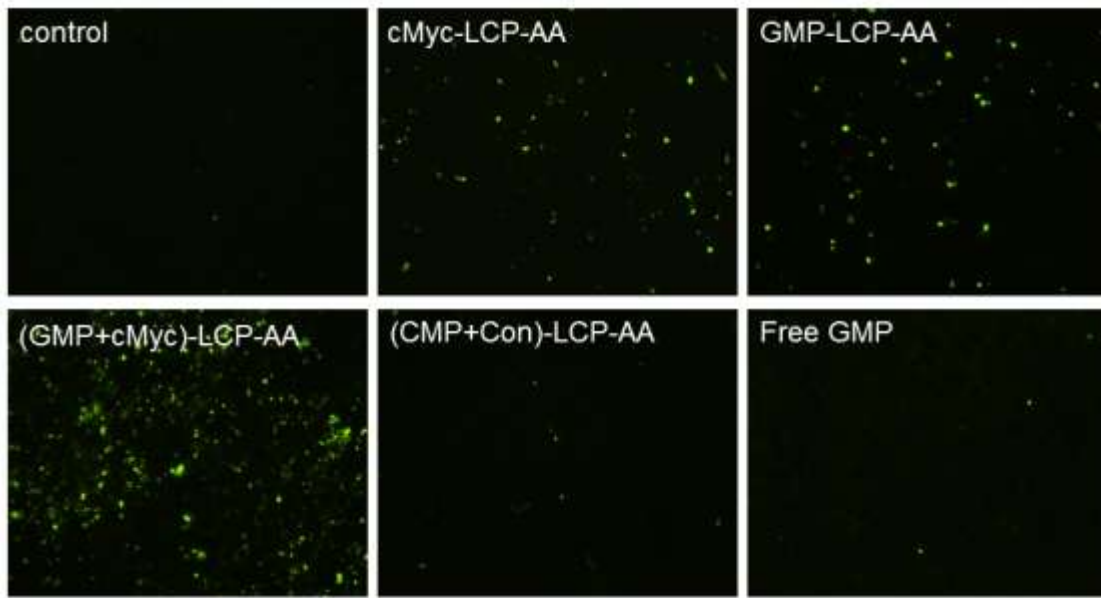
We also measured the apoptotic induction in A549 lung orthotopic tumor nodules using the TdT-mediated dUTP Nick-End Labeling (TUNEL) assay. Twenty-four h after 3 daily IV injections, (GMP+cMyc)-LCP-AA triggered a dramatic killing effect, inducing more than 40% apoptotic cells in tumors. GMP-LCP-AA and VEGF-LCP-AA led to about 10% apoptotic tumor cells. (CMP+Con)-LCP-AA and free GMP did not elicit tumor cell apoptosis (**Fig 5.4B**). The tumor cell apoptotic induction of (GMP+cMyc)-LCP-AA was significantly higher than GMP-LCP-AA and VEGF-LCP-AA, indicating a profound therapeutic effect of the combined LCP.



---

The figure legend of Figure 5.4A is on the next page.

B



C

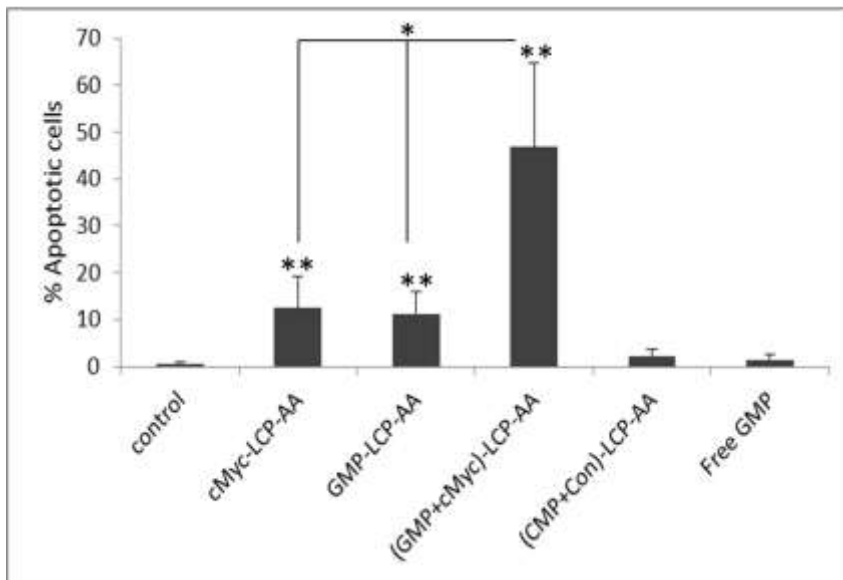
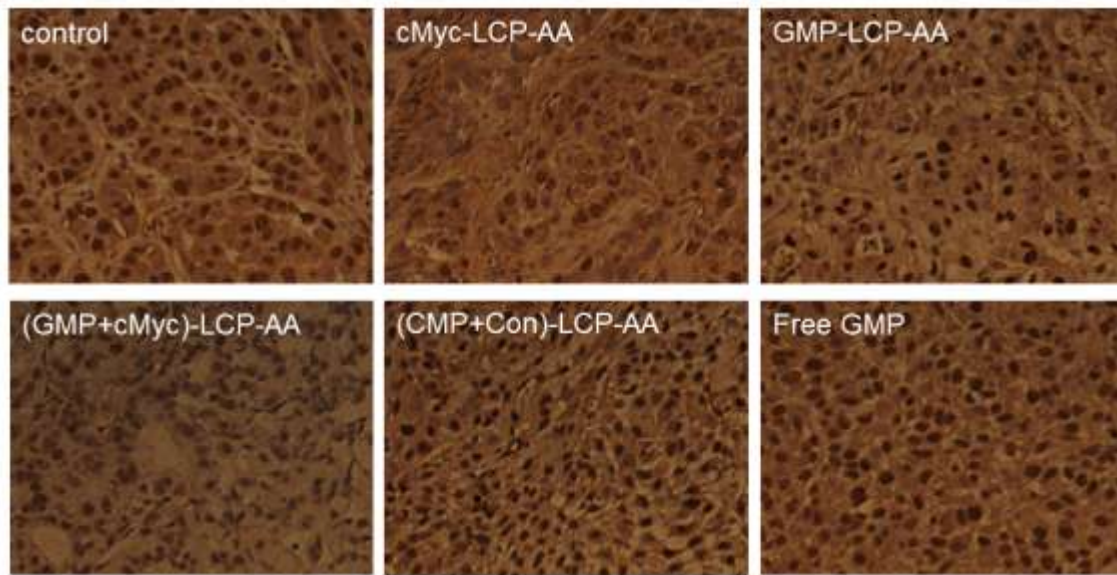


**Figure 5.4** The caspase activation and induction of apoptosis after the systemic administration of different LCPs in A549 lung orthotopic xenografts (n=4). (A) *In vivo* caspase-3/7 activity in tumors. \*\* $p < 0.01$ , \* $p < 0.05$ . (B) *In vivo* tumor apoptosis by TUNEL assay. (C) The percentage (%) of apoptotic cells in the TUNEL assay. \*\* $p < 0.00001$  vs. control, \* $p < 0.0001$ .

#### **5.3.4 Drug-loaded LCPs inhibited tumor cell proliferation *in vivo***

The A549 lung orthotopic tumor-bearing mice were given three daily IV injections of different LCP formulations. One day after the final injection, the mice were sacrificed and the tumor nodules were sectioned for PCNA immunohistochemistry. PCNA is expressed in the cell nuclei during DNA synthesis and can be used as a marker for cell proliferation. As shown in **Fig 5.5**, (GMP+cMyc)-LCP-AA significantly decreased the number of PCNA positive cells. cMyc-LCP-AA and GMP-LCP-AA also caused reductions in the proliferation of tumor cells, but not as potent as the combined therapy. (CMP+Con)-LCP-AA and free GMP showed little anti-proliferative effect.

A



B

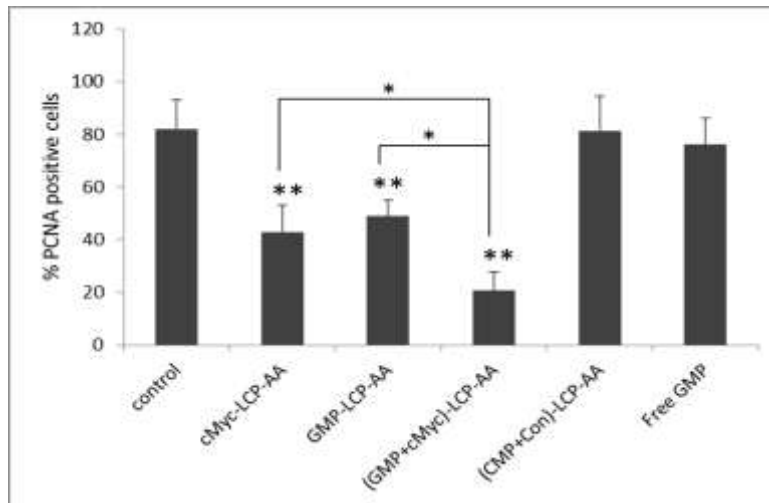


**Figure 5.5 Tumor cell proliferation after the systemic administration of different LCPs in A549 lung orthotopic xenografts.** cMyc-LCP-AA, GMP-LCP-AA, (GMP+cMyc)-LCP-AA, (GMP+Con)-LCP-AA and free GMP were administered intravenously over consecutive three days (n=4). One day after the last injection, mice were sacrificed and tumor nodules were sectioned for (A) PCNA immunohistochemistry in A549 lung orthotopic tumor nodules. (B) Statistics of the PCNA immunohistochemistry in A549 orthotopic xenografts: \*\* $p<0.0001$  vs. control, \* $p<0.01$ .



### 5.3.5 Tumor growth inhibition

Due to the heterogeneity of tumor formation in the orthotopic model, the tumor growth inhibition was evaluated in nude mice bearing H460 subcutaneous tumors. Mice were treated every other day for a total of 4 IV injections with a dose of 25.2  $\mu\text{mol/Kg}$  GMP and/or 0.2 mg/Kg c-Myc siRNA. As shown in **Fig 5.6**, (GMP+cMyc)-LCP-AA exhibited the most effective tumor growth inhibition; growth was almost completely arrested during the combined therapeutic regimen. GMP-LCP-AA, cMyc-LCP-AA and each particle mixture also suppressed tumor growth effectively, but not as potently as the combined nanoparticle treatment. The (CMP+Con)-LCP-AA had little effect on tumor growth inhibition compared to the control. There were no body weight changes among different treatment groups. At the treatment end point, the tumor weights in combined treatment group were much lower than other groups.

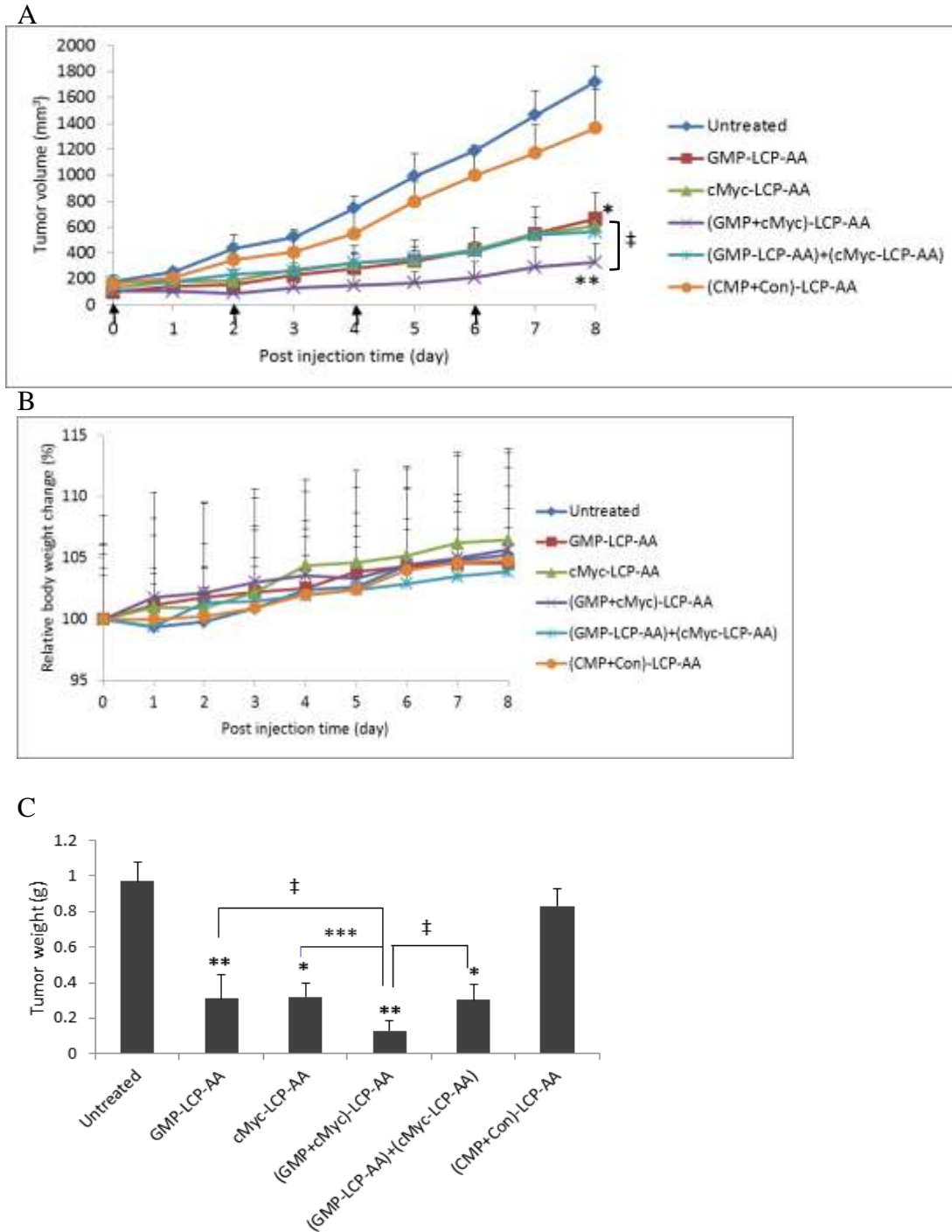


**Figure 5.6 Tumor growth inhibition after systemic treatment of different LCPs.** (A) Tumor growth inhibition on H460 xenografts. \* $p < 0.0005$  vs. Untreated. \*\* $p < 0.00001$  vs. Untreated. ‡ $p < 0.05$ . (B) The relative body weight changes of H460 xenografts. Data are mean  $\pm$  S.D. (n=5). (C) The tumor weights in different treatment groups at the end time point. \* $p < 0.005$ , \*\* $p < 0.001$ , ‡ $p < 0.05$ , \*\*\* $p < 0.01$ .

### 5.3.6 *In vivo* toxicity

To test whether GMP and c-Myc siRNA loaded LCPs would induce *in vivo* toxicity, especially hepatic and renal dysfunction after long term treatment, blood samples were obtained for hematological analysis. Long term treatment was characterized as every other day IV injections, total 4 injections, and the blood was drawn two days after the last injection from the venous plexus of the eyes of the mice. As shown in **Table 5.1**, There was little elevation of BUN, creatinine and liver enzymes (AST, ALT) in blood serum compared to the control, and all parameter values were in the normal range. Thus, GTP-loaded LCPs, at the therapeutic dose, did not elicit any toxicity in kidney and liver and there were no significant safety issues.

**Table 5.1 Serum levels of BUN, creatinine, AST, ALT after long term treatment (n=4).** Balb/c mice were given every other day IV injections, total 4 injections. Two days after the final injection, blood serum were collected for hematological analysis. Data are shown as mean  $\pm$  SD.

	BUN (mg/dL)	Creatinine (mg/dL)	AST (U/L)	ALT (U/L)
Control	26.0 $\pm$ 3.0	0.2	140 $\pm$ 5.0	46.0 $\pm$ 2.0
GMP-LCP-AA	27.3 $\pm$ 6.0	0.2	134 $\pm$ 14.2	47.7 $\pm$ 6.1
cMyc-LCP-AA	22.3 $\pm$ 3.5	0.2	144 $\pm$ 37.6	56.7 $\pm$ 12.5
(GMP+cMyc)-LCP-AA	23.6 $\pm$ 4.0	0.2	131 $\pm$ 26.6	54.7 $\pm$ 5.5
(GMP-LCP-AA)+(cMyc-LCP-AA)	23.8 $\pm$ 4.1	0.2	123 $\pm$ 22.0	53.8 $\pm$ 8.3
(CMP+Con)-LCP-AA	25.0 $\pm$ 3.4	0.2	141 $\pm$ 10.2	53.0 $\pm$ 4.1
Reference Range	8–33	0.2–0.9	54–298	17–132

## 5.4 DISCUSSION

There are now a number of active chemotherapeutic regimens developed for NSCLC, including gemcitabine based regimens, these chemotherapeutic treatments provide only

modest extensions of life and do not provide curative treatment. The advent of RNA interference has significantly enhanced the possibility of therapeutic intervention for cancer. In recent years, significant efforts have been made to identify agents (small molecules or biological such as antibodies and small interfering RNA (siRNA)) that selectively target cancer cells and/or genes that are expressed mainly in cancer-associated pathways. However, some of these targets are pleiotropic or lack an active drug-binding site, rendering them “undruggable” (or, at least, have not been successful exploited from a pharmaceutical perspective). These targets include cancer-associated protein such as transcription factors, which are attractive alternative therapeutic targets. Specifically, selective oncogene silencing via siRNA has shown great promise for cancer therapy as these have been shown to inhibit the mRNA synthesis that can lead to down-regulation of the associated protein<sup>244</sup>. Moreover, such nucleic acid sequences can potentially be combined with chemotherapeutics in the same delivery vehicle to strategically disrupt tumor progression at protein synthesis level (siRNA) and the at DNA synthesis level (chemotherapeutics), which makes the nanoparticle-based co-delivery an efficient therapeutic tool for cancer treatment in coordinated fashion, by simultaneously targeting unique points in the cancer –signaling cascade.

Despite being one of the earliest oncogenes identified, the c-Myc transcription factor remains “undruggable” by small molecules and/or antibodies. The c-Myc oncogene is overexpressed in numerous tumors, such as, lung, breast, pancreatic, gallbladder and colon carcinomas, where its downstream target genes promote cell growth, proliferation, invasion, expansion and angiogenesis<sup>242, 243, 245</sup>. c-Myc remains a challenging anti-tumor drug target for a variety of reasons. The basic helix-loop-helix structure of its

transcription factor protein does not possess drug-accessible domains. Also, as with other transcription factors, c-Myc carries out a multitude of physiological functions and its prolonged down-regulation can adversely affect healthy cells<sup>246</sup>. Nevertheless, c-Myc represents a promising target for siRNA-mediated protein down-regulation; several reports demonstrate the feasibility of this approach for tumor growth inhibition in multiple cancer models<sup>247, 248</sup>.

While targeted molecular therapy is attractive, there are still many lung cancer patients without precise determination of the molecular mutation(s) involved. Gemcitabine (Gemzar®) is a commonly used chemotherapeutic drug, especially for non-small cell lung carcinoma. It is a nucleoside analog of cytosine transported into mammalian cells via the nucleoside transporter and phosphorylated into mono-, di- and tri-nucleotides inside the cells. Gemcitabine triphosphate then enters the nucleus to be incorporated into cellular DNA during the S phase of the cell cycle and blocks the cell cycle. Thus, Gemcitabine is actually a prodrug which requires further cellular metabolism for its activity. Furthermore, pharmacokinetics of gemcitabine indicates that it is rapidly deaminated in the blood to become inactive difluorouridine and cleared from the blood by renal excretion<sup>249</sup>. The amount of intact drug taken up by the tumor is estimated to be less than 10%. Nucleotides, such as gemcitabine monophosphate (GMP) are not transported by the nucleoside transporter which presents a significant barrier to their use as a drug. Using a drug carrier to protect and to bring more gemcitabine to the tumor is an excellent strategy to enhance the efficacy and to reduce the toxicity of the drug.

Thus, taken together, we choose to use c-Myc siRNA as a viable and sound “undruggable” candidate, as being the one combination partner to the conventional

chemotherapeutic agent gemcitabine derivatives. The combinational therapeutic agents were co-delivered via a “smart” LCP nanovector.

Co-delivery of c-myc siRNA and GMP will obstruct tumor cell progression through two independent pathways; one that alters the physiological microenvironment of the tumor (c-Myc siRNA), and another that inhibits cell cycle progression through the intracellular delivery of GMP. c-Myc siRNA and GMP can be co-entrapped in ligand targeted LCP nanoparticles, delivered and cross the lung tumor cell membrane *in vivo* through receptor-mediated up-take, and get released through the acidic pH of the endosome into the cytoplasm. Once released in the cytoplasm, c-Myc siRNA can enter the RNA interference pathway that guides the sequence-specific mRNA degradation leading to down regulation of the c-Myc protein. Simultaneously the nucleotide analog GMP is delivered from the cytoplasm to the nucleus of the lung cancer cells where it can induce cellular apoptosis through its incorporation into the DNA transcription mechanism. Together, the development of a single nanoparticle formulation with multifunctional anti-cancer activity will overcome their individual innate limitations; delivery, release, and resistance. Additionally co-delivery will expand the potential of each mono-therapeutic treatment and facilitate superior efficacy.

The LCP nanoparticle is composed of a biocompatible and biodegradable amorphous CaP precipitation core, which can encapsulate siRNA, plasmid DNA and phosphorylated chemodrugs with high affinity. Moreover, CaP rapidly dissolves at the acidic pH of the endosome, increasing endosomal osmotic pressure and releasing the particle cargo into the cytoplasm. In LCP, the CaP core is stabilized with dioleoylphosphatic acid (DOPA), a phospholipid and further coated with cationic lipid to form an outer-lipid membrane. The

resulting NPs possess a spherical hollow core structure with an asymmetric lipid bilayer at the surface that can be modified with a polyethylene glycol (PEG)-phospholipid conjugate to shield the cationic charge of the lipid bilayer. Additionally, the NP can be augmented with PEGylated targeting ligand, such as PEG-Anisamide which allows for more efficient cargo delivery to tumor cells, a prolonged NP circulation time and less reticuloendothelial/mononuclear phagocyte system uptake.

## **6.0 SUMMARY**

### **6.1 SUMMARY OF RESEARCH RESULTS**

In this study, our objective was to enhance the activity and expand the therapeutic applications of LCP nanoparticles for cancer therapy, aiming for the systemic delivery of chemotherapeutics and siRNAs. First, phosphorylated nucleoside or nucleotide analogues (i.e. gemcitabine triphosphate (GTP), gemcitabine monophosphate (GMP)) loaded LCP nanoparticles were constructed. Our studies demonstrate that LCP can significantly improve the *in vivo* delivery efficiency of GTP and GMP in mice, as evidenced by its superior ability relative to gemcitabine to induce tumor cell apoptosis and suppress tumor cell proliferation *in vivo*. Dramatic tumor growth inhibitions were observed after long term treatment, and there were no safety issues raised at the therapeutic dose.

To further improve the therapeutic efficacy, especially for the refractory human NSCLC, we combine angiogenesis therapy together with chemotherapy, by co-delivering GMP and VEGF siRNA in a single LCP nanoparticle to eventually eradicate the tumor progression in mice. The improved therapeutic response, as compared to either VEGF siRNA or GMP therapy alone, was supported by the observation of effective induction of tumor cell apoptosis, significant reduction of tumor cell proliferation and tumor microvessel density. The combination therapy led to dramatic inhibition of tumor growth, with little *in vivo* toxicity. In the H460 xenograft mouse model, the tumor growth



was almost completely arrested by the combined LCP. Chemotherapy alone (GMP-LCP) also suppressed the tumor growth effectively, but not as potent as the combined nanoparticle. Anti-angiogenesis monotherapy (VEGF-LCP) stabilized the tumor growth at early stage, but was associated with the tumor progression at later stages, which indicated VEGF-LCP alone was not sufficient to obtain long term tumor suppression.

RNAi provides an alternative approach to knockdown oncogenes, especially some undruggable targets, such as c-Myc. The studies conducted herein have validated the anticancer potency of GMP. In this study, we co-encapsulate c-Myc siRNA together with GMP in a single LCP nanoparticle. Our results suggested that LCP co-encapsulating both c-Myc siRNA and GMP was more effective than LCP loading each agent individually, in terms of apoptosis induction and proliferation inhibition, in both NSCLC subcutaneous and orthotopic xenograft models.

The current studies demonstrated the possibility of incorporating multiple nucleic acid molecules and phosphorylated small molecule drugs into a single nanoparticle formulation, which leads to superior therapeutic improvement in many human diseases (e.g. various animal cancer models), and to modulate multiple therapeutic pathways simultaneously.

Combination therapy is becoming increasingly important in cancer treatment regimen for providing long-term effectiveness and prognosis, as well as decreasing side effects.<sup>252</sup>

Choosing an appropriate target is essential for gene therapy. In this thesis, VEGF siRNA and c-Myc siRNA were chosen as therapeutic partners to chemotherapy. VEGF is a key regulator of angiogenesis. VEGF overexpression induces microvascular proliferation

within the tumor by the VEGF/VEGFR interactions and the following signaling cascades, promoting cancer malignancy. VEGF siRNA would kill cancer cells indirectly by damaging tumor endothelial cells via VEGF down-regulation, thus, deprived tumors of nutrients. NSCLC shows increased levels of c-Myc oncogene which is considered as an “undruggable” target, correlating with a poor prognosis for patients. c-Myc is an oncogenic transcription factor. Mutated and highly amplified c-Myc leads to the dysregulation of cell proliferation, differentiation, cell cycle, cellular metabolism and genomic stability, resulting in the formation of cancer. c-Myc overexpression can also induce DNA damage and compromise the damaging-sensing mechanism of cells.<sup>251</sup> Since down-regulation of c-Myc shows some similar effects as GMP chemotherapy, in order to achieve synergistic efficacy and decrease potential toxicity, the dose of GMP in (GMP+cMyc)-LCP-AA was reduced to half compared to that of (GMP+VEGF)-LCP-AA. We need further validation to compare which siRNA serves as a better partner with GMP in terms of the anti-tumor efficacy of the combined treatment.

The advantage of multidrug-containing nanoparticles investigated in this study relative to co-administration of multiple different single drug-containing vehicles is that they can offer the unique features of vehicle uniformity, ratiometric drug loading and temporal drug release, as well as their ability to unify the pharmacokinetics of different drugs by simultaneously delivering multiple therapeutic agents to the target site, leading to profound therapeutic effects.

## **6.2 FUTURE DIRECTIONS**

We will further optimize the ratiometric drug loading, including the total drug loading and the loading ratio of each individual agent (i.e. optimal combination ratio of gene and chemotherapy). The LCP nanoplatfrom has wide application and can allow various therapeutic combinations, including gene therapy (i.e. siRNA, pDNA, mRNA), chemotherapy (i.e. phosphorylated nucleosides, antiviral drugs), immunotherapy (i.e. phosphor-modified antigen peptide), and their combinations.

## APPENDIX

### YUAN ZHANG's publication

#### Peer-reviewed Papers

- **Yuan Zhang**, William Y Kim, Leaf Huang. Systemic delivery of gemcitabine triphosphate via LCP nanoparticles for NSCLC and pancreatic cancer therapy. *Biomaterials*, 2013 (*In press*)
- **Yuan Zhang**, Nicole Schwerbrock, Arlin Rogers, Leaf Huang. Co-delivery of VEGF siRNA and gemcitabine monophosphate in a single nanoparticle formulation for effective treatment of NSCLC. (*submitted*)
- **Yuan Zhang**, Leaf Huang. Co-delivery of c-Myc siRNA and gemcitabine monophosphate via LCP nanoparticles for NSCLC treatment. (*in preparation*)
- Jing Yao\*, **Yuan Zhang**\*, Sirinivas Ramiseti, Yuhua Wang, Leaf Huang. Turning an antiviral into an anticancer drug: Nanoparticle delivery of acyclovir monophosphate. (*submitted*, \*equal contribution)
- Elizabeth A. Vasievich, Sirinivas Ramiseti, **Yuan Zhang**, Leaf Huang. Trp2 peptide vaccine with the adjuvant R-DOTAP able to break tolerance in an advanced melanoma solid tumor model. *Molecular Pharmaceutics*. 9 (2): 261-268, 2012

#### Review Papers and Book Chapters

- **Yuan Zhang**, Andrew Satterlee, Leaf Huang. In vivo gene delivery by non-viral vectors: overcoming hurdles? *Molecular Therapy*. 20 (7): 1298-304, 2012
- **Yuan Zhang**, Leaf Huang. Drug Delivery in Oncology—From Basic Research to Cancer Therapy. Volume 3. Chapter 'RNA Drug Delivery Approaches'. WILEY-VCH publication 2010.

## **Selected Poster Presentations**

- **Yuan Zhang**, Nicole Schwerbrock, Leaf Huang. Co-delivery of VEGF siRNA and gemcitabine monophosphate in a single LCP nanoparticle for effective treatment of NSCLC. Liposome Research Day Conference, Hangzhou, China, 2012
- **Yuan Zhang**, William Y Kim, Leaf Huang. Systemic delivery of gemcitabine triphosphate via LCP nanoparticles for cancer therapy. Gordon Research Conference, Waterville Valley, NH, 2012

## BIBLIOGRAPHY

1. Oh, Y.K. and T.G. Park, *siRNA delivery systems for cancer treatment*. Adv Drug Deliv Rev, 2009. **61**(10): p. 850-62.
2. de Fougères, A., et al., *Interfering with disease: a progress report on siRNA-based therapeutics*. Nat Rev Drug Discov, 2007. **6**(6): p. 443-53.
3. Bumcrot, D., et al., *RNAi therapeutics: a potential new class of pharmaceutical drugs*. Nat Chem Biol, 2006. **2**(12): p. 711-9.
4. Kim, D.H. and J.J. Rossi, *Strategies for silencing human disease using RNA interference*. Nat Rev Genet, 2007. **8**(3): p. 173-84.
5. John, M., et al., *Effective RNAi-mediated gene silencing without interruption of the endogenous microRNA pathway*. Nature, 2007. **449**(7163): p. 745-7.
6. Judge, A. and I. MacLachlan, *Overcoming the innate immune response to small interfering RNA*. Hum Gene Ther, 2008. **19**(2): p. 111-24.
7. Chiu, Y.L. and T.M. Rana, *siRNA function in RNAi: a chemical modification analysis*. Rna, 2003. **9**(9): p. 1034-48.
8. Capodici, J., K. Kariko, and D. Weissman, *Inhibition of HIV-1 infection by small interfering RNA-mediated RNA interference*. J Immunol, 2002. **169**(9): p. 5196-201.
9. Allerson, C.R., et al., *Fully 2'-modified oligonucleotide duplexes with improved in vitro potency and stability compared to unmodified small interfering RNA*. J Med Chem, 2005. **48**(4): p. 901-4.
10. Judge, A.D., et al., *Design of noninflammatory synthetic siRNA mediating potent gene silencing in vivo*. Mol Ther, 2006. **13**(3): p. 494-505.
11. Veedu, R.N. and J. Wengel, *Locked nucleic acids: promising nucleic acid analogs for therapeutic applications*. Chem Biodivers. **7**(3): p. 536-42.
12. Elmen, J., et al., *Locked nucleic acid (LNA) mediated improvements in siRNA stability and functionality*. Nucleic Acids Res, 2005. **33**(1): p. 439-47.
13. Braasch, D.A., et al., *RNA interference in mammalian cells by chemically-modified RNA*. Biochemistry, 2003. **42**(26): p. 7967-75.
14. Mook, O.R., et al., *Evaluation of locked nucleic acid-modified small interfering RNA in vitro and in vivo*. Mol Cancer Ther, 2007. **6**(3): p. 833-43.
15. Sipa, K., et al., *Effect of base modifications on structure, thermodynamic stability, and*

*gene silencing activity of short interfering RNA*. Rna, 2007. **13**(8): p. 1301-16.

16. Abes, S., et al., *Efficient splicing correction by PNA conjugation to an R6-Penetratin delivery peptide*. Nucleic Acids Res, 2007. **35**(13): p. 4495-502.

17. Moulton, H.M., et al., *Cell-penetrating peptide-morpholino conjugates alter pre mRNA splicing of DMD (Duchenne muscular dystrophy) and inhibit murine coronavirus replication in vivo*. Biochem Soc Trans, 2007. **35**(Pt 4): p. 826-8.

18. Martinez, J., et al., *Single-stranded antisense siRNAs guide target RNA cleavage in RNAi*. Cell, 2002. **110**(5): p. 563-74.

19. Schwarz, D.S., et al., *Evidence that siRNAs function as guides, not primers, in the Drosophila and human RNAi pathways*. Mol Cell, 2002. **10**(3): p. 537-48.

20. Corey, D.R., *Chemical modification: the key to clinical application of RNA interference?* J Clin Invest, 2007. **117**(12): p. 3615-22.

21. Jackson, A.L., et al., *Position-specific chemical modification of siRNAs reduces "off-target" transcript silencing*. Rna, 2006. **12**(7): p. 1197-205.

22. Li, S.D. and L. Huang, *Stealth nanoparticles: high density but sheddable PEG is a key for tumor targeting*. J Control Release. **145**(3): p. 178-81.

23. Wagner, E., *Effects of membrane-active agents in gene delivery*. J Control Release, 1998. **53**(1-3): p. 155-8.

24. Wagner, E., et al., *Coupling of adenovirus to transferrin-polylysine/DNA complexes greatly enhances receptor-mediated gene delivery and expression of transfected genes*. Proc Natl Acad Sci U S A, 1992. **89**(13): p. 6099-103.

25. Aagaard, L. and J.J. Rossi, *RNAi therapeutics: principles, prospects and challenges*. Adv Drug Deliv Rev, 2007. **59**(2-3): p. 75-86.

26. Marques, J.T. and B.R. Williams, *Activation of the mammalian immune system by siRNAs*. Nat Biotechnol, 2005. **23**(11): p. 1399-405.

27. Hornung, V., et al., *Sequence-specific potent induction of IFN-alpha by short interfering RNA in plasmacytoid dendritic cells through TLR7*. Nat Med, 2005. **11**(3): p. 263-70.

28. Judge, A.D., et al., *Sequence-dependent stimulation of the mammalian innate immune response by synthetic siRNA*. Nat Biotechnol, 2005. **23**(4): p. 457-62.

29. Jackson, A.L., et al., *Expression profiling reveals off-target gene regulation by RNAi*. Nat Biotechnol, 2003. **21**(6): p. 635-7.

30. Fedorov, Y., et al., *Different delivery methods-different expression profiles*. Nat Methods, 2005. **2**(4): p. 241.
31. Omid, Y., et al., *Toxicogenomics of non-viral vectors for gene therapy: a microarray study of lipofectin- and oligofectamine-induced gene expression changes in human epithelial cells*. J Drug Target, 2003. **11**(6): p. 311-23.
32. Liu, F., Y. Song, and D. Liu, *Hydrodynamics-based transfection in animals by systemic administration of plasmid DNA*. Gene Ther, 1999. **6**(7): p. 1258-66.
33. Suda, T., K. Suda, and D. Liu, *Computer-assisted hydrodynamic gene delivery*. Mol Ther, 2008. **16**(6): p. 1098-104.
34. Andre, F. and L.M. Mir, *DNA electrotransfer: its principles and an updated review of its therapeutic applications*. Gene Ther, 2004. **11 Suppl 1**: p. S33-42.
35. Ugen, K.E. and R. Heller, *Electroporation as a method for the efficient in vivo delivery of therapeutic genes*. DNA Cell Biol, 2003. **22**(12): p. 753.
36. Liu, F. and L. Huang, *A syringe electrode device for simultaneous injection of DNA and electrotransfer*. Mol Ther, 2002. **5**(3): p. 323-8.
37. Geng, T., et al., *Flow-through electroporation based on constant voltage for large-volume transfection of cells*. J Control Release. **144**(1): p. 91-100.
38. Johnston, S.A., et al., *Mitochondrial transformation in yeast by bombardment with microprojectiles*. Science, 1988. **240**(4858): p. 1538-41.
39. Klein, T.M., et al., *Transformation of microbes, plants and animals by particle bombardment*. Biotechnology (N Y), 1992. **10**(3): p. 286-91.
40. Tros de Ilarduya, C., Y. Sun, and N. Duzgunes, *Gene delivery by lipoplexes and polyplexes*. Eur J Pharm Sci. **40**(3): p. 159-70.
41. Simberg, D., et al., *DOTAP (and other cationic lipids): chemistry, biophysics, and transfection*. Crit Rev Ther Drug Carrier Syst, 2004. **21**(4): p. 257-317.
42. Tseng, Y.C., S. Mozumdar, and L. Huang, *Lipid-based systemic delivery of siRNA*. Adv Drug Deliv Rev, 2009. **61**(9): p. 721-31.
43. Koltover, I., et al., *An inverted hexagonal phase of cationic liposome-DNA complexes related to DNA release and delivery*. Science, 1998. **281**(5373): p. 78-81.
44. Simberg, D., et al., *Phase behavior, DNA ordering, and size instability of cationic lipoplexes. Relevance to optimal transfection activity*. J Biol Chem, 2001. **276**(50): p. 47453-9.



45. Zhou, X. and L. Huang, *DNA transfection mediated by cationic liposomes containing lipopolylysine: characterization and mechanism of action*. Biochim Biophys Acta, 1994. **1189**(2): p. 195-203.
46. Xu, Y. and F.C. Szoka, Jr., *Mechanism of DNA release from cationic liposome/DNA complexes used in cell transfection*. Biochemistry, 1996. **35**(18): p. 5616-23.
47. Hafez, I.M., N. Maurer, and P.R. Cullis, *On the mechanism whereby cationic lipids promote intracellular delivery of polynucleic acids*. Gene Ther, 2001. **8**(15): p. 1188-96.
48. Rejman, J., et al., *Characterization and transfection properties of lipoplexes stabilized with novel exchangeable polyethylene glycol-lipid conjugates*. Biochim Biophys Acta, 2004. **1660**(1-2): p. 41-52.
49. Akinc, A., et al., *Targeted delivery of RNAi therapeutics with endogenous and exogenous ligand-based mechanisms*. Mol Ther. **18**(7): p. 1357-64.
50. Semple, S.C., et al., *Rational design of cationic lipids for siRNA delivery*. Nat Biotechnol. **28**(2): p. 172-6.
51. Akinc, A., et al., *A combinatorial library of lipid-like materials for delivery of RNAi therapeutics*. Nat Biotechnol, 2008. **26**(5): p. 561-9.
52. Akinc, A., et al., *Development of lipidoid-siRNA formulations for systemic delivery to the liver*. Mol Ther, 2009. **17**(5): p. 872-9.
53. Mahon, K.P., et al., *Combinatorial Approach to Determine Functional Group Effects on Lipidoid-Mediated siRNA Delivery*. Bioconjug Chem. **21**(8): p. 1448-54.
54. Curiel, D.T., et al., *Adenovirus enhancement of transferrin-polylysine-mediated gene delivery*. Proc Natl Acad Sci U S A, 1991. **88**(19): p. 8850-4.
55. Neu, M., D. Fischer, and T. Kissel, *Recent advances in rational gene transfer vector design based on poly(ethylene imine) and its derivatives*. J Gene Med, 2005. **7**(8): p. 992-1009.
56. Fischer, D., et al., *A novel non-viral vector for DNA delivery based on low molecular weight, branched polyethylenimine: effect of molecular weight on transfection efficiency and cytotoxicity*. Pharm Res, 1999. **16**(8): p. 1273-9.
57. Weecharansan, W., et al., *Evaluation of chitosan salts as non-viral gene vectors in CHO-K1 cells*. Int J Pharm, 2008. **348**(1-2): p. 161-8.
58. Duceppe, N. and M. Tabrizian, *Factors influencing the transfection efficiency of ultra low molecular weight chitosan/hyaluronic acid nanoparticles*. Biomaterials, 2009. **30**(13): p.

2625-31.

59. Jiang, H.L., et al., *Efficient gene delivery using chitosan-polyethylenimine hybrid systems*. Biomed Mater, 2008. **3**(2): p. 025013.

60. Bartlett, D.W. and M.E. Davis, *Physicochemical and biological characterization of targeted, nucleic acid-containing nanoparticles*. Bioconjug Chem, 2007. **18**(2): p. 456-68.

61. Yezhelyev, M.V., et al., *Proton-sponge coated quantum dots for siRNA delivery and intracellular imaging*. J Am Chem Soc, 2008. **130**(28): p. 9006-12.

62. Bielinska, A., et al., *Regulation of in vitro gene expression using antisense oligonucleotides or antisense expression plasmids transfected using starburst PAMAM dendrimers*. Nucleic Acids Res, 1996. **24**(11): p. 2176-82.

63. Kukowska-Latallo, J.F., et al., *Efficient transfer of genetic material into mammalian cells using Starburst polyamidoamine dendrimers*. Proc Natl Acad Sci U S A, 1996. **93**(10): p. 4897-902.

64. Rozema, D.B., et al., *Dynamic PolyConjugates for targeted in vivo delivery of siRNA to hepatocytes*. Proc Natl Acad Sci U S A, 2007. **104**(32): p. 12982-7.

65. Li, S., et al., *Characterization of cationic lipid-protamine-DNA (LPD) complexes for intravenous gene delivery*. Gene Ther, 1998. **5**(7): p. 930-7.

66. Nakamura, Y., et al., *Octaarginine-modified multifunctional envelope-type nano device for siRNA*. J Control Release, 2007. **119**(3): p. 360-7.

67. Li, S. and L. Huang, *In vivo gene transfer via intravenous administration of cationic lipid-protamine-DNA (LPD) complexes*. Gene Ther, 1997. **4**(9): p. 891-900.

68. Lee, R.J. and L. Huang, *Folate-targeted, anionic liposome-entrapped polylysine-condensed DNA for tumor cell-specific gene transfer*. J Biol Chem, 1996. **271**(14): p. 8481-7.

69. Brown, M.D., et al., *Preliminary characterization of novel amino acid based polymeric vesicles as gene and drug delivery agents*. Bioconjug Chem, 2000. **11**(6): p. 880-91.

70. Li, J., et al., *Biodegradable calcium phosphate nanoparticle with lipid coating for systemic siRNA delivery*. J Control Release. **142**(3): p. 416-21.

71. Kamiya, H., H. Akita, and H. Harashima, *Pharmacokinetic and pharmacodynamic considerations in gene therapy*. Drug Discov Today, 2003. **8**(21): p. 990-6.

72. Hatakeyama, H., et al., *Development of a novel systemic gene delivery system for cancer therapy with a tumor-specific cleavable PEG-lipid*. Gene Ther, 2007. **14**(1): p. 68-77.

73. Espina, V., et al., *Pathology of the future: molecular profiling for targeted therapy*. Cancer Invest, 2005. **23**(1): p. 36-46.
74. Wilson, D.S. and J.W. Szostak, *In vitro selection of functional nucleic acids*. Annu Rev Biochem, 1999. **68**: p. 611-47.
75. Dassie, J.P., et al., *Systemic administration of optimized aptamer-siRNA chimeras promotes regression of PSMA-expressing tumors*. Nat Biotechnol, 2009. **27**(9): p. 839-49.
76. McNamara, J.O., 2nd, et al., *Cell type-specific delivery of siRNAs with aptamer-siRNA chimeras*. Nat Biotechnol, 2006. **24**(8): p. 1005-15.
77. Wang, K.Y., et al., *A DNA aptamer which binds to and inhibits thrombin exhibits a new structural motif for DNA*. Biochemistry, 1993. **32**(8): p. 1899-904.
78. Stoltenburg, R., C. Reinemann, and B. Strehlitz, *SELEX--a (r)evolutionary method to generate high-affinity nucleic acid ligands*. Biomol Eng, 2007. **24**(4): p. 381-403.
79. Drolet, D.W., et al., *Pharmacokinetics and safety of an anti-vascular endothelial growth factor aptamer (NX1838) following injection into the vitreous humor of rhesus monkeys*. Pharm Res, 2000. **17**(12): p. 1503-10.
80. Khalil, I.A., et al., *High density of octaarginine stimulates macropinocytosis leading to efficient intracellular trafficking for gene expression*. J Biol Chem, 2006. **281**(6): p. 3544-51.
81. Mae, M. and U. Langel, *Cell-penetrating peptides as vectors for peptide, protein and oligonucleotide delivery*. Curr Opin Pharmacol, 2006. **6**(5): p. 509-14.
82. Xu, L., et al., *Systemic tumor-targeted gene delivery by anti-transferrin receptor scFv-immunoliposomes*. Mol Cancer Ther, 2002. **1**(5): p. 337-46.
83. Chen, Y., et al., *Nanoparticles Modified With Tumor-targeting scFv Deliver siRNA and miRNA for Cancer Therapy*. Mol Ther.
84. Gurrath, M., et al., *Conformation/activity studies of rationally designed potent anti-adhesive RGD peptides*. Eur J Biochem, 1992. **210**(3): p. 911-21.
85. Haubner, R.H., et al., *Radiotracer-based strategies to image angiogenesis*. Q J Nucl Med, 2003. **47**(3): p. 189-99.
86. Wang, L., et al., *Improving tumor-targeting capability and pharmacokinetics of (99m)Tc-labeled cyclic RGD dimers with PEG(4) linkers*. Mol Pharm, 2009. **6**(1): p. 231-45.
87. Kok, R.J., et al., *Preparation and functional evaluation of RGD-modified proteins as alpha(v)beta(3) integrin directed therapeutics*. Bioconjug Chem, 2002. **13**(1): p. 128-35.

88. Boturyn, D., et al., *Template assembled cyclopeptides as multimeric system for integrin targeting and endocytosis*. J Am Chem Soc, 2004. **126**(18): p. 5730-9.
89. Temming, K., et al., *RGD-based strategies for selective delivery of therapeutics and imaging agents to the tumour vasculature*. Drug Resist Updat, 2005. **8**(6): p. 381-402.
90. Sudimack, J. and R.J. Lee, *Targeted drug delivery via the folate receptor*. Adv Drug Deliv Rev, 2000. **41**(2): p. 147-62.
91. Chen, Y., J.J. Wu, and L. Huang, *Nanoparticles targeted with NGR motif deliver c-myc siRNA and doxorubicin for anticancer therapy*. Mol Ther. **18**(4): p. 828-34.
92. Santoro, A., et al., *Phase II study of NGR-hTNF, a selective vascular targeting agent, in patients with metastatic colorectal cancer after failure of standard therapy*. Eur J Cancer. **46**(15): p. 2746-52.
93. Lee, R.J. and P.S. Low, *Delivery of liposomes into cultured KB cells via folate receptor-mediated endocytosis*. J Biol Chem, 1994. **269**(5): p. 3198-204.
94. Banerjee, R., et al., *Anisamide-targeted stealth liposomes: a potent carrier for targeting doxorubicin to human prostate cancer cells*. Int J Cancer, 2004. **112**(4): p. 693-700.
95. Chono, S., et al., *An efficient and low immunostimulatory nanoparticle formulation for systemic siRNA delivery to the tumor*. J Control Release, 2008. **131**(1): p. 64-9.
96. Li, S.D., S. Chono, and L. Huang, *Efficient oncogene silencing and metastasis inhibition via systemic delivery of siRNA*. Mol Ther, 2008. **16**(5): p. 942-6.
97. Maurice, T. and T.P. Su, *The pharmacology of sigma-1 receptors*. Pharmacol Ther, 2009. **124**(2): p. 195-206.
98. Mukherjee, A., et al., *Haloperidol-associated stealth liposomes: a potent carrier for delivering genes to human breast cancer cells*. J Biol Chem, 2005. **280**(16): p. 15619-27.
99. Hadj-Slimane, R., et al., *Short interfering RNA (siRNA), a novel therapeutic tool acting on angiogenesis*. Biochimie, 2007. **89**(10): p. 1234-44.
100. Lu, P.Y., F.Y. Xie, and M.C. Woodle, *siRNA-mediated antitumorigenesis for drug target validation and therapeutics*. Curr Opin Mol Ther, 2003. **5**(3): p. 225-34.
101. Chen, Y., et al., *Targeted Nanoparticles Deliver siRNA to Melanoma*. J Invest Dermatol.
102. Siomi, M.C., *Short interfering RNA-mediated gene silencing; towards successful application in human patients*. Adv Drug Deliv Rev, 2009. **61**(9): p. 668-71.
103. Davis, M.E., et al., *Evidence of RNAi in humans from systemically administered siRNA*

*via targeted nanoparticles*. Nature. **464**(7291): p. 1067-70.

104. Lopez-Fraga, M., T. Martinez, and A. Jimenez, *RNA interference technologies and therapeutics: from basic research to products*. BioDrugs, 2009. **23**(5): p. 305-32.

105. Phalon, C., D.D. Rao, and J. Nemunaitis, *Potential use of RNA interference in cancer therapy*. Expert Rev Mol Med. **12**: p. e26.

106. Nguyen, T., et al., *RNAi therapeutics: an update on delivery*. Curr Opin Mol Ther, 2008. **10**(2): p. 158-67.

107. Aleku, M., et al., *Atu027, a liposomal small interfering RNA formulation targeting protein kinase N3, inhibits cancer progression*. Cancer Res, 2008. **68**(23): p. 9788-98.

108. Tiemann, K. and J.J. Rossi, *RNAi-based therapeutics-current status, challenges and prospects*. EMBO Mol Med, 2009. **1**(3): p. 142-51.

109. Kleinman, M.E., et al., *Sequence- and target-independent angiogenesis suppression by siRNA via TLR3*. Nature, 2008. **452**(7187): p. 591-7.

110. Leachman, S.A., et al., *First-in-human mutation-targeted siRNA phase Ib trial of an inherited skin disorder*. Mol Ther. **18**(2): p. 442-6.

111. Koldehoff, M., et al., *Therapeutic application of small interfering RNA directed against bcr-abl transcripts to a patient with imatinib-resistant chronic myeloid leukaemia*. Clin Exp Med, 2007. **7**(2): p. 47-55.

112. Elsbahy M, Nazarali A, Foldvari M. Non-viral nucleic acid delivery: key challenges and future directions. Curr Drug Deliv 2011;8(3): 235-44.

113. Monaghan M, Pandit A. RNA interference therapy via functionalized scaffolds. Adv Drug Deliv Rev 2011;63(4-5): 197-208.

114. Vickers TA, Lima WF, Wu H, Nichols JG, Linsley PS, Crooke ST. Off-target and a portion of target-specific siRNA mediated mRNA degradation is Ago2 'Slicer' independent and can be mediated by Ago1. Nucleic Acids Res 2009;37(20): 6927-41.

115. Jackson AL, Bartz SR, Schelter J, et al. Expression profiling reveals off-target gene regulation by RNAi. Nat Biotechnol 2003;21(6): 635-7.

116. Fedorov Y, King A, Anderson E, et al. Different delivery methods-different expression profiles. Nat Methods 2005;2(4): 241.

117. Robbins M, Judge A, MacLachlan I. siRNA and innate immunity. Oligonucleotides 2009;19(2): 89-102.

118. Czech MP, Aouadi M, Tesz GJ. RNAi-based therapeutic strategies for metabolic disease. *Nat Rev Endocrinol* 2011.
119. Judge AD, Bola G, Lee AC, MacLachlan I. Design of noninflammatory synthetic siRNA mediating potent gene silencing in vivo. *Mol Ther* 2006;13(3): 494-505.
120. Gao Y, Liu XL, Li XR. Research progress on siRNA delivery with nonviral carriers. *Int J Nanomedicine* 2011;6: 1017-25.
121. Pan X, Thompson R, Meng X, Wu D, Xu L. Tumor-targeted RNA-interference: functional non-viral nanovectors. *Am J Cancer Res* 2011;1(1): 25-42.
122. Wolff JA, Rozema DB. Breaking the bonds: non-viral vectors become chemically dynamic. *Mol Ther* 2008;16(1): 8-15.
123. Li SD, Huang L. Stealth nanoparticles: high density but sheddable PEG is a key for tumor targeting. *J Control Release* 2010;145(3): 178-81.
124. Tseng YC, Mozumdar S, Huang L. Lipid-based systemic delivery of siRNA. *Adv Drug Deliv Rev* 2009;61(9): 721-31.
125. Schipper ML, Iyer G, Koh AL, et al. Particle size, surface coating, and PEGylation influence the biodistribution of quantum dots in living mice. *Small* 2009;5(1): 126-34.
126. Seymour LW. Passive tumor targeting of soluble macromolecules and drug conjugates. *Crit Rev Ther Drug Carrier Syst* 1992;9(2): 135-87.
127. Drummond DC, Zignani M, Leroux J. Current status of pH-sensitive liposomes in drug delivery. *Prog Lipid Res* 2000;39(5): 409-60.
128. Guo X, Szoka FC, Jr. Steric stabilization of fusogenic liposomes by a low-pH sensitive PEG--diortho ester--lipid conjugate. *Bioconjug Chem* 2001;12(2): 291-300.
129. Walker GF, Fella C, Pelisek J, et al. Toward synthetic viruses: endosomal pH-triggered deshielding of targeted polyplexes greatly enhances gene transfer in vitro and in vivo. *Mol Ther* 2005;11(3): 418-25.
130. Hatakeyama H, Akita H, Ito E, et al. Systemic delivery of siRNA to tumors using a lipid nanoparticle containing a tumor-specific cleavable PEG-lipid. *Biomaterials* 2011;32(18): 4306-16.
131. Hatakeyama H, Akita H, Harashima H. A multifunctional envelope type nano device (MEND) for gene delivery to tumours based on the EPR effect: a strategy for overcoming the PEG dilemma. *Adv Drug Deliv Rev* 2011;63(3): 152-60.

132. Hatakeyama H, Akita H, Kogure K, et al. Development of a novel systemic gene delivery system for cancer therapy with a tumor-specific cleavable PEG-lipid. *Gene Ther* 2007;14(1): 68-77.
133. Romberg B, Hennink WE, Storm G. Sheddable coatings for long-circulating nanoparticles. *Pharm Res* 2008;25(1): 55-71.
134. Huang L, Liu Y. In vivo delivery of RNAi with lipid-based nanoparticles. *Annu Rev Biomed Eng* 2011;13: 507-30.
135. Sun W, Du L, Li M. Advances and perspectives in cell-specific aptamers. *Curr Pharm Des* 2011;17(1): 80-91.
136. Sawant R, Torchilin V. Intracellular transduction using cell-penetrating peptides. *Mol Biosyst* 2010;6(4): 628-40.
137. Manjappa AS, Chaudhari KR, Venkataraju MP, et al. Antibody derivatization and conjugation strategies: application in preparation of stealth immunoliposome to target chemotherapeutics to tumor. *J Control Release* 2011;150(1): 2-22.
138. Chen Y, Wu JJ, Huang L. Nanoparticles targeted with NGR motif deliver c-myc siRNA and doxorubicin for anticancer therapy. *Mol Ther* 2010;18(4): 828-34.
139. Chen Y, Bathula SR, Yang Q, Huang L. Targeted nanoparticles deliver siRNA to melanoma. *J Invest Dermatol* 2010;130(12): 2790-8.
140. Huang S, Li J, Han L, et al. Dual targeting effect of Angiopep-2-modified, DNA-loaded nanoparticles for glioma. *Biomaterials* 2011;32(28): 6832-8.
141. Diez S, Navarro G, de ICT. In vivo targeted gene delivery by cationic nanoparticles for treatment of hepatocellular carcinoma. *J Gene Med* 2009;11(1): 38-45.
142. Hafez IM, Maurer N, Cullis PR. On the mechanism whereby cationic lipids promote intracellular delivery of polynucleic acids. *Gene Ther* 2001;8(15): 1188-96.
143. Semple SC, Akinc A, Chen J, et al. Rational design of cationic lipids for siRNA delivery. *Nat Biotechnol* 2010;28(2): 172-6.
144. Akinc A, Querbes W, De S, et al. Targeted delivery of RNAi therapeutics with endogenous and exogenous ligand-based mechanisms. *Mol Ther* 2010;18(7): 1357-64.
145. Fella C, Walker GF, Ogris M, Wagner E. Amine-reactive pyridylhydrazone-based PEG reagents for pH-reversible PEI polyplex shielding. *Eur J Pharm Sci* 2008;34(4-5): 309-20.

146. Asayama S, Sudo M, Nagaoka S, Kawakami H. Carboxymethyl poly(L-histidine) as a new pH-sensitive polypeptide to enhance polyplex gene delivery. *Mol Pharm* 2008;5(5): 898-901.
147. West KR, Otto S. Reversible covalent chemistry in drug delivery. *Curr Drug Discov Technol* 2005;2(3): 123-60.
148. Zalipsky S, Qazen M, Walker JA, 2nd, Mullah N, Quinn YP, Huang SK. New detachable poly(ethylene glycol) conjugates: cysteine-cleavable lipopolymers regenerating natural phospholipid, diacyl phosphatidylethanolamine. *Bioconjug Chem* 1999;10(5): 703-7.
149. Mok H, Veisheh O, Fang C, et al. pH-Sensitive siRNA nanovector for targeted gene silencing and cytotoxic effect in cancer cells. *Mol Pharm* 2010;7(6): 1930-9.
150. Pak CC, Erukulla RK, Ahl PL, Janoff AS, Meers P. Elastase activated liposomal delivery to nucleated cells. *Biochim Biophys Acta* 1999;1419(2): 111-26.
151. Hatakeyama H, Ito E, Akita H, et al. A pH-sensitive fusogenic peptide facilitates endosomal escape and greatly enhances the gene silencing of siRNA-containing nanoparticles in vitro and in vivo. *J Control Release* 2009;139(2): 127-32.
152. Sakurai Y, Hatakeyama H, Sato Y, et al. Endosomal escape and the knockdown efficiency of liposomal-siRNA by the fusogenic peptide shGALA. *Biomaterials* 2011;32(24): 5733-42.
153. Li J, Chen YC, Tseng YC, Mozumdar S, Huang L. Biodegradable calcium phosphate nanoparticle with lipid coating for systemic siRNA delivery. *J Control Release* 2010;142(3): 416-21.
154. Bolhassani A. Potential efficacy of cell-penetrating peptides for nucleic acid and drug delivery in cancer. *Biochim Biophys Acta* 2011;1816(2): 232-46.
155. Collas P, Alestrom P. Nuclear localization signal of SV40 T antigen directs import of plasmid DNA into sea urchin male pronuclei in vitro. *Mol Reprod Dev* 1996;45(4): 431-8.
156. Vacik J, Dean BS, Zimmer WE, Dean DA. Cell-specific nuclear import of plasmid DNA. *Gene Ther* 1999;6(6): 1006-14.
157. Grandinetti G, Smith AE, Reineke TM. Membrane and Nuclear Permeabilization by Polymeric pDNA Vehicles: Efficient Method for Gene Delivery or Mechanism of Cytotoxicity? *Mol Pharm* 2012;9(3): 523-38.
158. Grandinetti G, Ingle NP, Reineke TM. Interaction of poly(ethylenimine)-DNA polyplexes with mitochondria: implications for a mechanism of cytotoxicity. *Mol Pharm* 2011;8(5): 1709-19.



159. Shim MS, Kwon YJ. Efficient and targeted delivery of siRNA in vivo. *FEBS J* 2010;277(23): 4814-27.
160. Tsai LR, Chen MH, Chien CT, et al. A single-monomer derived linear-like PEI-co-PEG for siRNA delivery and silencing. *Biomaterials* 2011;32(14): 3647-53.
161. Yin Q, Gao Y, Zhang Z, Zhang P, Li Y. Bioreducible poly (beta-amino esters)/shRNA complex nanoparticles for efficient RNA delivery. *J Control Release* 2011;151(1): 35-44.
162. Wagner E. Polymers for siRNA Delivery: Inspired by Viruses to be Targeted, Dynamic, and Precise. *Acc Chem Res* 2011.
163. Schaffert D, Troiber C, Salcher EE, et al. Solid-phase synthesis of sequence-defined T-, i-, and U-shape polymers for pDNA and siRNA delivery. *Angew Chem Int Ed Engl* 2011;50(38): 8986-9.
164. Li SD, Huang L. Targeted delivery of antisense oligodeoxynucleotide and small interference RNA into lung cancer cells. *Mol Pharm* 2006;3(5): 579-88.
165. Li SD, Chen YC, Hackett MJ, Huang L. Tumor-targeted delivery of siRNA by self-assembled nanoparticles. *Mol Ther* 2008;16(1): 163-9.
166. Li SD, Chono S, Huang L. Efficient oncogene silencing and metastasis inhibition via systemic delivery of siRNA. *Mol Ther* 2008;16(5): 942-6.
167. Lee RJ, Huang L. Folate-targeted, anionic liposome-entrapped polylysine-condensed DNA for tumor cell-specific gene transfer. *J Biol Chem* 1996;271(14): 8481-7.
168. Chono S, Li SD, Conwell CC, Huang L. An efficient and low immunostimulatory nanoparticle formulation for systemic siRNA delivery to the tumor. *J Control Release* 2008;131(1): 64-9.
169. Chen Y, Zhu X, Zhang X, Liu B, Huang L. Nanoparticles modified with tumor-targeting scFv deliver siRNA and miRNA for cancer therapy. *Mol Ther* 2010;18(9): 1650-6.
170. Perche F, Benvegna T, Berchel M, et al. Enhancement of dendritic cells transfection in vivo and of vaccination against B16F10 melanoma with mannosylated histidylated lipopolyplexes loaded with tumor antigen messenger RNA. *Nanomedicine* 2011;7(4): 445-53.
171. Kormann MS, Hasenpusch G, Aneja MK, et al. Expression of therapeutic proteins after delivery of chemically modified mRNA in mice. *Nat Biotechnol* 2011;29(2): 154-7.
172. Kogure K, Akita H, Yamada Y, Harashima H. Multifunctional envelope-type nano device (MEND) as a non-viral gene delivery system. *Adv Drug Deliv Rev* 2008;60(4-5): 559-71.

173. Wang KY, McCurdy S, Shea RG, Swaminathan S, Bolton PH. A DNA aptamer which binds to and inhibits thrombin exhibits a new structural motif for DNA. *Biochemistry* 1993;32(8): 1899-904.
174. Esposito CL, Catuogno S, de Franciscis V, Cerchia L. New insight into clinical development of nucleic acid aptamers. *Discov Med* 2011;11(61): 487-96.
175. McNamara JO, 2nd, Andrechek ER, Wang Y, et al. Cell type-specific delivery of siRNAs with aptamer-siRNA chimeras. *Nat Biotechnol* 2006;24(8): 1005-15.
176. Dassie JP, Liu XY, Thomas GS, et al. Systemic administration of optimized aptamer-siRNA chimeras promotes regression of PSMA-expressing tumors. *Nat Biotechnol* 2009;27(9): 839-49.
177. Suzuki R, Takizawa T, Negishi Y, et al. Tumor specific ultrasound enhanced gene transfer in vivo with novel liposomal bubbles. *J Control Release* 2008;125(2): 137-44.
178. Negishi Y, Omata D, Iijima H, et al. Enhanced laminin-derived peptide AG73-mediated liposomal gene transfer by bubble liposomes and ultrasound. *Mol Pharm* 2010;7(1): 217-26.
179. Chumakova OV, Liopo AV, Andreev VG, et al. Composition of PLGA and PEI/DNA nanoparticles improves ultrasound-mediated gene delivery in solid tumors in vivo. *Cancer Lett* 2008;261(2): 215-25.
180. Bardhan R, Lal S, Joshi A, Halas NJ. Theranostic Nanoshells: From Probe Design to Imaging and Treatment of Cancer. *Acc Chem Res* 2011.
181. Ni X, Zhang Y, Ribas J, et al. Prostate-targeted radiosensitization via aptamer-shRNA chimeras in human tumor xenografts. *J Clin Invest* 2011;121(6): 2383-90.
182. Wang C, Ding C, Kong M, et al. Tumor-targeting magnetic lipoplex delivery of short hairpin RNA suppresses IGF-1R overexpression of lung adenocarcinoma A549 cells in vitro and in vivo. *Biochem Biophys Res Commun* 2011;410(3): 537-42.
183. Achanta G, Pelicano H, Feng L, Plunkett W, Huang P. Interaction of p53 and DNA-PK in response to nucleoside analogues: potential role as a sensor complex for DNA damage. *Cancer Res* 2001;61(24): 8723-9.
184. Parker WB. Enzymology of purine and pyrimidine antimetabolites used in the treatment of cancer. *Chem Rev* 2009;109(7): 2880-93.
185. Senanayake TH, Warren G, Vinogradov SV. Novel anticancer polymeric conjugates of activated nucleoside analogues. *Bioconjug Chem* 2011;22(10): 1983-93.
186. van Moorsel CJ, Peters GJ, Pinedo HM. Gemcitabine: Future Prospects of Single-Agent and Combination Studies. *Oncologist* 1997;2(3): 127-34.

187. Hung SW, Mody HR, Govindarajan R. Overcoming nucleoside analog chemoresistance of pancreatic cancer: a therapeutic challenge. *Cancer Lett* 2012;320(2): 138-49.
188. Allain V, Bourgaux C, Couvreur P. Self-assembled nucleolipids: from supramolecular structure to soft nucleic acid and drug delivery devices. *Nucleic Acids Res* 2012;40(5): 1891-903.
189. Rejiba S, Reddy LH, Bigand C, Parmentier C, Couvreur P, Hajri A. Squalenoyl gemcitabine nanomedicine overcomes the low efficacy of gemcitabine therapy in pancreatic cancer. *Nanomedicine* 2011;7(6): 841-9.
190. Li J, Chen YC, Tseng YC, Mozumdar S, Huang L. Biodegradable calcium phosphate nanoparticle with lipid coating for systemic siRNA delivery. *J Control Release* 2010;142(3): 416-21.
191. Matsumura Y, Maeda H. A new concept for macromolecular therapeutics in cancer chemotherapy: mechanism of tumoritropic accumulation of proteins and the antitumor agent smancs. *Cancer Res* 1986;46(12 Pt 1): 6387-92.
192. Li SD, Huang L. Nanoparticles evading the reticuloendothelial system: role of the supported bilayer. *Biochim Biophys Acta* 2009;1788(10): 2259-66.
193. Banerjee R, Tyagi P, Li S, Huang L. Anisamide-targeted stealth liposomes: a potent carrier for targeting doxorubicin to human prostate cancer cells. *Int J Cancer* 2004;112(4): 693-700.
194. Li J, Yang Y, Huang L. Calcium phosphate nanoparticles with an asymmetric lipid bilayer coating for siRNA delivery to the tumor. *J Control Release* 2012;158(1): 108-14.
195. Zhang Y, Wang X, Wang J, Zhang X, Zhang Q. Octreotide-modified polymeric micelles as potential carriers for targeted docetaxel delivery to somatostatin receptor overexpressing tumor cells. *Pharm Res* 2011;28(5): 1167-78.
196. Risbood PA, Kane CT, Jr., Hossain MT, Vadapalli S, Chadda SK. Synthesis of gemcitabine triphosphate (dFdCTP) as a tris(triethylammonium) salt. *Bioorg Med Chem Lett* 2008;18(9): 2957-8.
197. Karl DM, Craven DB. Effects of alkaline phosphatase activity on nucleotide measurements in aquatic microbial communities. *Appl Environ Microbiol* 1980;40(3): 549-61.
198. Kim IY, Kang YS, Lee DS, et al. Antitumor activity of EGFR targeted pH-sensitive immunoliposomes encapsulating gemcitabine in A549 xenograft nude mice. *J Control Release* 2009;140(1): 55-60.

199. Johnson SA. Clinical pharmacokinetics of nucleoside analogues: focus on haematological malignancies. *Clin Pharmacokinet* 2000;39(1): 5-26.
200. Cohen GM. Caspases: the executioners of apoptosis. *Biochem J* 1997;326 ( Pt 1): 1-16.
201. Arya G, Vandana M, Acharya S, Sahoo SK. Enhanced antiproliferative activity of Herceptin (HER2)-conjugated gemcitabine-loaded chitosan nanoparticle in pancreatic cancer therapy. *Nanomedicine* 2011;7(6): 859-70.
202. Tang SN, Fu J, Shankar S, Srivastava RK. EGCG Enhances the Therapeutic Potential of Gemcitabine and CP690550 by Inhibiting STAT3 Signaling Pathway in Human Pancreatic Cancer. *PLoS One* 2012;7(2): e31067.
203. Andreeva ER, Orekhov AN. Evaluation of cell proliferation in human atherosclerotic lesions. *Methods Mol Med* 2001;52: 213-8.
204. Hornick JR, Spitzer D, Goedegebuure P, Mach RH, Hawkins WG. Therapeutic targeting of pancreatic cancer utilizing sigma-2 ligands. *Surgery* 2012;152(3 Suppl 1): S152-6.
205. Riganas S, Papanastasiou I, Foscolos GB, et al. Synthesis, sigma(1), sigma(2)-receptors binding affinity and antiproliferative action of new C1-substituted adamantanes. *Bioorg Med Chem* 2012;20(10): 3323-31.
206. Everaert H, Flamen P, Franken PR, Verhaeghe W, Bossuyt A. Sigma-receptor imaging by means of I123-IDAB scintigraphy: clinical application in melanoma and non-small cell lung cancer. *Anticancer Res* 1997;17(3B): 1577-82.
207. White JC, Rathmell JP, Capizzi RL. Membrane transport influences the rate of accumulation of cytosine arabinoside in human leukemia cells. *J Clin Invest* 1987;79(2): 380-7.
208. Brusa P, Immordino ML, Rocco F, Cattel L. Antitumor activity and pharmacokinetics of liposomes containing lipophilic gemcitabine prodrugs. *Anticancer Res* 2007;27(1A): 195-9.
209. Immordino ML, Brusa P, Rocco F, Arpicco S, Ceruti M, Cattel L. Preparation, characterization, cytotoxicity and pharmacokinetics of liposomes containing lipophilic gemcitabine prodrugs. *J Control Release* 2004;100(3): 331-46.
210. Lansakara PD, Rodriguez BL, Cui Z. Synthesis and in vitro evaluation of novel lipophilic monophosphorylated gemcitabine derivatives and their nanoparticles. *Int J Pharm* 2012;429(1-2): 123-34.
211. Sarpietro MG, Ottimo S, Giuffrida MC, Rocco F, Ceruti M, Castelli F. Synthesis of n-squalenoyl cytarabine and evaluation of its affinity with phospholipid bilayers and monolayers. *Int J Pharm* 2011;406(1-2): 69-77.

212. Li Q, Du YZ, Yuan H, et al. Synthesis of lamivudine stearate and antiviral activity of stearic acid-g-chitosan oligosaccharide polymeric micelles delivery system. *Eur J Pharm Sci* 2010;41(3-4): 498-507.
213. Meier C, Balzarini J. Application of the cycloSal-prodrug approach for improving the biological potential of phosphorylated biomolecules. *Antiviral Res* 2006;71(2-3): 282-92.
214. Zhang Y, Satterlee A, Huang L. In Vivo Gene Delivery by Nonviral Vectors: Overcoming Hurdles? *Mol Ther* 2012.
215. Xu Y, Szoka FC, Jr. Mechanism of DNA release from cationic liposome/DNA complexes used in cell transfection. *Biochemistry* 1996;35(18): 5616-23.
216. Han M, Lv Q, Tang XJ, et al. Overcoming drug resistance of MCF-7/ADR cells by altering intracellular distribution of doxorubicin via MVP knockdown with a novel siRNA polyamidoamine-hyaluronic acid complex. *J Control Release* 2012.
217. Saharinen P, Eklund L, Pulkki K, Bono P, Alitalo K. VEGF and angiopoietin signaling in tumor angiogenesis and metastasis. *Trends Mol Med* 2011;17(7): 347-62.
218. Yancopoulos GD, Davis S, Gale NW, Rudge JS, Wiegand SJ, Holash J. Vascular-specific growth factors and blood vessel formation. *Nature* 2000;407(6801): 242-8.
219. Zhang C, Tan C, Ding H, Xin T, Jiang Y. Selective VEGFR inhibitors for anticancer therapeutics in clinical use and clinical trials. *Curr Pharm Des* 2012;18(20): 2921-35.
220. Poindessous V, Ouaret D, El Ouadrani K, et al. EGFR- and VEGF(R)-targeted small molecules show synergistic activity in colorectal cancer models refractory to combinations of monoclonal antibodies. *Clin Cancer Res* 2011;17(20): 6522-30.
221. Pestourie C, Tavitian B, Duconge F. Aptamers against extracellular targets for in vivo applications. *Biochimie* 2005;87(9-10): 921-30.
222. Chames P, Van Regenmortel M, Weiss E, Baty D. Therapeutic antibodies: successes, limitations and hopes for the future. *Br J Pharmacol* 2009;157(2): 220-33.
223. Kamba T, McDonald DM. Mechanisms of adverse effects of anti-VEGF therapy for cancer. *Br J Cancer* 2007;96(12): 1788-95.
224. Oguri T, Achiwa H, Sato S, et al. The determinants of sensitivity and acquired resistance to gemcitabine differ in non-small cell lung cancer: a role of ABCC5 in gemcitabine sensitivity. *Mol Cancer Ther* 2006;5(7): 1800-6.
225. Nakano Y, Tanno S, Koizumi K, et al. Gemcitabine chemoresistance and molecular markers associated with gemcitabine transport and metabolism in human pancreatic cancer cells. *Br J Cancer* 2007;96(3): 457-63.

226. Waterhouse DN, Yapp D, Verreault M, Anantha M, Sutherland B, Bally MB. Lipid-based nanoformulation of irinotecan: dual mechanism of action allows for combination chemo/angiogenic therapy. *Nanomedicine (Lond)* 2011;6(9): 1645-54.
227. Chauhan VP, Stylianopoulos T, Martin JD, et al. Normalization of tumour blood vessels improves the delivery of nanomedicines in a size-dependent manner. *Nat Nanotechnol* 2012;7(6): 383-8.
228. Chaitanya GV, Steven AJ, Babu PP. PARP-1 cleavage fragments: signatures of cell-death proteases in neurodegeneration. *Cell Commun Signal* 2010;8: 31.
229. Nunez G, Benedict MA, Hu Y, Inohara N. Caspases: the proteases of the apoptotic pathway. *Oncogene* 1998;17(25): 3237-45.
230. Amoh Y, Li L, Tsuji K, et al. Dual-color imaging of nascent blood vessels vascularizing pancreatic cancer in an orthotopic model demonstrates antiangiogenesis efficacy of gemcitabine. *J Surg Res* 2006;132(2): 164-9.
231. Solorzano CC, Hwang R, Baker CH, et al. Administration of optimal biological dose and schedule of interferon alpha combined with gemcitabine induces apoptosis in tumor-associated endothelial cells and reduces growth of human pancreatic carcinoma implanted orthotopically in nude mice. *Clin Cancer Res* 2003;9(5): 1858-67.
232. Ma J, Waxman DJ. Combination of antiangiogenesis with chemotherapy for more effective cancer treatment. *Mol Cancer Ther* 2008;7(12): 3670-84.
233. Liang Y, Brekken RA, Hyder SM. Vascular endothelial growth factor induces proliferation of breast cancer cells and inhibits the anti-proliferative activity of anti-hormones. *Endocr Relat Cancer* 2006;13(3): 905-19.
234. Goel A, Goel H. Oral leiomyoma extending in retromolar region. *J Indian Soc Pedod Prev Dent* 2011;29(6 Suppl 2): S61-5.
235. Zhang Y, Satterlee A, Huang L. In vivo gene delivery by nonviral vectors: overcoming hurdles? *Mol Ther* 2012;20(7): 1298-304.
236. Li J, Chen YC, Tseng YC, Mozumdar S, Huang L. Biodegradable calcium phosphate nanoparticle with lipid coating for systemic siRNA delivery. *J Control Release* 2010;142(3): 416-21.
237. Tseng YC, Mozumdar S, Huang L. Lipid-based systemic delivery of siRNA. *Adv Drug Deliv Rev* 2009;61(9): 721-31.
238. Tredan O, Galmarini CM, Patel K, Tannock IF. Drug resistance and the solid tumor microenvironment. *J Natl Cancer Inst* 2007;99(19): 1441-54.
239. Hu CM, Aryal S, Zhang L. Nanoparticle-assisted combination therapies for effective cancer treatment. *Ther Deliv* 2010;1(2): 323-34.

240. Banerjee R, Tyagi P, Li S, Huang L. Anisamide-targeted stealth liposomes: a potent carrier for targeting doxorubicin to human prostate cancer cells. *Int J Cancer* 2004;112(4): 693-700.
241. Li J, Yang Y, Huang L. Calcium phosphate nanoparticles with an asymmetric lipid bilayer coating for siRNA delivery to the tumor. *J Control Release* 2012;158(1): 108-14.
242. de Nigris F, Balestrieri ML, Napoli C. Targeting c-Myc, Ras and IGF cascade to treat cancer and vascular disorders. *Cell Cycle* 2006;5(15): 1621-8.
243. Dang CV. MYC on the path to cancer. *Cell* 2012;149(1): 22-35.
244. Wang Z, Rao DD, Senzer N, Nemunaitis J. RNA interference and cancer therapy. *Pharm Res* 2011;28(12): 2983-95.
245. Baudino TA, McKay C, Pendeville-Samain H, et al. c-Myc is essential for vasculogenesis and angiogenesis during development and tumor progression. *Genes Dev* 2002;16(19): 2530-43.
246. Soucek L, Evan GI. The ups and downs of Myc biology. *Curr Opin Genet Dev* 2010;20(1): 91-5.
247. Kabilova TO, Chernolovskaya EL, Vladimirova AV, Vlassov VV. Inhibition of human carcinoma and neuroblastoma cell proliferation by anti-c-myc siRNA. *Oligonucleotides* 2006;16(1): 15-25.
248. Wang YH, Liu S, Zhang G, et al. Knockdown of c-Myc expression by RNAi inhibits MCF-7 breast tumor cells growth in vitro and in vivo. *Breast Cancer Res* 2005;7(2): R220-8.
249. Shipley LA, Brown TJ, Cornpropst JD, Hamilton M, Daniels WD, Culp HW. Metabolism and disposition of gemcitabine, and oncolytic deoxycytidine analog, in mice, rats, and dogs. *Drug Metab Dispos* 1992;20(6): 849-55.
250. Toyoshima M, Howie HL, Imakura M, et al. Functional genomics identifies therapeutic targets for MYC-driven cancer. *Proc Natl Acad Sci U S A* 2012;109(24): 9545-50.
251. Vafa O, Wade M, Kern S, et al. c-Myc can induce DNA damage, increase reactive oxygen species, and mitigate p53 function: a mechanism for oncogene-induced genetic instability. *Mol Cell* 2002;9(5): 1031-44.
252. Che-Ming Jack Hu, Santosh Aryal, Liangfang Zhang. Nanoparticle-assisted combination therapies for effective cancer treatment. *Therapeutic Delivery* 2010; 1(2): 323-334.
253. K.C. Cundy. Clinical pharmacokinetics of the antiviral nucleotide analogues cidofovir and adefovir. *Clin Pharmacokinet*. 1999; 36 (2): 127-143.

254. Data Sheet GEMZAR. <http://www.medsafe.govt.nz/profs/datasheet/g/gemzarinj.pdf>